MODULATION OF PULMONARY EPITHELIAL TO MESENCHYMAL TRANSITIONS THROUGH CONTROL OF EXTRACELLULAR MATRIX MICROENVIRONMENTS

A Dissertation
Presented to
The Academic Faculty

by

Ashley Carson Brown

In Partial Fulfillment
of the Requirements for the Degree
Doctor of Philosophy in Bioengineering in the
Wallace H. Coulter Department of Biomedical Engineering at Georgia Tech and Emory University

Georgia Institute of Technology
August 2011

MODULATION OF PULMONARY EPITHELIAL TO MESENCHYMAL TRANSITIONS THROUGH CONTROL OF EXTRACELLULAR MATRIX MICROENVIRONMENTS

Approved by:

Dr. Thomas H. Barker, Advisor
Wallace H. Coulter Department of Biomedical Engineering
Georgia Institute of Technology

Dr. Douglas Eaton
Department of Physiology
Emory University School of Medicine

Dr. Andrés Garcia
George W. Woodruff School of Mechanical Engineering
Georgia Institute of Technology

Dr. Melissa Kemp
Wallace H. Coulter Department of Biomedical Engineering
Georgia Institute of Technology

Dr. Evan Zamir
George W. Woodruff School of Mechanical Engineering
Georgia Institute of Technology

Date Approved: [May 12, 2011]

I dedicate this work to my husband Chris. You are my rock, constant support, and best friend.

ACKNOWLEDGEMENTS

This work could not have been accomplished without the guidance, support, encouragement, and input from a number of people. I would first like to thank my advisor, Dr. Thomas H. Barker for taking me on as the first graduate student in the Matrix Biology and Engineering Lab. My experience in a new lab was exciting and I felt as though I really had the chance to contribute to the overall direction of the research. I especially want to thank Tom for his guidance and mentoring over the past 5 years, for giving me the opportunity to expand my horizons, pursue research that was of great interest to me, and for encouraging me to be my own biggest critic. I would secondly like to thank my committee members, Dr. Douglas Eaton, Dr. Andres Garcia, Dr. Melissa Kemp, and Dr. Evan Zamir for their valuable insight about alveolar epithelial cell biology, fibronectin integrin interactions and cell signaling, and also for their comments and suggestions that improved the depth of this work. Specifically, I would like to thank Dr. Douglas Eaton and Ms. Julie Self for assistance with primary ATII isolation and for providing me with L2 cells and Dr. Andres Garcia for providing reagents. In addition, I would like to thank Dr. Andres Garcia for his mentorship during my tenure on the Cell and Tissue Engineering Training grant. I thoroughly enjoyed our journal clubs and I am grateful for his continual encouragement to complete an industrial internship, which was an invaluable experience.

I would like to thank the members of the Matrix Biology and Engineering Lab, who all work extremely diligently to produce the highest quality research. First, I would like to thank Allyson Soon, who joined the lab shortly after I did. I am grateful for Allyson's expertise and assistance with cloning, protein production, and purification; she

always had the answers to my many questions regarding the FPLC. I also thank Allyson for her friendship and her willingness to listen and despair with me about experiments gone awry. Secondly, I would like to thank Dr. Sarah Stabenfeldt for her assistance with SPR. I am very grateful that she learned the ins and outs of SPR and bestowed all of that knowledge upon me, taking the time to train me to use the machine and for assistance in data analysis. It was a pleasure working with Sarah and I wish her the best of luck as she establishes her independent research at Arizona State University. I thank Vince Fiore for his assistance with polyacrylamide gel production and for his many contributions to the investigation of the role of substrate stiffness in EMT. Specifically, I thank Vince Fiore for his work on characterizing tissue stiffness in normal and fibrotic mouse models and also for his AFM analysis of single cell stiffness in response to increasing stiffness. I thank Lizhi Cao for insightful conversations about fibronectin structure and also for his lab antics including a messy bench and occasional out of control flame that always made me laugh. I thank Sarah Jordan for taking over the administrative aspects of the lab and for her assistance with numerous protocols, most importantly for her assistance with western blots. I would like to thank the most recent members of the lab, Alison Douglas, Saranya Sathananthan, Dr. Kelly Clause, and Dr. Rodney Avery for helpful comments and feedback; I look forward to the results from their exciting research projects. I specifically thank Alison Douglas for her contribution to my caffeine addiction and thesis writing by bringing a Keurig brewer into lab during the critical last months of my thesis writing. I thank several undergraduate students who I had the pleasure of working with during my thesis. I thank Nikhil Dewan for his technical assistance on the fibronectin fragment EMT project and Justin Chen for his contributions to the stiffness mediated

EMT project. I would especially like to thank Jessie Rowe for her contributions to characterization of EMT in response to integrin specific fibronectin fragments. It was a pleasure working with such a motivated and talented undergraduate student.

I would like to thank the several graduate students for their scientific contributions and invaluable friendships. I thank Andres Bratt-Leal for always providing reagents when I realized I needed something in the middle of an experiment, Jeremy Lim for his help with qPCR, and Dr. Randy Ankey for advice related to western blots. I thank Casey Holliday for her assistance with flow cytometry and for her friendship; I could not ask for a better birthday buddy. I thank Erin Spinner for her tremendous friendship and for sharing my passion for yoga and for introducing me to running, an activity which has become such an integral part of my life. I further thank Erin and Casey, along with Dr. Fernie Goh, Rachel Whitmire, Laura Hansen, Dr. Sarah Griffiths, Nnenna Finn, Julia Henkels, and Gina Cremona, for their numerous conversations, coffee breaks, encouragement, and advice; friends are so important in this journey.

Most importantly I would like to thank my family. Donny Carson, my dad, Catherine Carson, my mom, Bradley Carson and Eric Carson, my brothers, for their love and support through the years. Thank you for your constant encouragement and for always being proud in me. I love you all so very much. I would also like to thank my new family members, Lou and Tim Jackson, Roger Brown, Christine Anton, Lauren and Robert Krawczyk, and Meg Brown for welcoming me into your family and for all of your encouragement. To my friends who are as close as family: I would like to thank Ms. Erin Pardue and Ms. Marisa Arms for their support through the many years I have known them. I thank Erin for being a wonderful roommate and friend during our time together

at Clemson, and for continuing to be a great friend and colleague in the field matrix biology.

Finally to my husband Chris, to whom I have dedicated this work, words cannot truly express my gratitude. Chris endured my long hours, frustration when experiments were not working, and complete lack of attention to housework with nothing but encouragement and total faith in my abilities. After proofreading all of my abstracts and papers, and listening to me practice talks and presentations, Chris knows more about fibronectin, integrins, and EMT than any other electrical engineer I know. Furthermore, Chris was instrumental in several aspects of my data analysis through providing Matlab code for determining qPCR reaction efficiency and for plotting SPR curves. Chris continually kept me motivated, and was always willing to accompany me to lab late into the night and on weekends, or simply provide assistance in any way that would help me progress in my work. Most of all I thank Chris for his love, laughter, positive attitude, and unwavering support. You always know how to make me smile, and I am so grateful that you are a part of my life.

TABLE OF CONTENTS

LIST OF TABLES

LIST OF FIGURES

LIST OF SYMBOLS AND ABBREVIATIONS

α	alpha
α-SMA	alpha smooth muscle actin
β	beta
k_a	kinetic association rate constant
k_d	kinetic dissociation rate constant
K_d	equilibrium dissociation rate constant
AFM	atomic force microscopy
ATI	alveolar epithelial type I
ATII	alveolar epithelial type II
cDNA	complimentary deoxyribonucleic acid
ECM	extracellular matrix
EMT	epithelial to mesenchymal transition
Fn	fibronectin
FnIII9'10	fibronectin 9^{th} and 10^{th} type III domain with stabilizing point mutation
Ln	laminin
mRNA	messenger ribonucleic acid
qPCR	quantitative polymerase chain reaction
RU	response units
SPR	surface plasmon resonance
P4H	prolyl-4-hydroxylase
TGFβ	transforming growth factor beta

SUMMARY

The extracellular matrix (ECM) is a dynamic environment that provides important cues for directing cell fate. Cells respond to and also actively remodel their ECM, and this dynamic remodeling of the ECM is essential for development, wound healing, and normal tissue homeostastis. However, severe pathological conditions can arise when ECM remodeling becomes excessive or uncontrolled. Dysregulation of the biochemical and biophysical properties of the ECM are observed in many types of disease including cancer and fibrotic pathologies such as pulmonary fibrosis and cardiovascular disease. These changes force cells into a non-homeostatic niche. Specifically in the case of pulmonary fibrosis, biochemically the ECM is known to shift from a predominantly laminin/elastin matrix to a more provisional matrix comprised of fibrin and fibronectin (Fn). In addition, the elasticity of fibrotic tissue has been shown to increase approximately nine-fold, drastically modifying the biophysical properties of the ECM. The stiffness of the underlying matrix has been shown to have many implications in directing cell fate. For example, it has been shown that in response to increases in substrate stiffness, cells will adjust their internal stiffness to match that of their surroundings. As a consequence of this mechanical homeostasis between the cell and its ECM, cells in increasingly rigid, or stiff, environments display increased activation of contractile signals like Rho and Rho associated kinase (ROCK), which likely has multiple and diverse secondary effects, such as increases in forces applied by cells to the ECM. As a consequence of stress application in the ECM, proteins comprising structural fibers (such as Fn) are known to display significant conformational changes (i.e. force-

mediated partial unfolding), further contributing to biochemical alterations to the ECM. In the case of Fn, conformational changes can have great consequences on cell phenotype by altering integrin binding. In this dissertation, it was hypothesized that such alterations in the ECM, mechanochemical alterations and stiffness, would lead to pathological cellular processes such as epithelial to mesenchymal transitions (EMT).

EMT, the phenotypic transdifferentiation of cells from epithelial to mesenchymal lineages, has been shown to contribute to the onset and progression of pulmonary fibrosis, as well as other types of fibrotic diseases and cancer metastasis. While EMT is critical for wound healing and embryonic development, dysregulation of EMT leads to significant tissue and organ defects. EMT is a highly orchestrated process involving the integration of biochemical signals from ECM receptors (integrins) and growth factor receptors like transforming growth factor-β (TGFβ) receptor and receptor tyrosine kinases. TGFβ has been identified as a potent inducer of EMT. TGFβ must be activated in order to bind to its receptors, which can occur through several mechanisms, one of which is through mechanical activation as a result of cell contractile forces. Because it is a cell-mediated process, mechanical activation of TGFβ is also influenced by both the biophysical and biochemical state of the ECM. Therefore, it was hypothesized that both increases in substrate stiffness or changes in integrin engagement would modulate cell contractility, leading to TGFβ activation and subsequently EMT.

This dissertation seeks to connect the biochemical and biophysical changes observed in the ECM during fibrosis to the pathological process of EMT. Biochemically, the role of alterations in Fn conformation in the progression of EMT was investigated. Utilizing recombinant Fn fragments modeling different conformational states of the

molecule, integrin specific binding to the fragments and resulting downstream phenotypes were investigated. Furthermore, the ability of the central cell binding domain of Fn to facilitate interactions with the classical laminin (Ln) receptor, integrin α3β1 were characterized. Finally, the contribution of biophysical changes in the ECM to EMT was investigated, specifically analyzing the role of increased tissue stiffness in the onset and progression of EMT. Utilizing poly-acrylamide gels of varying stiffness, EMT responses were characterized and the role of TGFβ activation/signaling in stiffness-mediated EMT was investigated.

The results presented here show that both the biochemical and biophysical state of the ECM contribute to the pathological progression of EMT. Biochemically, Fn fragments displaying both the RGD and PHSRN binding sites facilitate cell binding through α5β1 and α3β1 integrins, and lead to maintenance of epithelial phenotype, while Fn fragments displaying only the RGD site facilitate cell binding through αv integrins and lead to enhanced activation of TGFβ and EMT. Furthermore, an in depth investigation into α3β1 binding to Fn fragments indicates that α3β1 integrin binding to Fn is dependent on both the presence and orientation of the PHSRN site. Biophysically, increasingly rigid Fn substrates are sufficient to induce EMT and these responses are mediated by enhanced activation of TGFβ. These results suggest that the cellular micromechanical environment is a significant contributor to the emergence of pathological phenotypes associated with disease progression.

CHAPTER 1

INTRODUCTION

Fibrosis, a potentially deadly pathology, is characterized by excessive deposition of extracellular matrix leading to stiffening of the surrounding tissue and ultimately loss of tissue structure and function. Many lung diseases such as pulmonary fibrosis, COPD, lung cancer, and emphysema, are extracellular matrix (ECM)-centric pathologies, meaning that the ECM, the structural scaffolding of the tissue, drives many of the pathological phenotypes contributing to the disease. (1-6)

Despite general scientific acceptance and significant published data illustrating the role of mechanical forces on cell phenotype, (7-12) there has been a considerable lack of attention to the role of ECM mechanics in the progression of lung pathologies. During fibrosis, cells experience changes in their mechanical microenvironment at both the biophysical and biochemical level, such that their underlying ECM becomes stiffer, (13) while the biochemical composition of the ECM changes from a predominantly laminin/elastin matrix to exhibiting higher levels of provisional matrix proteins such as fibronectin (Fn). (14) The precise mechanisms of the biophysical changes are not entirely clear, but could occur through changes in ECM composition through changed in gene expression, increased glycosylation, or increased cross linking of the matrix through tissue transglutaminases, lysyl oxidase, or other mechanisms. (15, 16) In addition, shifts in cell populations to more contractile phenotypes can also contribute significantly to the mechanical-state of the ECM. This phenomenon is highlighted by studies demonstrating that physiologically relevant fibroblast subpopulations associated with pulmonary fibrosis

generate Fn ECMs with markedly different mechanical signatures. (17) Increased mechanical input from contractile cells can have great consequences on the state of the matrix by increasing the stiffness of the matrix as well as through altering the biochemical nature of fibrillar ECM proteins such as Fn. Fn is highly sensitive to force-mediated unfolding, and small force inputs can lead to distention within the cell-binding region, such that the RGD and PHSRN integrin binding sites are moved away from one other. The relative positioning of the RGD and PHSRN site has been shown to influence α5β1 integrin binding, therefore, alterations in their positions can lead to differential integrin engagement, ultimately having great consequence on cell fate. (14, 18-20)

Recently, epithelial to mesenchymal transitions (EMT) have been implicated in the onset and progression of numerous fibrotic pathologies, including pulmonary fibrosis, renal fibrosis, and abhorrent wound healing/scar tissue formation. (21, 22) EMT is characterized by a loss of cell-cell contacts, decreased expression of e-cadherin, and loss of polarity, accompanied by an increase in expression of mesenchymal markers including α-SMA, increased ECM production, and an increase in stress-fiber formation, cell contractility and mobility. (23, 24) EMT has been observed *in vivo* in bleoymycin-induced pulmonary fibrosis in fibrotic regions of the lung. (25) Furthermore, *in vitro*, alveolar epithelial type II (ATII) cells have been shown to undergo EMT in response to the underlying matrix; when cultured on Ln/collagen matrices epithelial cells maintain their phenotype, but when cultured on provisional Fn matrices the cells undergo EMT. (26) Though the precise mechanisms leading to the onset of EMT are not well defined, it is clear that transforming growth factor beta (TGFβ) is a potent inducer of EMT. (26-36) TGFβ must be activated in order to bind to its receptor(s), and can be activated through

several mechanisms including proteolytic cleavage, increases in pH, reactive oxygen species, and integrins. (37-42) Interestingly, TGFβ can also be mechanically activated through cell contractile forces, which can be mediated through both biophysical events, as observed in fibroblasts in response to increases in substrate stiffness, (43) or through biochemical events, such as αv integrin engagement of Fn. (26) Though it is clear that TGFβ is a potent inducer of EMT and TGFβ activation can be regulated by mechanical input, there is a little known about how force-induced changes in the ECM affect EMT.

The *overall objective* of this project was to characterize how the biophysical and biochemical nature of the ECM contribute to TGFβ activation and subsequently EMT. The *central hypothesis* of this work was that both increases in substrate stiffness and changes in integrin engagement would modulate cell contractility, leading to TGFβ activation and subsequently EMT. In this dissertation, the influence of substrate stiffness and integrin specific interactions, on ATII cell contractility, TGFβ activation, and downstream regulation of EMT was investigated. Integrin-specific recombinant fragments of Fn type III repeats or polyacrylamide gels of varying stiffness were used to address the hypothesis through 3 specific aims: 1) Investigate modulation of EMT through α3/α5 vs. αv integrin binding to engineered integrin-specific Fn fragments; 2) Further characterize conformation specific binding of α3β1 integrin to Fn fragments; 3) Investigate the role of substrate stiffness-mediated increases in contractility in modulation of EMT. This work will provide insight into the pathological progression of pulmonary fibrosis and could uncover potential targets for therapeutics.

Specific Aim 1: Investigate modulation of EMT through α3/α5 vs. αv integrin binding to Fn fragments

The hypothesis of this aim was that epithelial cells would engage FnIII9'10 displaying both the RGD and PHSRN sites predominantly through α5 and α3 integrins, and FnIII10 displaying only the RGD site predominantly through αv integrins. Because of α3 and α5 integrins' known role in wound healing and αv integrins' known role in fibrotic progression, it was hypothesized that cells cultured on FnIII9'10 would maintain an epithelial phenotype while cells cultured on FnIII10 would undergo EMT. Integrin specific attachment to the Fn fragments was first determined through cell attachment assays and immunofluorescence staining for integrin subunits. EMT was then analyzed through q-PCR and immunofluorescence staining for various epithelial and mesenchymal markers. Furthermore, proper wound healing was assessed through an *in vitro* wound healing assay. The role of TGFβ signaling was analyzed through q-PCR analysis of Pai-1 mRNA expression.

Specific Aim 2: Establish the conformation specific binding of α3β1 integrin to FN fragments.

Based on initial results from cell attachment assays and immunofluorescence staining on Fn fragments indicating that epithelial cells engage FnIII9'10 via α3β1 integrin but not FnIII10, it was hypothesized that α3β1 integrin binds to the central cell binding domain of Fn in a PHSRN-dependent manner. To explore this hypothesis, a variety of recombinant Fn III9'10 variants displaying an ARG to ALA mutation in the synergy site (FnIII9$^{R\rightarrow A}$10), and a 2 GLY insertion (FnIII9^{2G}10) or a 4 GLY insertion (FNIII9^{4G}10) between FnIII9 and FnIII10 were created. Surface plasmon resonance (SPR) was used to

determine binding kinetics of integrin α3β1 binding to the Fn fragments. In addition, cells spreading responses on Fn fragments were investigated.

Specific Aim 3: Investigate the role of substrate stiffness in modulating EMT

The working hypothesis of this aim was that cells on increasingly stiffness substrates will become more contractile, leading to increased TGFβ activation/signaling, and subsequently increased EMT. Stiffness mediated EMT was investigated by culturing alveolar epithelial cells on polyacrylamide gels of varying stiffness with Fn cross-linked to the surface or on Fn or Ln-coated glass as controls. EMT was investigated through western blot and immunofluorescence analysis of various epithelial and mesenchymal markers. Cell contractility was investigated through analysis of stress-fiber formation and quantification of single cell stiffness through AFM probing. Based on the hypothesis that increases in cell contractility contribute to stiffness-mediated EMT, EMT was characterized on substrates of varying stiffness in the presence of the contractility inhibitor, Y-27632. The role of TGFβ activation/signaling in response to increasingly rigid substrates in the presence or absence of Y-27632 was investigated through qPCR for the TGFβ responsive gene, Pai-1. The role of TGFβ signaling was further analyzed by analysis of EMT events and Pai-1 signaling in the presence of active TGFβ on soft substrates and in the presence of TGFβ neutralizing antibodies on rigid substrates.

This body of work focuses on a highly significant unknown in the field of pulmonary repair, remodeling, and pathogenesis by investigating the role of the integrin specific binding and stiffness of the ECM in modulating EMT. While traditional approaches have sought to understand the role of full length Fn on rigid surfaces on epithelial cells, this study focuses on 1) the role of mechanically unstable, integrin

binding regions of Fn that likely display altered conformations over time and their role in the progression of interstitial pulmonary disorders through the regulation of cell-integrin engagement and 2) the role of increases in tissue stiffness, over the range of tissue stiffness observed in pulmonary fibrosis *in vivo*, in modulating EMT. Understanding these processes will provide insight into how mechanical forces, ECM remodeling, and mechanical regulation of TGFβ signaling contribute to the pathological progression of pulmonary fibrosis and could uncover potential targets for therapeutics. Furthermore, most of what is known about EMT has been performed on rigid substrates. This work is significant, because it illustrates the integration of both biochemical and biophysical signals from the ECM in TGFβ activation and the pathological progression of EMT. Current therapeutics for fibrotic diseases such as TGFβ antibodies focus on treating the cells, but this work suggests that the state of the matrix should also be considered in development of effective therapeutics.

References

1. Spruit MA, Janssen DJ, Franssen FM, Wouters EF. Rehabilitation and palliative care in lung fibrosis. Respirology.14:781-7. 2009.

2. Hallgren O, Nihlberg K, Dahlback M, Bjermer L, Eriksson LT, Erjefalt JS, et al. Altered fibroblast proteoglycan production in COPD. Respir Res.11:55.

3. Zandvoort A, Postma DS, Jonker MR, Noordhoek JA, Vos JT, Timens W. Smad gene expression in pulmonary fibroblasts: indications for defective ECM repair in COPD. Respir Res.9:83. 2008.

4. Horowitz JC, Martinez FJ, Thannickal VJ. Mesenchymal cell fate and phenotypes in the pathogenesis of emphysema. COPD.6:201-10. 2009.

5. Buttery RC, Rintoul RC, Sethi T. Small cell lung cancer: the importance of the extracellular matrix. Int J Biochem Cell Biol.36:1154-60. 2004.

6. Cox TR, Erler JT. Remodeling and homeostasis of the extracellular matrix: implications for fibrotic diseases and cancer. Dis Model Mech.4:165-78.

7. Engler AJ, Griffin MA, Sen S, Bonnemann CG, Sweeney HL, Discher DE. Myotubes differentiate optimally on substrates with tissue-like stiffness: pathological implications for soft or stiff microenvironments. J Cell Biol.166:877-87. 2004.

8. Engler AJ, Sen S, Sweeney HL, Discher DE. Matrix elasticity directs stem cell lineage specification. Cell.126:677-89. 2006.

9. Paszek MJ, Zahir N, Johnson KR, Lakins JN, Rozenberg GI, Gefen A, et al. Tensional homeostasis and the malignant phenotype. Cancer Cell.8:241-54. 2005.

10. Pelham RJ, Jr., Wang Y. Cell locomotion and focal adhesions are regulated by substrate flexibility. Proc Natl Acad Sci U S A.94:13661-5. 1997.

11. Pelham RJ, Jr., Wang YL. Cell locomotion and focal adhesions are regulated by the mechanical properties of the substrate. Biol Bull.194:348-9; discussion 9-50. 1998.

12. Wozniak MA, Desai R, Solski PA, Der CJ, Keely PJ. ROCK-generated contractility regulates breast epithelial cell differentiation in response to the physical properties of a three-dimensional collagen matrix. J Cell Biol.163:583-95. 2003.

13. Liu F, Mih JD, Shea BS, Kho AT, Sharif AS, Tager AM, et al. Feedback amplification of fibrosis through matrix stiffening and COX-2 suppression. J Cell Biol.190:693-706.

14. Smith ML, Gourdon D, Little WC, Kubow KE, Eguiluz RA, Luna-Morris S, et al. Force-induced unfolding of fibronectin in the extracellular matrix of living cells. PLoS Biol.5:e268. 2007.

15. Levental KR, Yu H, Kass L, Lakins JN, Egeblad M, Erler JT, et al. Matrix crosslinking forces tumor progression by enhancing integrin signaling. Cell.139:891-906. 2009.

16. Santhanam L, Tuday EC, Webb AK, Dowzicky P, Kim JH, Oh YJ, et al. Decreased S-nitrosylation of tissue transglutaminase contributes to age-related increases in vascular stiffness. Circ Res.107:117-25.

17. Barker TH, Grenett HE, MacEwen MW, Tilden SG, Fuller GM, Settleman J, et al. Thy-1 regulates fibroblast focal adhesions, cytoskeletal organization and migration through modulation of p190 RhoGAP and Rho GTPase activity. Exp Cell Res.295:488-96. 2004.

18. Krammer A, Craig D, Thomas WE, Schulten K, Vogel V. A structural model for force regulated integrin binding to fibronectin's RGD-synergy site. Matrix Biol.21:139-47. 2002.

19. Baneyx G, Baugh L, Vogel V. Fibronectin extension and unfolding within cell matrix fibrils controlled by cytoskeletal tension. Proc Natl Acad Sci U S A.99:5139-43. 2002.

20. Garcia AJ, Vega MD, Boettiger D. Modulation of cell proliferation and differentiation through substrate-dependent changes in fibronectin conformation. Mol Biol Cell.10:785-98. 1999.

21. Chaffer CL, Thompson EW, Williams ED. Mesenchymal to epithelial transition in development and disease. Cells Tissues Organs.185:7-19. 2007.

22. Lopez-Novoa JM, Nieto MA. Inflammation and EMT: an alliance towards organ fibrosis and cancer progression. EMBO Mol Med.1:303-14. 2009.

23. Thiery JP, Sleeman JP. Complex networks orchestrate epithelial-mesenchymal transitions. Nat Rev Mol Cell Biol.7:131-42. 2006.

24. Zeisberg M, Neilson EG. Biomarkers for epithelial-mesenchymal transitions. J Clin Invest.119:1429-37. 2009.

25. Wu Z, Yang L, Cai L, Zhang M, Cheng X, Yang X, et al. Detection of epithelial to mesenchymal transition in airways of a bleomycin induced pulmonary fibrosis model derived from an alpha-smooth muscle actin-Cre transgenic mouse. Respir Res.8:1. 2007.

26. Kim KK, Kugler MC, Wolters PJ, Robillard L, Galvez MG, Brumwell AN, et al. Alveolar epithelial cell mesenchymal transition develops in vivo during pulmonary fibrosis and is regulated by the extracellular matrix. Proc Natl Acad Sci U S A.103:13180-5. 2006.

27. Jain R, Shaul PW, Borok Z, Willis BC. Endothelin-1 induces alveolar epithelial-mesenchymal transition through endothelin type A receptor-mediated production of TGF-beta1. Am J Respir Cell Mol Biol.37:38-47. 2007.

28. Kasai H, Allen JT, Mason RM, Kamimura T, Zhang Z. TGF-beta1 induces human alveolar epithelial to mesenchymal cell transition (EMT). Respir Res.6:56. 2005.

29. Lamouille S, Derynck R. Cell size and invasion in TGF-beta-induced epithelial to mesenchymal transition is regulated by activation of the mTOR pathway. J Cell Biol.178:437-51. 2007.

30. Lenferink AE, Magoon J, Cantin C, O'Connor-McCourt MD. Investigation of three new mouse mammary tumor cell lines as models for transforming growth factor (TGF)-beta and Neu pathway signaling studies: identification of a novel model for TGF-beta-induced epithelial-to-mesenchymal transition. Breast Cancer Res.6:R514-30. 2004.

31. Park SH, Choi MJ, Song IK, Choi SY, Nam JO, Kim CD, et al. Erythropoietin decreases renal fibrosis in mice with ureteral obstruction: role of inhibiting TGF-beta-induced epithelial-to-mesenchymal transition. J Am Soc Nephrol.18:1497-507. 2007.

32. Willis BC, Liebler JM, Luby-Phelps K, Nicholson AG, Crandall ED, du Bois RM, et al. Induction of epithelial-mesenchymal transition in alveolar epithelial cells by transforming growth factor-beta1: potential role in idiopathic pulmonary fibrosis. Am J Pathol.166:1321-32. 2005.

33. Wynn TA. Cellular and molecular mechanisms of fibrosis. J Pathol.214:199-210. 2008.

34. Xu J, Lamouille S, Derynck R. TGF-beta-induced epithelial to mesenchymal transition. Cell Res.19:156-72. 2009.

35. Yao HW, Xie QM, Chen JQ, Deng YM, Tang HF. TGF-beta1 induces alveolar epithelial to mesenchymal transition in vitro. Life Sci.76:29-37. 2004.

36. Willis BC, Borok Z. TGF-beta-induced EMT: mechanisms and implications for fibrotic lung disease. Am J Physiol Lung Cell Mol Physiol.293:L525-34. 2007.

37. Yue J, Mulder KM. Transforming growth factor-beta signal transduction in epithelial cells. Pharmacol Ther.91:1-34. 2001.

38. Stetler-Stevenson WG, Aznavoorian S, Liotta LA. Tumor cell interactions with the extracellular matrix during invasion and metastasis. Annu Rev Cell Biol.9:541-73. 1993.

39. Barcellos-Hoff MH, Dix TA. Redox-mediated activation of latent transforming growth factor-beta 1. Mol Endocrinol.10:1077-83. 1996.

40. Yu Q, Stamenkovic I. Cell surface-localized matrix metalloproteinase-9 proteolytically activates TGF-beta and promotes tumor invasion and angiogenesis. Genes Dev.14:163-76. 2000.

41. Munger JS, Huang X, Kawakatsu H, Griffiths MJ, Dalton SL, Wu J, et al. The integrin alpha v beta 6 binds and activates latent TGF beta 1: a mechanism for regulating pulmonary inflammation and fibrosis. Cell.96:319-28. 1999.

42. Annes JP, Munger JS, Rifkin DB. Making sense of latent TGFbeta activation. J Cell Sci.116:217-24. 2003.

43. Wipff PJ, Rifkin DB, Meister JJ, Hinz B. Myofibroblast contraction activates latent TGF-beta1 from the extracellular matrix. J Cell Biol.179:1311-23. 2007.

CHAPTER 2

BACKGROUND

Fibrosis and EMT

Fibrotic pathologies are characterized by excessive ECM production, interstitial scar tissue formation, and an increase in tissue stiffness. During the course of idiopathic pulmonary fibrosis (IPF), the experimental disease model utilized for this work, functional lung tissue of the alveoli is replaced with collagen-rich ECM, leading to rapid and severe decreases in lung compliance and irreversible loss of lung function. (1, 2) IPF is a currently untreatable and ultimately fatal condition with 3 and 5 year mortality rates of 50% and 80%, respectively. (3) In addition to formation of scar tissue, another hallmark of IPF and other fibrotic conditions is the influx of extremely contractile myofibroblasts. The influx of myofibroblasts further perpetuates the disease through persistent matrix production and contraction, contributing to increased cytokine activation. Lack of effective treatment options for this disease, and many other fibrotic diseases is largely due to lack of understanding of the exact mechanisms initiating fibrosis, however recent studies implicate alveolar epithelial to mesenchymal transitions (EMT) in the onset and progression of fibrosis. (4-9) EMT has been theorized to increase the number of ECM secreting mesenchymal cells, and cell tracking studies have demonstrated that a considerable number of myofibroblasts arise from EMT. (6, 10)

EMT is the de-differentiation of an epithelial cell into a mesenchymal cell, and is defined through the loss of apical-basolateral polarity, loss of tight cell junctions, and a marked down-regulation of E-cadherin. These changes are accompanied by concomitant up-regulation of α-smooth muscle actin (α-SMA), increased stress fiber formation and

alignment, increased migration through filopodia and lamellopodia formation, and an increased synthesis of ECM. EMT is important during normal cellular processes in wound healing, embryogenesis, and development, contributing to wound-closure, blastocyst implantation, gastrulation, generation of the neural crest, and palate closure. (11-13) Highlighting the importance of EMT in wound healing of the skin, keratinocytes at the wound edge undergo partial EMT, acquiring an intermediate phenotype characterized by loose cell-cell contacts and migration that allow for wound closure. (14) Though EMT is clearly an important cellular transition, if not tightly regulated, EMT can lead to abhorrent wound healing and scar tissue formation in mature tissues, contributing to pathological conditions such as keloids, pulmonary fibrosis, and renal fibrosis, or through a similar process of endothelial to mesenchymal transition, an contribute to cardiac fibrosis. Furthermore, EMT contributes to cancer metastisis, as epithelial cells take on a migratory mesenchymal phenotype that allows them to invade secondary epithelia.

EMT has been shown to occur in response to several factors such as growth factors including transforming growth factor beta (TGFβ), tumor necrosis factor alpha (TNFα), epidermal growth factor (EGF), and reactive oxygen species, as well as in response to extracellular matrix proteins including fibronectin (Fn). (15-19) The role of TGFβ is most well defined of all these factors, and is known to be a potent inducer of EMT. TGFβ signaling is quite complex and can activate a number of different pathways, including SMAD-dependent and independent pathways. (20-22) SMAD dependent signaling can lead to Snail1 activation, which plays a role in EMT by down regulating E-cadherin expression and up regulating a number of mesenchymal genes including

vimentin and α-SMA. (23-25) Though many advances have been made in understanding factors contributing to EMT, precise events leading to the initiation of EMT remain unclear. This dissertation focuses on the role of the extracellular matrix microenvironment in the onset of EMT of ATII cells.

Alveolar Type II Epithelial Cells

ATII cells in pulmonary homeostasis/repair:

Understanding normal pulmonary homeostasis and repair can provide insight into anomalous cellular interactions that lead to pathological EMT in pulmonary fibrosis. Pulmonary remodeling and repair follows roughly the same process as healing of any epithelial barrier, namely the proliferation, migration and differentiation of epithelial cells in response to provisional and intermediate ECMs. In pulmonary tissue, disruption of underlying vasculature results in the initiation of the clotting cascade and the creation of a fibrin-rich provisional ECM with interspersed cross-linked Fn, which is ultimately degraded by invading interstitial mesenchymal fibroblasts and replaced with an intermediate Fn-rich ECM. (26) Alveolar epithelial cells interact with the provisional and intermediate matrix through cell surface ECM-binding receptors known as integrins. The intermediate Fn-rich ECM provides important biochemical cues directing apical epithelial cell proliferation and differentiation as well as other functions (27) and acts as the initial template for the more permanent collagen-laminin-elastin matrix of the lung. (28)

The ATII cell is the primary cell type associated with proper maintenance of pulmonary tissue, i.e. alveolar homeostasis and repair. (29) Adult pulmonary tissue is composed of over 40 different cell types and possesses over 300 million alveoli, the primary functional

structure of lung. Two primary epithelial cells populate the alveolus, Type I and II alveolar epithelial cells (ATI and ATII). ATI cells, separated from capillaries by only a thin basement membrane, are the primary gas-exchange cells and comprise 90% of the alveolar surface yet only 10% of the epithelial cell number. (30) ATII cells are pseudo-cuboidal, multifunctional cells that are considered the "protector of the alveolus" due to their central role in defense and repair. ATII cells act as the primary surfactant-secreting cell, precursors to ATI cells, and in many instances as non-professional antigen-presenting cells. (31) ATII cells also contribute significantly to the fluid balance across the epithelial barrier through sodium transport functions. (32) These various functions underscore the vital importance of these cells in maintaining pulmonary function. During normal repair, ATII cells are thought to proliferate, migrate onto a provisional matrix and differentiate into ATI cells.

Despite their obvious beneficial effects, recent evidence suggests that repeated injury of ATII cells may be the primary cause of pulmonary fibrotic disorders. (31, 33-35) Lung biopsies of patients with pulmonary fibrosis show fragmented DNA (indicative of apoptosis) in alveolar epithelium (36) and apoptotic alveolar epithelial cells are observed adjacent to foci of myofibroblasts. (24, 25, 37) As discussed, an important emerging hypothesis is that ATII cells may serve as the source of EMT. (4, 6, 38) It has been demonstrated that ATII cell EMT can be potently induced by transforming growth factor beta-1 (TGFβ) in vitro and in vivo. (4, 18, 38-40) The extracellular matrix has also been shown to play a critical role in alveolar EMT. (6) Primary ATII cells cultured on provisional matrices (fibrin-fibronectin) undergo EMT via αvβ6 integrin-dependent activation of endogenous TGFβ, while cells cultured on laminin/collagen mixtures do not

activate TGFβ. (6) This response is integrin-dependent, such that integrins are required not only in the binding to matrix proteins, but also for activation of TGFβ, therefore ATII integrin binding/signaling plays a pivotal role in modulating EMT, though this has not been thoroughly investigated.

ATII cell integrins: expression and functions:

ATII cells have been shown to express a wide range of integrins. At least 7 integrin pairs are expressed in healthy adult ATII cells including α2β1, α3β1, α6β4, α9β1, αvβ5, αvβ6, and αvβ8. Though not present in healthy airway epithelium, α5β1 integrin expression is rapidly induced in response to injury, and is therefore important for wound healing responses. (41) These integrins are known to have various roles in epithelial homeostasis, repair, and possibly pathologic responses, including maintaining epithelial integrity (α6β4 and α3β1 (41)), regulating wound-repair processes, (27) and activation of TGFβ (αvβ6 and αvβ8 (42, 43)).

Recent studies have illustrated the importance of α3β1 integrin in maintaining epithelial integrity. The classical ligand for α3β1 is laminin (41, 44) but is also known to bind collagen and fibronectin. (45-47) Integrin α3 is important in alveolar epithelial monolayer formation. (48) ATII α3 mRNA has been shown to decrease in response to TGFβ, (49) implying a role for α3β1 in regulating EMT in the lung. Downregulation of α3 integrin has been noted in response to EMT driven by the transcription factor Slug. (49, 50). In addition, a decrease in expression of α3β1 integrin is commonly seen in cancer related EMT and is associated with a more malignant phenotype and poor patient prognosis. (51) Antibody inhibition experiments with airway epithelial cells shows a

significant decrease in wound-repair in the presence of either anti-β1, anti-α3, anti-α5, or anti-fibronectin antibodies, suggesting that α3 may also play a role in the wound repair process. (27) α3β1 null keratinocytes display higher concentrations of actin-associated proteins such as vinculin, tailin, and α-actin at focal contact sites compared to wild type cells, indicating that this integrin is important in the regulation of focal adhesion and stress fiber formation. (52) α3β1 causes a suppression of cytokine responses by epithelial cells indicating an important role for this integrin during inflammation or wound healing. (53) Interestingly, it has also been suggested that α3β1 may act as a transdominant inhibitor of other integrins; α3-null keratinocytes show an increase in Fn and CollIV receptors. (52) This transdominant effect of α3 has also been shown to play a pivotal role in anti-tumorigenic activities. (54) This data suggests a potential role for α3 integrin in the prevention/inhibition of EMT through the regulation of other integrins associated with pathological states (such as αV). Taken together, this evidence suggests a role for α3β1 signaling in preventing alveolar EMT by maintenance of monolayer formation, inhibition of focal adhesion and stress fiber formation, suppression of cytokine responses, and transdominant inhibition of other integrins.

The provisional matrix protein Fn has the capacity to bind many of the integrins expressed by ATII cells, including αvβ3, αvβ6, α3β1, and α5β1 (during injury). (27, 45, 47, 55) Integrin α3β1 binding to Fn has been shown to occur in an RGD dependent fashion, but interestingly, α3β1 binding to Ln and Col is not through RGD sites. (45) Integrin α3β1 binding to Fn can be affected by the presence of α5β1 integrin such that α3β1 binding is low in cells expressing α3β1 and α5β1 at comparable levels, but α3β1

binding to Fn is greatly enhanced in H69 cells that highly express α3β1 compared to other integrins. Because ATII cells only express α5β1 integrin in response to injury, (27) it is likely that integrin α3β1 binds Fn with great affinity in this cell type under normal conditions. Though α5β1 appears to be the main Fn receptor during alveolar wound repair, integrin blocking experiments with airway epithelial cells showed that in addition to α5, β1, and Fn blocking antibodies that α3 blocking antibodies also resulted in a significant decrease in wound repair. (27) This suggests that initial binding of α3β1 to Fn may modulate wound repair. The competing effects of ATII cell engagement of various integrins likely plays a significant role in the determination of cell phenotype leading to normal alveolar repair or pathological EMT events. This dissertation specifically addresses the role of Fn in the progression of ATII cell EMT versus maintenance of epithelial phenotype. A central hypothesis of this dissertation was that mechanical forces activate integrin "switches", based on domain unfolding, within Fn that regulate integrin specificity and thus activation of different cell signaling cascades.

Fibronectin

Although Fn has a wide variety of functions, it is the capacity to bind multiple integrins and initiate specific intracellular signals that give this protein such importance in directing cell and tissue state. Biochemically, Fn is a soluble dimeric glycoprotein composed of two nearly identical 230-270 kDa monomers linked covalently near their C-termini by a pair of disulfide bonds. (reviewed by (47, 56)) Each monomeric subunit consists of three types of repeating modules, type I, II and III. These modules comprise functional domains that mediate interactions with other ECM components, cell surface receptors, and Fn itself. (47) Whereas type I and II repeats are structurally stabilized with

two intrachain disulfide bonds in each repeat, type III repeats have no disulfide bonds and therefore are highly sensitive to force-mediated unfolding. Fn is encoded by a single gene yet as many as 20 variants of human Fn are produced each having slight differences in the composition and number of type I, II, and III repeats. All isoforms are capable of being incorporated into a fibrillar polymer.

As mentioned, Fn's role in directing cell and tissue homeostasis and repair is through the binding and activation of the cell surface ECM receptors known as integrins. The most studied integrin recognition sequence, RGD (Arg-Gly-Asp), is located on the 10th type III repeat. The recognition of this simple tripeptide sequence can be quite complex and greatly depends on flanking residues, its three dimensional presentation, and individual features of the integrin-binding pockets. For example, RGD in concert with a second recognition sequence (PHSRN), the so-called "synergy" site, in the adjacent 9th type III repeat is known to promote the specific interaction of $\alpha 5\beta 1$ integrin binding to Fn through interactions with the $\alpha 5$ subunit. (57, 58) Importantly, the spatial orientation, and thus synergistic activity, of the RGD and synergy cell adhesion peptides is highly sensitive to mechanical forces generated by resident cells.

Force-mediated unfolding of Fn:

Fn is extremely sensitive to mechanical forces, a fact that is exemplified by its own polymerization into fibrillar form. (59, 60) Soluble Fn is compact and has very few sites for interaction with other proteins. Thus Fn must undergo significant conformation changes to allow self-binding to cryptic sites near the N-terminus during polymerization and to engage cellular integrins via the central cell-binding domain (7^{th}-10^{th} type-III repeats). These conformation changes are naturally driven by the input of cellular energy

in the form of cell contractile forces. The type-III repeats that comprise the cell-binding domain within Fn are particularly sensitive to mechanical forces since these individual domains are stabilized only by van der Waals forces and hydrogen bonding between amino acid side-chains of opposing beta sheets. While it has long been observed that the alveolar wall experiences levels of approximately 25% cyclic strain due to inhalation, (61) it is improbable that this level of strain significantly contributes to the tension observed in native Fn ECMs within the lung. Recent studies on cell-mediated Fn molecular unfolding provide evidence to this fact. Specifically, loss of in vitro cellular contraction through inhibition of actin polymerization results in significant relaxation of Fn into a more compact conformation (62) while inhibition of cell contractility in excised (*ex vivo*) frog embryo tissue results in a completely collapsed Fn conformation. (63) Furthermore, extraction of cells from fibroblast-derived Fn ECMs and quantification of the Fn molecular collapse indicates that cells strain Fn fibers (and unfold type-III repeats) between 200 and 700%; (64) values greater than an order of magnitude more than could be accounted for by inhalation-mediated strain. Strain associated with inhalation clearly has significant effects on epithelial cell behavior, however these recent studies emphasize that tension in the underlying ECM resulting in Fn molecular unfolding originates from resident mesenchymal cells (e.g. pulmonary interstitial fibroblasts) rather than bulk organ-level mechanics.

Fn conformational changes direct changes in integrin specificity:

The best-defined model of Fn unfolding at the secondary level having a significant impact on integrin engagement and subsequent cell fate is domain unfolding of the RGD-containing 10^{th} type III repeat. Due to the elasticity of type III repeats, the 9th and 10th

type III repeats together present multiple conformations that direct integrin specificity to this region. The synergy site, located on the 9th type III repeat is located approximately 32Å from the RGD-loop on the 10th type III repeat in solution. In this conformation the two motifs act synergistically to bind $\alpha5\beta1$ integrin. (43) Under small forces (<100 pN) the 10^{th} type-III repeat, prior to complete unfolding, assumes an intermediate state characterized by the RGD loop translocating away from the 9^{th} type-III repeat. In this state, the synergy–RGD distance is increased from 32Å to approximately 55Å, a distance too large for both sites to co-bind the same receptor. This is further evidenced by experiments that demonstrate increasing the length of the linker chain between the two repeats by insertion mutation reduces $\alpha5\beta1$ binding. (65) These data suggest that $\alpha5\beta1$ binding attributed to the synergy site can be turned off mechanically by stretching these domains into this intermediate state or beyond. The effect of force-mediated unfolding of Fn on integrin engagement and activity levels may be further explained by studies showing the degrees of conformational stability of the 9^{th} (or 10^{th}) type III repeat, can modulate integrin accessibility of the RGD motif. A stabilization of the 9^{th} repeat via a Leu to Pro point mutation at amino acid 1408 (66) or stabilization of the hydrogen bonding within the 10^{th} type-III repeat (67) increases affinity for $\alpha5\beta1$ over $\alpha V\beta3$.

Importantly, the exact composition of Fn isoforms, with respect to its type-III repeats, will play a significant role in determining the overall stability of the molecule since the stability of type-III repeats are critically dependent on neighboring type-III repeats. (68) This fact has particular relevance to pulmonary fibrosis. Fn-EDA, which has been consistently linked to fibrosis and is expressed at high levels in pulmonary fibrosis, (69) contains an extra type-III repeat, the EDA domain (inserted following the

11^{th} type-III repeat) which is extraordinarily unstable. The NMR spectra of the EDA domain demonstrates that it is mostly in an unfolded state at 37°C and can be completely unfolded upon the removal of four amino acids at its N-terminus. (70) This data suggest the EDA type-III repeat is a "hyper" mechano-sensitive type-III repeat of Fn that is predicted to cause local conformational alterations through the potential destabilization of the remaining type-III repeats. This example is particularly interesting, since the presence of EDA could result in destabilization of the 9^{th} and 10^{th} type-III repeats resulting in preferential engagement of certain integrins over others.

Integrin specificity is clearly linked to cell fate determination and differentiation and proliferation processes. For example, the β1 integrin subunit enhances the progression of differentiation of precursor cells, (71, 72) while αv integrins, like αvβ3, correlate with increased cell adhesion, (73) enhanced cell proliferation, and decreased differentiation. (74) Fn has been shown to cause a switch between stimulation of proliferation and differentiation of mouse C2C12 myoblasts to myotubes (75) and MC3T3-E1 osteoblast-like cells (72) by a yet to be identified structural change that results in an increase of the α5β1-to-αvβ3 binding ratio.

From these published studies it is clear that the application of mechanical forces to Fn ECM, resulting in conformation changes, likely has a significant impact on the integrin specificity with which cells engage Fn, and in turn modulate cell behavior through intracellular signaling events. The first aim of this project applies these fundamental principles of Fn dynamics to the process of integrin engagement and epithelial cell fate during pulmonary remodeling and progression of fibrosis by determining the effects of altering the stretched state of Fn ECM on ATII cell integrin

engagement and phenotypic alteration. The second aim of this project further characterizes the dependence of epithelial cell integrin interactions with a dynamic Fn molecule by investigating the role of the Fn synergy site in integrin α3β1 binding.

TGFβ Activation and Signaling

Cell-mediated mechanical forces play an integral role in Fn unfolding and conformation changes that alter integrin specificity. Recent studies have shown that cell contractility and regulation of integrin expression also play a critical role in TGFβ-1 activation, which, as previously mentioned, is a critical mediator of EMT. TGFβ regulates a wide-array of cellular processes associated with normal homeostasis and repair, including proliferation, differentiation, motility, apoptosis, and tumor suppression. (76, 77) Because TGFβ is a potent inducer of EMT and many other cellular events, its presentation must be tightly controlled. TGFβ exists in an inactive form, and must be activated in order to bind to its receptor. In its inactive form, TGFβ forms a complex with the latency-associated peptide (LAP), and this non-covalent association is termed the small latent complex. This small latent complex can go on to form a large latent complex by binding the latent TGFβ binding protein, which allows for immobilization of the inactive TGFβ the ECM. (78-80) The latent complex of TGFβ can be activated in the lung through two distinct mechanosensitive events. First, activation can occur through binding of the latency-associated protein complex to integrins αvβ6 or αvβ8 via RGD sequences. (42, 81, 82) Application of cell contractile forces to the integrin-LAP complex results in a prying of the LAP complex away from TGFβ and either releasing the active growth factor in a soluble form (when bound through αvβ8 integrin) or exposing it temporally to neighboring cells (when bound through αvβ6 integrin). (83)

Second, activation has been proposed to occur through a similar releasing process of TGFβ bound within the ECM via the large latent complex. (84) Both processes of TGFβ activation are directly related to integrin expression and cell contractility. As mentioned before, engagement of α3β1 integrin has been shown to regulate the expression and engagement of other integrins (such as αv) and regulate cell contractility. Recent reports have linked α3β1 integrin to TGFβ-induced alveolar EMT. In response to active TGFβ, alveolar epithelial cells have been shown to form complexes of E-cadherin, TGFβ receptors, and α3β1 integrins which then go on to generate phospho-Smad2(p-Smad2)-pY654-β-catenin complexes. These p-Smad2-pY654-β-catenin complexes then translocate to the nucleus and through some unknown mechanism upregulate EMT-related mesenchymal genes. Presumably if α3β1 is otherwise engaged, such as in binding to an extracellular matrix ligand or in complexes with E-cadherin in adheren junctions, then it cannot form complexes with E-cadherin and TGFβ receptors, therefore preventing EMT. (85) Preferential binding of α3β1 to "unstrained", and, therefore, more compact, Fn could then potentially regulate activation of TGFβ through these or other unknown mechanisms. The first two aims of this project investigate whether force-mediated unfolding of Fn domains modulates ATII cell α3 integrin engagement and the downstream consequences of α3β1-Fn engagement relative to TGFβ activation, signaling, and subsequent EMT.

Mechanotransduction: Cells and Stiffness

The composition of the extracellular matrix surrounding a cell has great consequences on cell fate; however, evidence is mounting that, in addition, cells sense and respond to the

mechanical properties of the ECM, particularly the stiffness of the matrix. The process of cellular sensing of the underlying properties of the ECM has been termed mechanotransduction. Matrix stiffness has been shown to influence many aspects of cellular behavior including stem cell, myoblast, and breast epithelial cell differentiation; cellular motility; contractility; and focal adhesion formation, and it has also been shown to contribute or prevent a malignant phenotype. (86-94) Reports by Engler *et al.* showed that stem cell differentiation can be guided by underlying matrix mechanics, with mesenchymal stem cells on hard substrates differentiating down an osteoblastic lineage and mesenchymal stem cells on soft substrates differentiating down a neuronal lineage, which suggests a potential mechanism through which stem cells "match" their differentiation based on the surrounding tissue. Interestingly, as previously described, changes in tissue stiffness, specifically an increase in stiffness and hardening of tissue, is associated with the pathological progression of fibrotic responses. Recent AFM analysis of fibrotic tissue from mice with bleomycin-induced pulmonary fibrosis shows a nine-fold increase in stiffness of fibrotic tissue compared to that of normal tissue. (95) In addition, increases in tissue elasticity in pathological conditions of tumor formation and muscular dystrophy have been reported to be increases approximately nine-fold and 1.5-fold, respectively. (86, 88)

Interestingly, it has recently been shown that mesenchymal cells respond to substrate stiffness by engaging their actinomyosin contractile machinery in a manner that facilitates cell-ECM compliance matching. This has been demonstrated by AFM analysis of single cell stiffness, showing fibroblasts become increasingly stiff on increasingly rigid substrates, indicating a cell may adjust its internal stress through

contraction to "match" its external environment. (94) As a consequence of this mechano-homeostasis between the cell and its ECM, cells in increasingly rigid, or stiff, environments display increased activation of contractile signals like Rho and Rho associated kinase (ROCK), resulting in multiple and diverse secondary effects. An elegant example of this is shown by Wipff *et. al.* who demonstrated that fibroblast activation of TGFβ increases on increasingly rigid substrates, leading to greater myofibroblast differentiation on stiff, but not compliant, substrates. (96) Because fibrotic diseases are characterized by increased tissue stiffness, and because of TGFβ's prominent role in the onset of EMT, it was hypothesized that a similar mechanism of increased TGFβ activation with increasing stiffness would contribute to EMT on increasingly rigid substrates.

While many studies have shown the important role of mechanical properties in influencing cell phenotype, little is known about how a cell actually senses mechanical properties. Because of their role in ECM ligand interactions, it is hypothesized that integrins play a critical role in mechanotransduction, (97-99) but how integrins interact with specific extracellular ligands to determine transduction of matrix mechanical properties is not well understood. Integrin binding to an ECM ligand can result in physical linkage between integrin and the cytoskeleton, allowing force transmission through the attachment site and reinforcement of the protein complex. (93, 100) Force application to the focal adhesion complex leads to recruitment and activation of signaling proteins like FAK, Src, and Shc whose major downstream targets are Rho GTPases. Importantly, activation of the Rho signaling cascade leads to cytoskeletal rearrangement and increased cell contractility, having numerous influences on cell phenotype, and

implications in EMT, by potentially increasing TGFβ activation. (101, 102) In addition, differential integrin binding to Fn can lead to differences in adhesion dynamics and adhesion reinforcement. (103, 104) Recent reports by Rosa-Cusachs *et al*. reported dynamic stiffening of the attachment site when physiological forces were applied via mainly αvβ3, whereas binding and clustering of α5β1 resulted in enhanced adhesion strength, indicating αvβ3 integrins may play a key role mechanotransduction.

While the precise mechanism of cell stiffness sensing remains unknown, it likely involves the binding of specific integrins that result in transduction of stiffness-mediated signaling via increased cell contractility. This dissertation explores the role of two mechano-transduction events in the onset and progression of EMT: 1) the role of Fn conformation changes, such as those that arise from molecular unfolding, in integrin specific binding and downstream EMT and 2) the role of substrate stiffness in Fn-mediated EMT. These studies provide insights into the role of mechanotransduction in the onset and progression of fibrotic pathologies.

References

1. Maher TM, Wells AU, Laurent GJ. Idiopathic pulmonary fibrosis: multiple causes and multiple mechanisms? Eur Respir J.30:835-9. 2007.

2. Meltzer EB, Noble PW. Idiopathic pulmonary fibrosis. Orphanet J Rare Dis.3:8. 2008.

3. Spruit MA, Janssen DJ, Franssen FM, Wouters EF. Rehabilitation and palliative care in lung fibrosis. Respirology.14:781-7. 2009.

4. Willis BC, Liebler JM, Luby-Phelps K, Nicholson AG, Crandall ED, du Bois RM, et al. Induction of epithelial-mesenchymal transition in alveolar epithelial cells by transforming growth factor-beta1: potential role in idiopathic pulmonary fibrosis. Am J Pathol.166:1321-32. 2005.

5. Kasai H, Allen JT, Mason RM, Kamimura T, Zhang Z. TGF-beta1 induces human alveolar epithelial to mesenchymal cell transition (EMT). Respir Res.6:56. 2005.

6. Kim KK, Kugler MC, Wolters PJ, Robillard L, Galvez MG, Brumwell AN, et al. Alveolar epithelial cell mesenchymal transition develops in vivo during pulmonary fibrosis and is regulated by the extracellular matrix. Proc Natl Acad Sci U S A.103:13180-5. 2006.

7. Xu J, Lamouille S, Derynck R. TGF-beta-induced epithelial to mesenchymal transition. Cell Res.19:156-72. 2009.

8. Wynn TA. Cellular and molecular mechanisms of fibrosis. J Pathol.214:199-210. 2008.

9. Degryse AL, Tanjore H, Xu XC, Polosukhin VV, Jones BR, Boomershine CS, et al. TGF{beta} SIGNALING IN LUNG EPITHELIUM REGULATES BLEOMYCIN INDUCED ALVEOLAR INJURY AND FIBROBLAST RECRUITMENT. American journal of physiology.

10. Iwano M, Plieth D, Danoff TM, Xue C, Okada H, Neilson EG. Evidence that fibroblasts derive from epithelium during tissue fibrosis. J Clin Invest.110:341-50. 2002.

11. Duband JL, Thiery JP. Appearance and distribution of fibronectin during chick embryo gastrulation and neurulation. Dev Biol.94:337-50. 1982.

12. Vicovac L, Aplin JD. Epithelial-mesenchymal transition during trophoblast differentiation. Acta Anat (Basel).156:202-16. 1996.

13. Hay ED. An overview of epithelio-mesenchymal transformation. Acta Anat (Basel).154:8-20. 1995.

14. Thiery JP, Acloque H, Huang RY, Nieto MA. Epithelial-mesenchymal transitions in development and disease. Cell.139:871-90. 2009.

15. Camara J, Jarai G. Epithelial-mesenchymal transition in primary human bronchial epithelial cells is Smad-dependent and enhanced by fibronectin and TNF-alpha. Fibrogenesis Tissue Repair.3:2.

16. Arnoux V, Nassour M, L'Helgoualc'h A, Hipskind RA, Savagner P. Erk5 controls Slug expression and keratinocyte activation during wound healing. Molecular biology of the cell.19:4738-49. 2008.

17. Felton VM, Borok Z, Willis BC. N-acetylcysteine inhibits alveolar epithelial-mesenchymal transition. American journal of physiology.297:L805-12. 2009.

18. Willis BC, Borok Z. TGF-beta-induced EMT: mechanisms and implications for fibrotic lung disease. American journal of physiology.293:L525-34. 2007.

19. Gharaee-Kermani M, Hu B, Phan SH, Gyetko MR. Recent advances in molecular targets and treatment of idiopathic pulmonary fibrosis: focus on TGFbeta signaling and the myofibroblast. Curr Med Chem.16:1400-17. 2009.

20. Shi Y, Massague J. Mechanisms of TGF-beta signaling from cell membrane to the nucleus. Cell.113:685-700. 2003.

21. Derynck R, Zhang YE. Smad-dependent and Smad-independent pathways in TGF-beta family signalling. Nature.425:577-84. 2003.

22. Rahimi RA, Leof EB. TGF-beta signaling: a tale of two responses. J Cell Biochem.102:593-608. 2007.

23. Boutet A, De Frutos CA, Maxwell PH, Mayol MJ, Romero J, Nieto MA. Snail activation disrupts tissue homeostasis and induces fibrosis in the adult kidney. EMBO J.25:5603-13. 2006.

24. Guaita S, Puig I, Franci C, Garrido M, Dominguez D, Batlle E, et al. Snail induction of epithelial to mesenchymal transition in tumor cells is accompanied by MUC1 repression and ZEB1 expression. The Journal of biological chemistry.277:39209-16. 2002.

25. Batlle E, Sancho E, Franci C, Dominguez D, Monfar M, Baulida J, et al. The transcription factor snail is a repressor of E-cadherin gene expression in epithelial tumour cells. Nat Cell Biol.2:84-9. 2000.

26. Magnusson MK, Mosher DF. Fibronectin: structure, assembly, and cardiovascular implications. Arterioscler Thromb Vasc Biol.18:1363-70. 1998.

27. Herard AL, Pierrot D, Hinnrasky J, Kaplan H, Sheppard D, Puchelle E, et al. Fibronectin and its alpha 5 beta 1-integrin receptor are involved in the wound-repair process of airway epithelium. The American journal of physiology.271:L726-33. 1996.
28. Sottile J, Hocking DC. Fibronectin polymerization regulates the composition and stability of extracellular matrix fibrils and cell-matrix adhesions. Mol Biol Cell.13:3546-59. 2002.

29. Matthay MA, Robriquet L, Fang X. Alveolar epithelium: role in lung fluid balance and acute lung injury. Proc Am Thorac Soc.2:206-13. 2005.

30. Mason RJ. Biology of alveolar type II cells. Respirology.11 Suppl:S12-5. 2006.

31. Fehrenbach H. Alveolar epithelial type II cell: defender of the alveolus revisited. Respir Res.2:33-46. 2001.

32. Jain L, Chen XJ, Ramosevac S, Brown LA, Eaton DC. Expression of highly selective sodium channels in alveolar type II cells is determined by culture conditions. Am J Physiol Lung Cell Mol Physiol.280:L646-58. 2001.

33. Selman M, Pardo A. Role of epithelial cells in idiopathic pulmonary fibrosis: from innocent targets to serial killers. Proc Am Thorac Soc.3:364-72. 2006.

34. Thannickal VJ, Horowitz JC. Evolving concepts of apoptosis in idiopathic pulmonary fibrosis. Proc Am Thorac Soc.3:350-6. 2006.

35. Konigshoff M, Kramer M, Balsara N, Wilhelm J, Amarie OV, Jahn A, et al. WNT1-inducible signaling protein-1 mediates pulmonary fibrosis in mice and is upregulated in humans with idiopathic pulmonary fibrosis. J Clin Invest.119:772-87. 2009.

36. Kuwano K, Kunitake R, Kawasaki M, Nomoto Y, Hagimoto N, Nakanishi Y, et al. P21Waf1/Cip1/Sdi1 and p53 expression in association with DNA strand breaks in idiopathic pulmonary fibrosis. American journal of respiratory and critical care medicine.154:477-83. 1996.

37. Uhal BD, Joshi I, Hughes WF, Ramos C, Pardo A, Selman M. Alveolar epithelial cell death adjacent to underlying myofibroblasts in advanced fibrotic human lung. The American journal of physiology.275:L1192-9. 1998.

38. Wu Z, Yang L, Cai L, Zhang M, Cheng X, Yang X, et al. Detection of epithelial to mesenchymal transition in airways of a bleomycin induced pulmonary fibrosis model derived from an alpha-smooth muscle actin-Cre transgenic mouse. Respir Res.8:1. 2007.

39. Willis BC, duBois RM, Borok Z. Epithelial origin of myofibroblasts during fibrosis in the lung. Proc Am Thorac Soc.3:377-82. 2006.

40. Yao HW, Xie QM, Chen JQ, Deng YM, Tang HF. TGF-beta1 induces alveolar epithelial to mesenchymal transition in vitro. Life Sci.76:29-37. 2004.

41. Sheppard D. Functions of pulmonary epithelial integrins: from development to disease. Physiol Rev.83:673-86. 2003.

42. Munger JS, Huang X, Kawakatsu H, Griffiths MJ, Dalton SL, Wu J, et al. The integrin alpha v beta 6 binds and activates latent TGF beta 1: a mechanism for regulating pulmonary inflammation and fibrosis. Cell.96:319-28. 1999.

43. Krammer A, Craig D, Thomas WE, Schulten K, Vogel V. A structural model for force regulated integrin binding to fibronectin's RGD-synergy site. Matrix Biol.21:139-47. 2002.

44. Eble JA, Wucherpfennig KW, Gauthier L, Dersch P, Krukonis E, Isberg RR, et al. Recombinant soluble human alpha 3 beta 1 integrin: purification, processing, regulation, and specific binding to laminin-5 and invasin in a mutually exclusive manner. Biochemistry.37:10945-55. 1998.

45. Elices MJ, Urry LA, Hemler ME. Receptor functions for the integrin VLA-3: fibronectin, collagen, and laminin binding are differentially influenced by Arg-Gly-Asp peptide and by divalent cations. The Journal of cell biology.112:169-81. 1991.

46. Kaufmann R, Frosch D, Westphal C, Weber L, Klein CE. Integrin VLA-3: ultrastructural localization at cell-cell contact sites of human cell cultures. The Journal of cell biology.109:1807-15. 1989.

47. Pankov R YK. Fibronectin at a glance. J Cell Sci.115:3861-3. 2002.

48. Lubman RL, Zhang XL, Zheng J, Ocampo L, Lopez MZ, Veeraraghavan S, et al. Integrin alpha(3)-subunit expression modulates alveolar epithelial cell monolayer formation. Am J Physiol Lung Cell Mol Physiol.279:L183-93. 2000.

49. Kumar NM, Sigurdson SL, Sheppard D, Lwebuga-Mukasa JS. Differential modulation of integrin receptors and extracellular matrix laminin by transforming growth factor-beta 1 in rat alveolar epithelial cells. Exp Cell Res.221:385-94. 1995.

50. Turner FE, Broad S, Khanim FL, Jeanes A, Talma S, Hughes S, et al. Slug regulates integrin expression and cell proliferation in human epidermal keratinocytes. The Journal of biological chemistry.281:21321-31. 2006.

51. Adachi M, Taki T, Huang C, Higashiyama M, Doi O, Tsuji T, et al. Reduced integrin alpha3 expression as a factor of poor prognosis of patients with adenocarcinoma of the lung. J Clin Oncol.16:1060-7. 1998.

52. Hodivala-Dilke KM, DiPersio CM, Kreidberg JA, Hynes RO. Novel roles for alpha3beta1 integrin as a regulator of cytoskeletal assembly and as a trans-dominant

inhibitor of integrin receptor function in mouse keratinocytes. The Journal of cell biology.142:1357-69. 1998.

53. Lubin FD, Segal M, McGee DW. Regulation of epithelial cell cytokine responses by the alpha3beta1 integrin. Immunology.108:204-10. 2003.
54. Borza CM, Pozzi A, Borza DB, Pedchenko V, Hellmark T, Hudson BG, et al. Integrin alpha3beta1, a novel receptor for alpha3(IV) noncollagenous domain and a trans-dominant Inhibitor for integrin alphavbeta3. The Journal of biological chemistry.281:20932-9. 2006.

55. Humphries J, Byron, A, Humphries, M. Integrin ligands at a glance. J Cell Sci.119:3901-3. 2006.

56. Mao Y, Schwarzbauer JE. Fibronectin fibrillogenesis, a cell-mediated matrix assembly process. Matrix Biol.24:389-99. 2005.

57. Mardon HJ, Grant KE. The role of the ninth and tenth type III domains of human fibronectin in cell adhesion. FEBS Lett.340:197-201. 1994.

58. Mould AP, Askari JA, Aota S, Yamada KM, Irie A, Takada Y, et al. Defining the topology of integrin alpha5beta1-fibronectin interactions using inhibitory anti-alpha5 and anti-beta1 monoclonal antibodies. Evidence that the synergy sequence of fibronectin is recognized by the amino-terminal repeats of the alpha5 subunit. The Journal of biological chemistry.272:17283-92. 1997.

59. Barker TH, Baneyx G, Cardo-Vila M, Workman GA, Weaver M, Menon PM, et al. SPARC regulates extracellular matrix organization through its modulation of integrin-linked kinase activity. The Journal of biological chemistry.280:36483-93. 2005.

60. Barker TH, Grenett HE, MacEwen MW, Tilden SG, Fuller GM, Settleman J, et al. Thy-1 regulates fibroblast focal adhesions, cytoskeletal organization and migration through modulation of p190 RhoGAP and Rho GTPase activity. Exp Cell Res.295:488-96. 2004.

61. Tschumperlin DJ, Margulies SS. Alveolar epithelial surface area-volume relationship in isolated rat lungs. J Appl Physiol.86:2026-33. 1999.

62. Baneyx G, Baugh L, Vogel V. Fibronectin extension and unfolding within cell matrix fibrils controlled by cytoskeletal tension. Proc Natl Acad Sci U S A.99:5139-43. 2002.

63. Davidson LA, Dzamba BD, Keller R, Desimone DW. Live imaging of cell protrusive activity, and extracellular matrix assembly and remodeling during morphogenesis in the frog, Xenopus laevis. Dev Dyn.237:2684-92. 2008.

64. Higashiyama H, Yoshimoto D, Okamoto Y, Kikkawa H, Asano S, Kinoshita M. Receptor-activated Smad localisation in bleomycin-induced pulmonary fibrosis. Journal of clinical pathology.60:283-9. 2007.

65. Grant RP, Spitzfaden C, Altroff H, Campbell ID, Mardon HJ. Structural requirements for biological activity of the ninth and tenth FIII domains of human fibronectin. The Journal of biological chemistry.272:6159-66. 1997.

66. Altroff H, Schlinkert R, van der Walle CF, Bernini A, Campbell ID, Werner JM, et al. Interdomain tilt angle determines integrin-dependent function of the ninth and tenth FIII domains of human fibronectin. The Journal of biological chemistry.279:55995-6003. 2004.

67. Ng SP, Billings KS, Ohashi T, Allen MD, Best RB, Randles LG, et al. Designing an extracellular matrix protein with enhanced mechanical stability. Proc Natl Acad Sci U S A.104:9633-7. 2007.

68. Zhu C, Bao G, Wang N. Cell mechanics: mechanical response, cell adhesion, and molecular deformation. Annu Rev Biomed Eng.2:189-226. 2000.

69. Muro AF, Moretti FA, Moore BB, Yan M, Atrasz RG, Wilke CA, et al. An essential role for fibronectin extra type III domain A in pulmonary fibrosis. American journal of respiratory and critical care medicine.177:638-45. 2008.

70. Niimi T, Osawa M, Yamaji N, Yasunaga K, Sakashita H, Mase T, et al. NMR structure of human fibronectin EDA. J Biomol NMR.21:281-4. 2001.

71. Gronthos S, Simmons PJ, Graves SE, Robey PG. Integrin-mediated interactions between human bone marrow stromal precursor cells and the extracellular matrix. Bone.28:174-81. 2001.

72. Stephansson SN, Byers BA, Garcia AJ. Enhanced expression of the osteoblastic phenotype on substrates that modulate fibronectin conformation and integrin receptor binding. Biomaterials.23:2527-34. 2002.

73. Koistinen P, Pulli T, Uitto VJ, Nissinen L, Hyypia T, Heino J. Depletion of alphaV integrins from osteosarcoma cells by intracellular antibody expression induces bone differentiation marker genes and suppresses gelatinase (MMP-2) synthesis. Matrix Biol.18:239-51. 1999.

74. Cheng SL, Lai CF, Blystone SD, Avioli LV. Bone mineralization and osteoblast differentiation are negatively modulated by integrin alpha(v)beta3. J Bone Miner Res.16:277-88. 2001.

75. Garcia AJ, Vega MD, Boettiger D. Modulation of cell proliferation and differentiation through substrate-dependent changes in fibronectin conformation. Mol Biol Cell.10:785-98. 1999.

76. Taipale J, Saharinen J, Keski-Oja J. Extracellular matrix-associated transforming growth factor-beta: role in cancer cell growth and invasion. Adv Cancer Res.75:87-134. 1998.

77. Yue J, Mulder KM. Transforming growth factor-beta signal transduction in epithelial cells. Pharmacol Ther.91:1-34. 2001.

78. Chen Q, Sivakumar P, Barley C, Peters DM, Gomes RR, Farach-Carson MC, et al. Potential role for heparan sulfate proteoglycans in regulation of transforming growth factor-beta (TGF-beta) by modulating assembly of latent TGF-beta-binding protein-1. The Journal of biological chemistry.282:26418-30. 2007.

79. Worthington JJ, Klementowicz JE, Travis MA. TGFbeta: a sleeping giant awoken by integrins. Trends Biochem Sci.36:47-54.

80. Kantola AK, Keski-Oja J, Koli K. Fibronectin and heparin binding domains of latent TGF-beta binding protein (LTBP)-4 mediate matrix targeting and cell adhesion. Experimental cell research.314:2488-500. 2008.

81. Mu D, Cambier S, Fjellbirkeland L, Baron JL, Munger JS, Kawakatsu H, et al. The integrin alpha(v)beta8 mediates epithelial homeostasis through MT1-MMP-dependent activation of TGF-beta1. The Journal of cell biology.157:493-507. 2002.

82. Jenkins RG, Su X, Su G, Scotton CJ, Camerer E, Laurent GJ, et al. Ligation of protease-activated receptor 1 enhances alpha(v)beta6 integrin-dependent TGF-beta activation and promotes acute lung injury. J Clin Invest.116:1606-14. 2006.

83. Wipff PJ, Hinz B. Integrins and the activation of latent transforming growth factor beta1 - an intimate relationship. Eur J Cell Biol.87:601-15. 2008.

84. Wells RG, Discher DE. Matrix elasticity, cytoskeletal tension, and TGF-beta: the insoluble and soluble meet. Sci Signal.1:pe13. 2008.

85. Kim Y, Kugler MC, Wei Y, Kim KK, Li X, Brumwell AN, et al. Integrin alpha3beta1-dependent beta-catenin phosphorylation links epithelial Smad signaling to cell contacts. The Journal of cell biology.184:309-22. 2009.

86. Engler AJ, Griffin MA, Sen S, Bonnemann CG, Sweeney HL, Discher DE. Myotubes differentiate optimally on substrates with tissue-like stiffness: pathological implications for soft or stiff microenvironments. The Journal of cell biology.166:877-87. 2004.

87. Engler AJ, Sen S, Sweeney HL, Discher DE. Matrix elasticity directs stem cell lineage specification. Cell.126:677-89. 2006.

88. Paszek MJ, Zahir N, Johnson KR, Lakins JN, Rozenberg GI, Gefen A, et al. Tensional homeostasis and the malignant phenotype. Cancer Cell.8:241-54. 2005.

89. Wozniak MA, Desai R, Solski PA, Der CJ, Keely PJ. ROCK-generated contractility regulates breast epithelial cell differentiation in response to the physical properties of a three-dimensional collagen matrix. J Cell Biol.163:583-95. 2003.

90. Pelham RJ, Jr., Wang Y. Cell locomotion and focal adhesions are regulated by substrate flexibility. Proc Natl Acad Sci U S A.94:13661-5. 1997.

91. Pelham RJ, Jr., Wang YL. Cell locomotion and focal adhesions are regulated by the mechanical properties of the substrate. Biol Bull.194:348-9; discussion 9-50. 1998.

92. Vogel V, Sheetz M. Local force and geometry sensing regulate cell functions. Nat Rev Mol Cell Biol.7:265-75. 2006.

93. Choquet D, Felsenfeld DP, Sheetz MP. Extracellular matrix rigidity causes strengthening of integrin-cytoskeleton linkages. Cell.88:39-48. 1997.

94. Georges PC, Janmey PA. Cell type-specific response to growth on soft materials. J Appl Physiol.98:1547-53. 2005.

95. Liu F, Mih JD, Shea BS, Kho AT, Sharif AS, Tager AM, et al. Feedback amplification of fibrosis through matrix stiffening and COX-2 suppression. The Journal of cell biology.190:693-706.

96. Wipff PJ, Rifkin DB, Meister JJ, Hinz B. Myofibroblast contraction activates latent TGF-beta1 from the extracellular matrix. J Cell Biol.179:1311-23. 2007.

97. Bershadsky AD, Balaban NQ, Geiger B. Adhesion-dependent cell mechanosensitivity. Annu Rev Cell Dev Biol.19:677-95. 2003.

98. Schwartz MA. Integrins and extracellular matrix in mechanotransduction. Cold Spring Harb Perspect Biol.2:a005066.

99. Li J, Zhao Z, Wang J, Chen G, Yang J, Luo S. The role of extracellular matrix, integrins, and cytoskeleton in mechanotransduction of centrifugal loading. Mol Cell Biochem.309:41-8. 2008.

100. Grashoff C, Hoffman BD, Brenner MD, Zhou R, Parsons M, Yang MT, et al. Measuring mechanical tension across vinculin reveals regulation of focal adhesion dynamics. Nature.466:263-6.

101. Chrzanowska-Wodnicka M, Burridge K. Rho-stimulated contractility drives the formation of stress fibers and focal adhesions. The Journal of cell biology.133:1403-15. 1996.

102. Tzima E, del Pozo MA, Shattil SJ, Chien S, Schwartz MA. Activation of integrins in endothelial cells by fluid shear stress mediates Rho-dependent cytoskeletal alignment. EMBO J.20:4639-47. 2001.

103. Jiang G, Huang AH, Cai Y, Tanase M, Sheetz MP. Rigidity sensing at the leading edge through alphavbeta3 integrins and RPTPalpha. Biophys J.90:1804-9. 2006.

104. Roca-Cusachs P, Gauthier NC, Del Rio A, Sheetz MP. Clustering of alpha(5)beta(1) integrins determines adhesion strength whereas alpha(v)beta(3) and talin enable mechanotransduction. Proc Natl Acad Sci U S A.106:16245-50. 2009.

CHAPTER 3

INTEGRIN SPECIFIC RESPONSES TO FIBRONECTIN TYPE III DOMAINS DETERMINE EPITHELIAL TO MESENCHYMAL TRANSITIONS (EMT) *

Introduction

The extracellular matrix (ECM) provides important directional cues for directing cellular processes, such as cell spreading, survival, proliferation, and differentiation. In pathological states such as fibrosis where the ECM has become modified, either in composition or in mechanical properties, cells are forced into a non-homeostatic niche, and the ECM can facilitate altered and potentially pathological phenotypes, such as epithelial to mesenchymal transitions.

Cells interact with their underlying ECM through transmembrane cell-surface receptors known as integrins, heterodimeric molecules comprised of transmembrane alpha and beta subunits, which are intracellularly linked to cytoskeletal proteins such as talin, vinculin, and/or paxillin. (1) Integrins bind to ECM molecules through specific and often multiple synergistic sequences on ECM proteins. Likewise, ECM proteins often contain several distinct binding sites for multiple integrins and some individual integrin binding sequences within the ECM can bind multiple integrins.

---

* Modified from:

Brown AC, Rowe JA, Barker TH. Guiding epithelial cell phenotypes with engineered integrin-specific recombinant fibronectin fragments. Tissue Eng Part A.17:139-50.

As a result, cells can exhibit different phenotypic responses to the same ECM molecule depending on the integrins that bind, (2, 3) which is in turn directed not only by cellular expression of particular integrins but also by the conformation of the ECM ligand, the availability of specific ligand sequences, and the avidity of particular integrins to competing sites of engagement. ECM-integrin interactions are of particular interest in dynamic ECMs, such as those observed in development and wound healing, because if not precisely controlled, alterations in these interactions can lead to pathological conditions.

As a part of their normal function in tissue development, repair, and remodeling, epithelial cells must display two distinct phenotypes, namely an epithelial phenotype characterized by tight cell-cell junctions and formation of 'high resistance' epithelial sheets, as determined by resistance to electrical current, (4) and a mesenchymal-like phenotype characterized by migratory/invasive behavior and ECM production. (5, 6) The processes of these phenotypic conversions are termed epithelial to mesenchymal and mesenchymal to epithelial transition (EMT and MET, respectively). Normal phenotypic switching associated with EMT and MET as a part of development, repair, and remodeling is not often associated with a complete and permanent conversion and thus is often referred to as partial-EMT or MET. (7-9) However, if chronically stimulated, epithelial cells are capable of a complete conversion to mesenchymal or fibroblastic phenotypes, such as in the case of metastatic cancer and fibrotic pathologies. (10, 11) In particular, complete EMT further perpetuates fibrotic responses by increasing the number of synthetic, ECM producing fibroblasts. Thus, the process of EMT and MET must be tightly regulated during normal events such as re-epithelialization.

Re-epithelialization during wound healing, and the phenotypic switching essential to this process, has been shown to be promoted by binding of specific integrins to ECM molecules, such as Fn, including but not limited to $\alpha5\beta1$, $\alpha3\beta1$, and $\alpha2\beta1$. (12, 13) For example, re-epithelization of airway epithelial cells has been shown to be modulated by binding of $\alpha5\beta1$ integrin to Fn. (12) On the other hand, engagement of other integrins associated with wound-healing, including the RGD-binding integrins $\alpha v\beta3$, $\alpha v\beta5$, $\alpha v\beta6$, and $\alpha v\beta8$ (13) have been associated with greater induction of EMT, through activation of cell contractile machinery, enhanced migration, and contraction. Interestingly, Fn has the capacity to interact with integrins that promote re-epithelization as well as those that have been shown to induce EMT. Integrin mediated activation of cell contractility has significant consequences to the force-mediated activation of the fibrogenic cytokine TGFβ. (14-17) The activation of TGFβ can be induced by contractile cells through mechanical release of TGFβ from the inactive complex leading to further enhancement of the EMT process and downstream cell contraction and ECM production. (10) While induction of cell contractility/mobility is critical for proper wound-healing, there is a critical balance that must be achieved in order to direct regeneration or formation of epithelial tissues without inducing fibrotic responses. The goal of this aim is to understand how integrin specific binding to recombinant Fn fragments modulates normal wound healing or EMT responses. Significant research has demonstrated that Fn has the capacity to bind many of the integrins involved in re-epithelization and wound repair, including $\alpha v\beta3$, $\alpha v\beta6$, $\alpha3\beta1$, and $\alpha5\beta1$, (12, 18-21) and could therefore direct differential cellular responses depending on specific integrin engagement.

Fn, a soluble dimeric glycoprotein consisting of two nearly identical monomers approximately 250 kD in size, is comprised of three repeating subunits known as type I, type II, and type III repeats. (20) The central cell binding domain of Fn, where most integrins bind the molecule, is comprised completely of type III repeats. More specifically the 9^{th} and 10^{th} type III repeats contain the integrin binding "synergy" site (PHSRN) and RGD sequences, respectively. (22, 23) Recently, the relative position of these two binding sites on adjacent type III repeats has been shown critical for $\alpha5\beta1$ integrin binding, such that $\alpha5\beta1$ binding is nearly abolished in the absence of the synergy site. (24-29) Based on the known integrin binding sites within Fn's 9^{th} and 10^{th} type III repeats and the reliance of $\alpha5\beta1$ integrin binding to the synergy sequence, recombinant Fn fragments were utilized comprising the 9^{th} and 10^{th} type III repeats (PHSRN and RGD sites) containing a point mutation previously shown to stabilize the relative position of these two domains, (24, 30) or the 10^{th} type III repeat alone to direct integrin binding. Based on Fn's known role in directing re-epithelialization (12) and/or EMT (10), it was hypothesized that the presence of the synergy site is critical to the regulation of epithelial cell phenotype, by directing integrin specificity. Here, utilizing engineered recombinant fragments of Fn to model two conformation of the molecule, the role of Fn conformation in directing epithelial attachment via αv, $\alpha3$, and $\alpha5$ integrins and the resulting downstream phenotypic determination (**Figure 3.1**) was established.

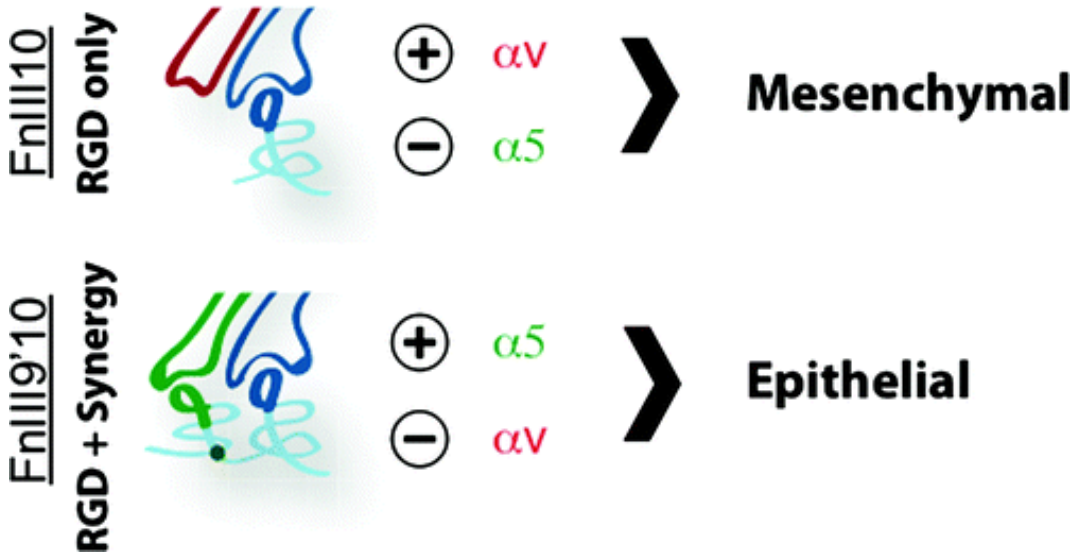

Figure 3.1: Schematic of recombinant fibronectin (Fn) fragments. FnIII10 contains only the Arg-Gly-Asp (RGD) site and is expected to interact with predominantly αv integrins and direct epithelial cells to undergo epithelial-to-mesenchymal transition. FnIII9'10 contains both the RGD and Pro-His-Ser-Arg-Asn (PHSRN) sites and is expected to interact predominantly with the α5 integrin subunit and direct epithelial cells to maintain their epithelial phenotypes. From (31)

Materials and Methods

Production of recombinant proteins

Recombinant Fn fragments were produced as previously described. (30) Briefly, expression vectors encoding the 9th and 10th type III repeats with a structural stabilizing Leu^{1408} to Pro point mutation (FnIII9'10 (24)) and the 10th type III repeat alone (FnIII10) were transformed into BL21 *E.coli* and Fn fragments purified by GST affinity chromatography (AKTA Purifier, GE Healthcare, Piscataway, NJ, USA). GST tags were removed using bovine thrombin (Sigma–Aldrich, St. Louis, MO, USA), and proteins were verified as >98% pure by SDS-PAGE.

Cell culture

RLE-6TN cells, an alveolar epithelial cell line, were obtained from ATCC (Manassas, VA, USA) and maintained in DMEM/F12 media supplemented with 10% FBS, 1% P/S. For experiments analyzing the role of Fn fragments in directing cell phenotype, cells were plated on 2μM Fn-fragment coated, 1% heat denatured (hd)-BSA blocked plates and cultured in serum-free DMEM/F12 media.

Attachment assay

Cell attachment assays were performed as previously described. (32) Briefly, surfaces were coated with 2 μM (30) Fn fragments (FnIII9'10 and FnIII10 have similar coating efficiencies (33)) and blocked with 1% hd-BSA. RLE-6TN cells were incubated with 5μg/mL anti-α3 (Ralph 3.2), anti-αv (H9.2B8), anti-α5 (HMα5-1) (Santa-Cruz Biotech, Santa Cruz, CA, USA), anti-β1 (HMβ1-1), or anti-β3 (2C9.G2) (Biolegend, San Diego, CA, USA) function blocking antibodies or normal mouse IgG control (Millipore) or with 1μg/mL synergy, RGD, synergy plus RGD, or control scrambled peptides (Anaspec, Fremont, CA, USA) for 30 minutes at 37°C in serum-free DMEM/F12 media. A concentration of 5 μg/mL was used for antibody blocking experiments based on dose response experiments demonstrating that this concentration was saturating for all antibodies utilized. Cells were allowed to attach for 20 minutes at 37°C, washed to remove unbound cells, fixed, and stained with crystal violet and absorbance quantified at 570 nm. Attachment values were normalized to cell attachment levels on hd-BSA (0% attachment) and to the test fragment with cells incubated with the IgG control or the scrambled peptide control (100% attachment). Data from triplicate experiments were

normalized and presented as averages +/- standard error. Both normalized (left) and total cell number (right) are presented on the y-axis.

Immunofluorescence integrin staining

RLE-6TN cells were cultured on 2μM FnIII9'10 or FnIII10 coated, hd-BSA blocked glass coverslips for 3 hours. Cells were washed with PBS, fixed with 4% formaldehyde, permeabilized with 0.2% Triton-X 100 and then blocked with 10% goat serum. Primary antibodies were incubated for 1 hour then washed thoroughly with PBS + 0.2% Tween-20. Integrin α3, α5, and αv antibodies utilized for attachment assays were also utilized for immunofluorescence as recommended by the manufacturer. Secondary antibodies (Alexa-Fluor-488 goat-anti-mouse, Invitrogen; FITC-conjugated goat anti-Armenian hamster, Santa-Cruz Biotech) were incubated for 1 hour then washed thoroughly with PBS + 0.2% Tween-20. Nuclei were stained with Hoescht (Invitrogen), coverslips mounted for imaging, and images acquired with a Nikon Eclipse (TiE) inverted fluorescence microscope at 100X magnification, (100X, PlanApo 1.4 NA oil-immersion objective) with a CoolSNAP HQ2 Monochromatic CCD camera. Experiments were performed in triplicate, and images presented are representative from at least 5-10 random fields for each independent experiment.

Analysis of gene expression

RLE-6TN cells were cultured on plates coated with 2μM Fn fragments and blocked with hdBSA. Epithelial cells were cultured in serum free DMEM/F12 media for 48 hours. For analysis of Pai-1, cells were cultured in the absence or presence of 5 ng/mL active TGFβ (R&D Systems, Minneapolis, MN) or 10μg/mL TGFβ neutralizing antibody (9016, R&D Systems). Cells were trypsinized, mRNA isolated (RNAeasy, Qiagen,

Valencia, CA, USA) and c-DNA generated (High Capacity cDNA Reverse Transcription Kit, Applied Biosystems, Foster City, CA, USA). Primers (Invitrogen, Carlsbad, CA, USA) used for q-PCR reactions were as follows: α-SMA forward TTCGTTACTACTGCTGAGCGTGAGA; α-SMA reverse AAAGATGGCTGGAAGAGGGTC (34); collagen I forward GGTAACGATGGTGCTGTCGG; collagen I reverse GGGACCTTGAACTCCAGCAG (35); GAPDH forward GGCAAGTTCAATGGCACAGT; GAPDH reverse AAGGTGGAGGA ATGGGAGTT (35); ZO-1 forward TCAGATCCCTGTAAGTCACC; ZO-1 reverse CCATCTCTTGCTGCCAAAC (36); N-cadherin forward AGGGCCTTAAAGCTGCTGACA; N-cadherin reverse TCATAGTCGAAGACTAAAAGGGAGTCATAT (37); Vimentin forward CCCAGATTCAGGAACAGCAT; Vimentin reverse CACCTGTCTCCGGTATTCGT (designed using Primer3Plus software); E-cadherin forward TGAGCATGCCCCAGTATCG ; E-cadherin reverse CTGCCTTCAGGTTTTCATCGA (37); Plasminogen activator inhibitor-1 (Pai-1) forward CACAGTGCTGGGTGTAATGG; Pai-1 reverse GTTTGTGGGGCAGCTATTGT (designed using Primer3Plus software). Q-PCR was performed on a Step One Plus ABI thermocycler (Applied Biosystems) using Power SYBR Green Master Mix (Applied Biosystems). Data was analyzed using the ΔΔCT method using GAPDH as the endogenous control and comparing expression levels to cells cultured on FnIII9'10. Q-PCR reactions were run in triplicate and performed for 3 independent experiments. Data shown was pooled from 3 independent experiments.

Immunofluorescence E-cadherin/α-SMA staining

RLE-6TN cells were cultured on 2μM Fn fragment-coated, hd-BSA blocked glass coverslips for 48 hours in the absence or presence of 5ng/mL active TGFβ. Cells were processed as described for integrin staining with the exception of using anti-E-cadherin (36/E-Cadherin; BD Transduction Laboratories, San Jose, CA, USA)) and anti-α-SMA (1A4, Sigma-Aldrich) antibodies. Alexa-Fluor-488-conjugated goat-anti-mouse (Invitrogen) was used as the secondary antibody. Images were acquired with a Nikon Eclipse (TiE) inverted fluorescence microscope at 20X magnification (PlanFluor 20X, 0.5 NA objective) with a CoolSNAP HQ2 Monochromatic CCD camera. Experiments were performed in triplicate, and images presented are representative from 5-10 random fields for each independent experiment.

Analysis of cell shape and cytoskeleton organization

RLE-6TN cells were cultured on FnIII9'10 (2μM), FnIII10 (2μM), Fn (0.1μM), or Ln (0.1μM) coated, hd-BSA blocked coverslips in serum-free DMEM/F12 media in the absence or presence of 5 ng/mL activated TGFβ for 48 hours and fixed with 4% formaldehyde. The concentration of Fn was chosen based on previous studies showing similar binding of an antibody specific to the 7-10 type III repeats of Fn (clone HFN7.1a1) (30) to Fn and the Fn fragments at 2 μM concentrations, and the concentration of Ln was chosen based on ELISAs showing maximal coating at 0.1 μM. Actin was stained with Texas-red phalloidin (Invitrogen) and nuclei were stained with Hoescht stain (Invitrogen). Coverslips were mounted and images acquired with a Nikon Eclipse (TiE) inverted fluorescence microscope at 100X magnification (PlanApo 100X, 1.4 NA oil-immersion objective) with a CoolSNAP HQ2 Monochromatic CCD camera.

Representative images are presented.

Analysis of circularity

Cells were cultured on FnIII9'10 (2μM), FnIII10 (2μM), Fn (0.1μM), or Ln (0.1 μM) for 48 hours in the absence or presence of 5ng/mL active TGFβ and the cytoskeleton visualized as described above. Area and perimeter of individual cells was determined for each condition using Image J (NIH Freeware) image processing software, then circularity was determined using the equation circularity = $4\pi(\text{area}/\text{perimeter}^2)$. Three independent images were analyzed for each condition, and at least 10 cells were analyzed per image. Data is pooled from all 3 images analyzed per condition.

Wound-healing assay

Wells of 24-well plates were coated with FnIII9'10 (2μM), FnIII10 (2μM), Fn (0.1μM), or Ln (0.1μM) and then blocked with hd-BSA. Cyto-select wound healing inserts (900μm wide, Cell Biolabs, Inc, San Diego, CA, USA) were then placed in coated wells and RLE-6TN cells seeded at 200,000 cells/cm^2 in serum-free DMEM/F12 media. To insure even distribution of cells, half of the cell suspension was plated on each side of wound field insert. Cells were allowed to form a monolayer for 5 hours, which was verified by phase contrast. The wound insert was then removed, cells were gently washed with PBS to remove any unattached cells, and media was replaced with fresh serum-free DMEM/F12 in the absence or presence of 5ng/mL active TGFβ. Cells were allowed to migrate and close the wound field for 15 hours, followed by gentle washing 2X with PBS, fixation and nuclei staining with DAPI (Cell Biolabs) and immediate imaging. At least 3 images were taken per condition, and conditions were run in triplicate. Percent wound closure was determined by measuring the wound gap area,

dividing by original wound area, and multiplying times 100%.

Statistical analysis

All statistical analysis was performed by multi-variate ANOVA using Prism (Graphpad Software Inc., La Jolla, CA, USA). Statistical significance was achieved for $p<0.05$.

Results

Fn fragments induce integrin specific adhesion

To determine if the presence/absence of the synergy site in concert with the RGD site affects epithelial cell integrin binding to Fn type III repeats, a series of attachment assays were performed with a number of integrin function blocking antibodies. The integrins analyzed were chosen because they are known to be expressed by RLE-6TN cells and also are reported to bind Fn. Attachment of epithelial cells to FnIII9'10 was particularly sensitive to anti-α3, anti-α5, and anti-β1 function-blocking antibodies and less so to anti-αv and anti-β3 antibodies. Epithelial cell attachment to FnIII9'10 was inhibited by 80% ($p<0.01$ with respect to IgG control) in the presence of α3 function-blocking antibodies, 105% ($p<0.001$ with respect to IgG control) in the presence of α5 function-blocking antibodies, and 90% ($p<0.001$ with respect to IgG control) in the presence of β1 function-blocking antibodies. Contrary to epithelial cell binding to FnIII9'10, adhesion to FnIII10, which only contains the integrin-binding RGD sequence but not the adjacent synergy motif (PHSRN) on FnIII9, was less integrin specific and was most notably inhibited by anti-αv integrin antibodies.

RLE-6TN cells demonstrated a 40% inhibition of binding to FnIII10 in response to anti-αv antibodies, while anti-α3, anti-α5, and anti-β1 antibody had negligible effect (**Figure 3.2A-B**). These data indicate that while epithelial cells are capable of binding the RGD motif when it is decoupled from the synergy motif, binding via α3, and predictably α5, integrins require the two motifs' synergistic activity and thus proper orientation.

To determine whether the synergy and RGD sites specifically contribute to epithelial cell binding to FnIII9'10 fragments, attachment assays were also performed with epithelial cells preincubated with soluble RGD and synergy mimetic peptides. Attachment values were normalized to the controls (100%, scrambled peptide; 0%, hd-BSA) and both normalized and total cell number presented on the y-axis (**Figure 3.2C-D**). Attachment of cells to FnIII9'10 was particularly sensitive to both RGD and PHSRN (synergy) peptides, with adhesion inhibited 63% ($p<0.05$) and 79% ($p<0.01$), respectively. Adhesion to FnIII9'10 was blocked most significantly with a combination of RGD and PHSRN peptides where adhesion was inhibited 122% ($p<0.001$). Contrary to the binding of FnIII9'10, adhesion to FnIII10 was most notably blocked by RGD peptides, with adhesion inhibited 46%, while PHSRN peptides had no considerable effect. In addition, the combination of RGD and PHSRN peptides showed approximately the same level of inhibition as RGD peptides alone, with adhesion inhibited 48%.

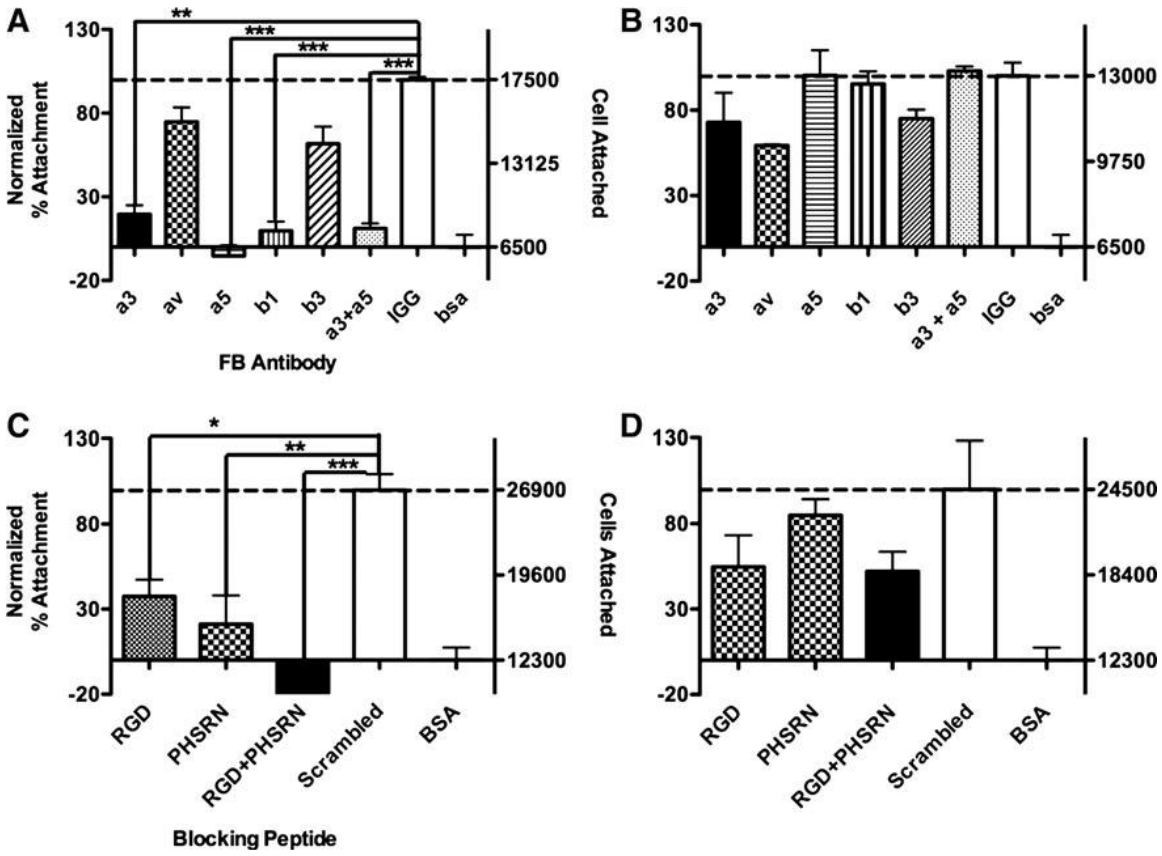

Figure 3.2: Attachment of RLE-6TN cells on Fn fragments. Attachment of epithelial cells to FnIII9'10 (**A, C**) or FnIII10 (**B, D**) fragments was analyzed +/- integrin function blocking (FB) antibodies (**A-B**) or +/- inhibitory peptides (**C-D**) through a standard attachment assay. Percent attachment (left y-axis) was determined by normalizing attachment to BSA (0%) and Fn fragment in the presence of control IgG (**A-B**) or scrambled peptide (**C-D**) (100%) and averages and standard errors are plotted. Total cell number is reported on the right y-axis. *** denotes $p < 0.001$, ** denotes $p < 0.01$, * denotes $p < 0.05$. From (31)

Specific integrin clustering is modulated by the Fn synergy site

To further characterize integrin specific responses to Fn fragments at early time points, RLE-6TN cells were cultured on Fn fragments for a period of 3 hours then stained for integrin subunits α3, α5, or αv. These integrin subunits were chosen for staining based on the differences in integrin binding to Fn fragments as determined through the attachment assays. Cells cultured on FnIII9'10 displayed distinct and strong punctate staining for α3 and α5 integrins indicative of epithelial focal contact formation (**Figure 3.3A, E**), while cells cultured on FnIII10 displayed minimal staining for α3 and α5 integrins (**Figure 3.3B, F**). In contrast, cells cultured on FnIII10 exhibited a stronger staining pattern for αv integrins (**Figure 3.3D**). Cells cultured on FnIII9'10 displayed minimal staining for αv integrins (**Figure 3.3C**).

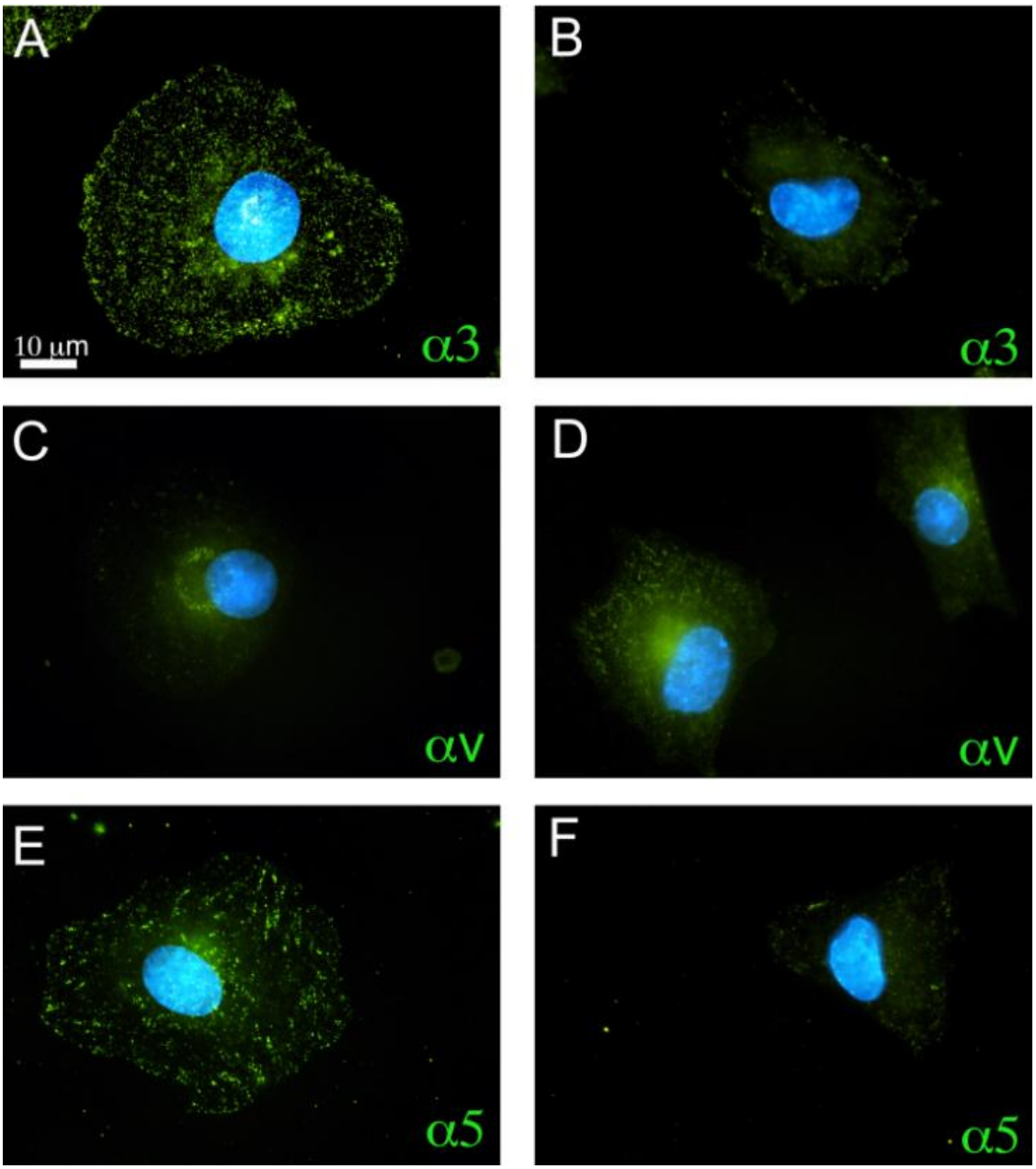

Figure 3.3: Integrin α3, αv, and α5 surface expression and distribution. Cells were analyzed for α3 (**A-B**), αv (**C-D**), and α5 (**E-F**) integrin surface expression and distribution by immunofluorescence 3 hours after plating cells on FnIII9'10 (**A, C, E**) or FnIII10 (**B, D, F**). Images were acquired with a Nikon Eclipse (TiE) inverted fluorescence microscope at 100X magnification. Images are representative of 3 independent experiments. From (31)

Epithelial cells exhibit differences in expression of epithelial and mesenchymal specific genes when cultured on Fn fragments displaying both RGD and synergy versus RGD alone

To determine if differences in initial integrin engagement of Fn fragments induced changes in EMT-related response genes, RLE-6TN cells were cultured on FnIII9'10 and FnIII10 for 48 hours in serum-free DMEM/F12 media, then expression of various epithelial and mesenchymal genes was determined by q-PCR (**Figure 3.4**). All epithelial genes analyzed were significantly down-regulated in cells cultured on FnIII10 compared to cells cultured on FnIII9'10, and all mesenchymal genes analyzed were up-regulated. Specifically, E-cadherin was down-regulated sevenfold ($p<0.05$), and ZO-1 was down-regulated approximately twofold ($p<0.05$) in cells cultured on FnIII10. In contrast, α-SMA was up-regulated 18-fold ($p<0.001$), vimentin was up-regulated 32-fold ($p<0.001$), N-cadherin was up-regulated 78-fold ($p<0.001$), and collagen I was up-regulated sevenfold ($p<0.05$) in cells cultured on FnIII10.

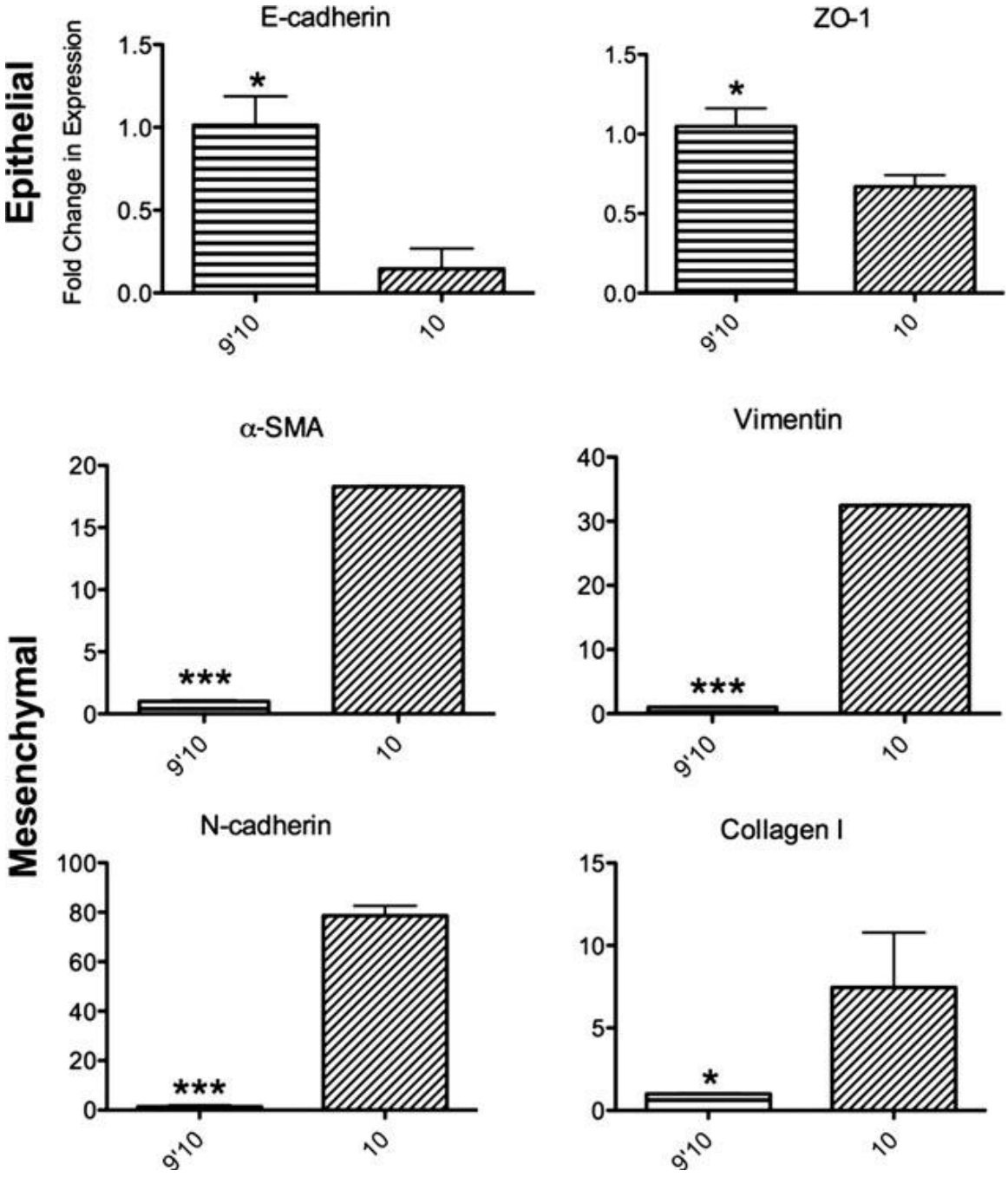

Figure 3.4: Gene expression analysis. RLE-6TN cells were cultured for 48 hours on Fn fragments (FnIII9'10 and FnIII10), then RNA was isolated for gene expression analysis. Levels of expression of epithelial (E-cad, ZO-1) and mesenchymal (α-SMA, Col I, Vimentin, N-cad) markers were determined by q-PCR. Fold changes in gene expression were determined by ΔΔCT analysis using GAPDH as the endogenous control and comparing expression to cells cultured on FnIII9'10. Reactions were performed in triplicate. *** denotes $p < 0.001$, * denotes $p < 0.05$ From (31)

Epithelial cells exhibit differences in E-cadherin and α-SMA protein expression and localization when cultured on Fn fragments displaying both RGD And synergy versus RGD alone

To characterize expression and cellular localization of select epithelial and mesenchymal proteins, RLE-6TN cells were cultured on FnIII9'10 or FnIII10 in the absence (**Figure 3.5A-B; E-F**) or presence (**Figure 3.5C-D; G-H**) of 5 ng/mL active TGFβ for 48 hours then stained for E-cadherin (epithelial marker) (**Figure 3.5A-D**) and α-SMA (mesenchymal marker) (**Figure 3.5E-H**). Cells cultured on FnIII9'10 displayed strong staining for E-cadherin at cell contacts, characteristic of an epithelial phenotype, with additional punctuate staining throughout the cell (**Figure 3.5A**). In contrast, epithelial cells seeded on FnIII10 displayed significantly less E-cadherin at cell-cell contacts, even after only 48 hours in culture (**Figure 3.5B**). The presence of 5 ng/mL active TGFβ drove similar E-cadherin staining patterns in epithelial cells regardless of the substrate, with some diffuse cell-cell contact staining and significant amounts of intracellular punctuate E-cadherin (**Figure 3.5C-D**). In support of a loss of epithelial character, a significant number of epithelial cells cultured on FnIII10 displayed staining for α-SMA (**Figure 3.5F**), while cells cultured on FnIII9'10 displayed no detectable staining (**Figure 3.5E**). As expected, cells cultured in the presence of TGFβ displayed significant staining for α-SMA regardless of underlying ligand (**Figure 3.5G-H**).

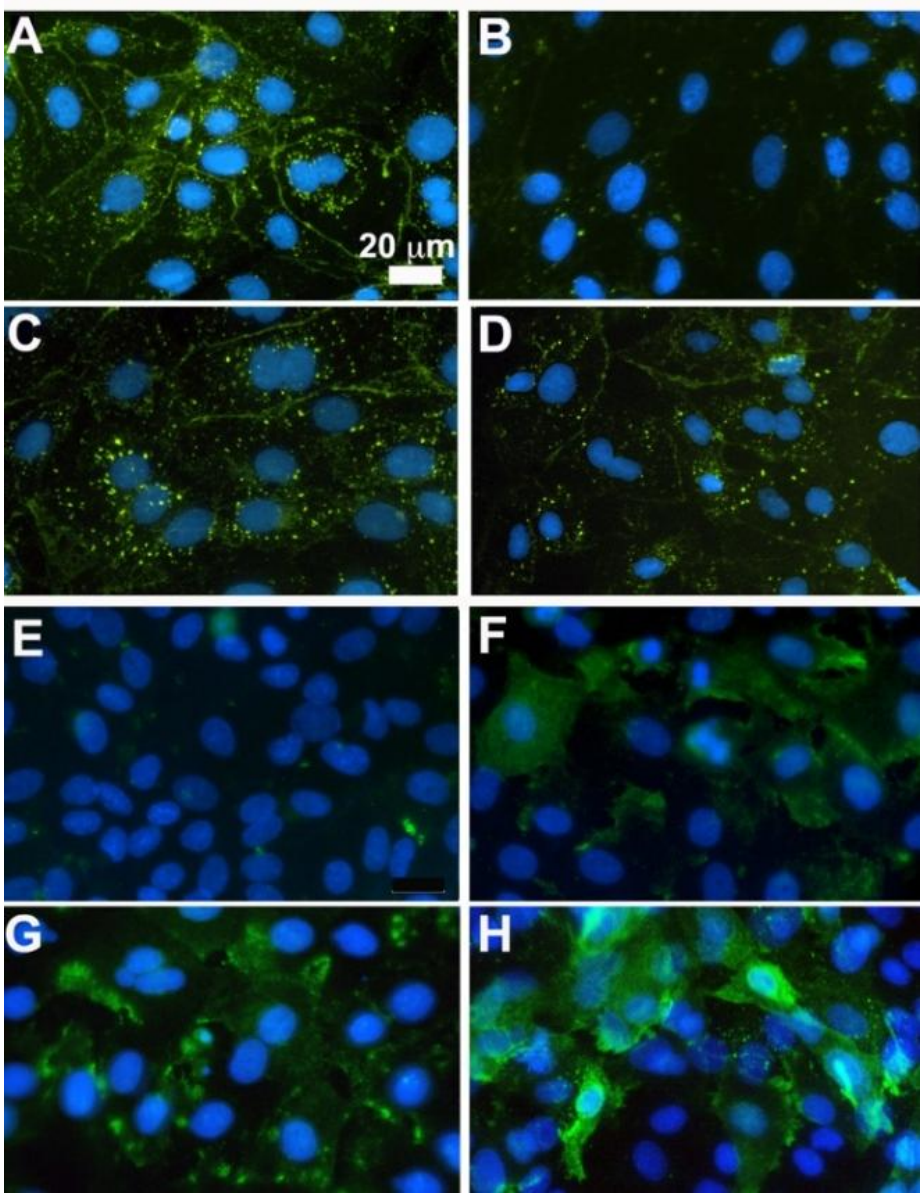

Figure 3.5: E-Cadherin and α-SMA staining in RLE-6TN cells cultured on Fn fragments. RLE-6TN cells were cultured on FnIII9'10 (**A, C, E, G)** or FnIII10 (**B, D, F, H)** in the absence (**A-B, E-F)** or presence (**C-D, G-H**) of 5ng/mL active TGFβ for 48 hours. Cells were then analyzed for E-cadherin (**A-D**) and α-SMA (**E-H**) expression and distribution via immunoflouresence staining. Fluorescent images were acquired with a Nikon Eclipse (TiE) inverted fluorescence microscope at 20X magnification. Images are of representative of at least 3 independent experiments. From (31)

Epithelial cells cultured on Fn fragments display different degrees of cytoskeletal organization

Next, cytoskeletal organization, stress fiber formation, and cell circularity were analyzed by culturing RLE-6TN cells for 48 hours on FnIII9'10, FnIII10, Fn, or Ln in the absence (**Figure 3.6A-D**) or presence (**Figure 3.6E-H**) of 5ng/mL active TGFβ. Cells were stained with Texas-red phallodin to visualize the actin cytoskeleton. Cells cultured on FnIII9'10 displayed a more rounded, cuboidal morphology and diffuse staining for actin (**Figure 3.6A**) similar to cellular responses to Ln (**Figure 3.6D**), while cells cultured on FnIII10 (**Figure 3.6B**) were more spread and displayed aligned, thick actin filaments characteristic of stress fibers similarly to cells cultured on full length Fn (**Figure 3.6C**). The addition of TGFβ enhanced actin filament alignment and stress fiber formation regardless of the adhesive ligand, with the exception of Ln which supported a more rounded epithelial phenotype (**Figure 3.6E-H**). Cell circularity was calculated to quantify differences observed in cell shape (**Figure 3.6I**); values closer to 1 indicated a more rounded cell. Cells cultured on FnIII9'10 exhibited a circularity value of 0.61, compared to cells on FnIII10 which were quite spread and displayed a circularity of 0.26 ($p<0.001$). The addition of TGFβ resulted in circularity values less than 0.35 on each substrate with the exception of Ln, which exhibited a circularity value of 0.47. The addition of TGFβ to cells cultured on FnIII9'10 significantly decreased the circularity to 0.27 ($p<0.001$).

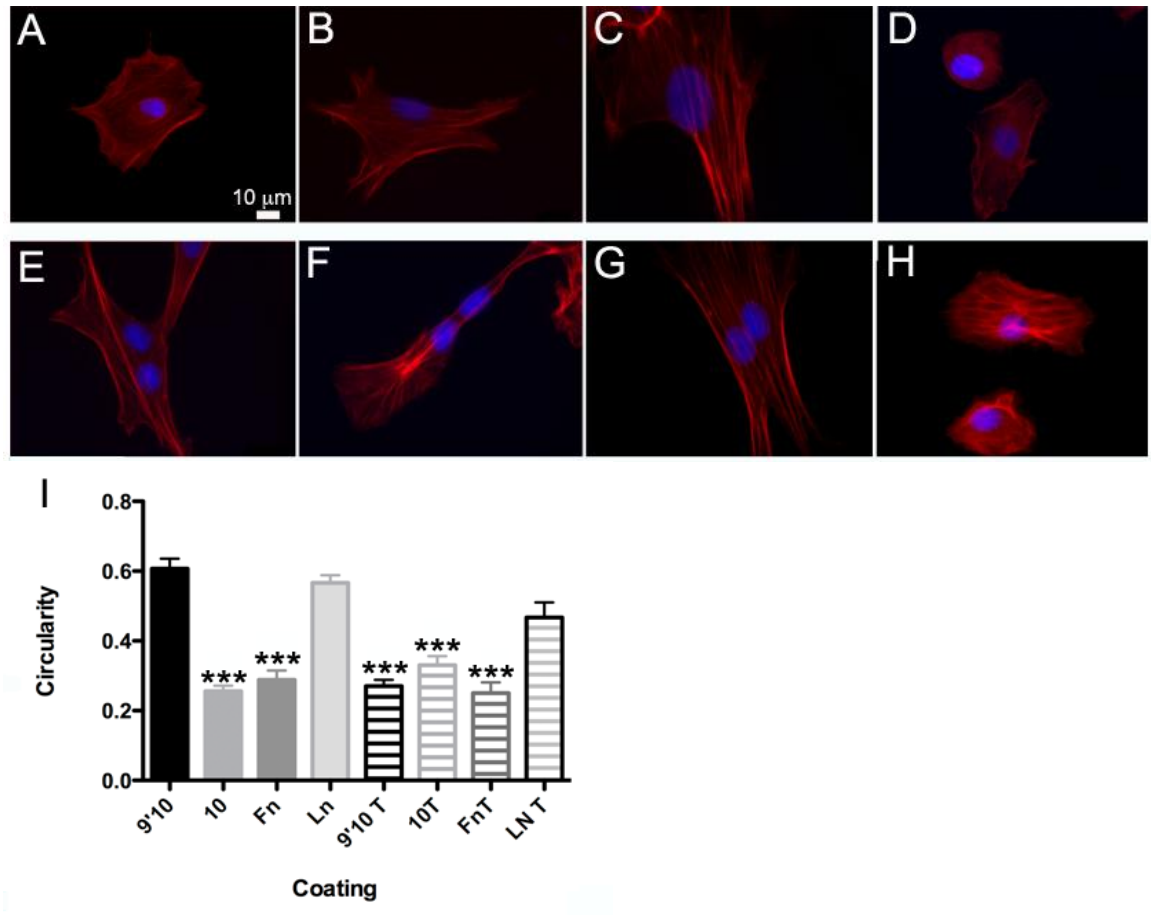

Figure 3.6: Actin cytoskeleton alignment, stress fiber formation, and changes in cell circularity in response to Fn fragments. RLE-6TN cells were cultured for 48 hours on FnIII9'10 (**A,E**), FnIII10 (**B, F),** Fn (**C, G**), or Ln (**D, H**) in the absence (**A-D**) of presence (**E-H)** of 5ng/mL active TGFβ. To analyze stress fiber formation, the actin cytoskeleton was visualized by staining with Texas-red phalloidin and the nuclei stained with Hoescht. Images are of representative of at least 3 independent experiments. Cell circularity was calculated to quantify differences observed in cell shape (**I**); values closer to 1 indicate a more rounded cell. Fluorescent images were acquired with a Nikon Eclipse (TiE) inverted fluorescence microscope at 100X magnification. Three independent images were analyzed for each condition and 10 cells were analyzed per image. Data is pooled from all 3 images analyzed per condition. *** denotes $p<0.001$ relative to cells cultured on FnIII9'10. From (31)

Epithelial cells exhibit differences in Pai-1 expression when cultured On FnIII10 compared to cells cultures on FnIII9'10

To determine if differences in initial integrin engagement of Fn fragments induced changes in Pai-1, a TGFβ-specific responsive gene, RLE-6TN cells were cultured on FnIII9'10, FnIII10, Fn, or Ln for 48 hours in serum-free DMEM/F12 media in the absence or presence of 5ng/mL active TGFβ or 10 μg/mL TGFβ inhibiting antibody and then expression of the Pai-1 gene was determined by q-PCR (**Figure 3.7**). Pai-1 was significantly up-regulated in cells cultured on FnIII10 compared to cells cultured on FnIII9'10, approximately twofold ($p<0.05$), and upon addition of active TGFβ, cells cultured on FnIII10 increased Pai-1 expression significantly (2.5-fold, $p<0.001$). This difference was negated upon the addition of TGFβ inhibiting antibody. Cells cultured on Fn up-regulated Pai-1 threefold compared to cells cultured on FnIII9'10, while cells cultured on Ln had equivalent expression levels as cells cultured on FnIII9'10. Again, as expected all differences were negated by the addition of the TGFβ inhibiting antibody.

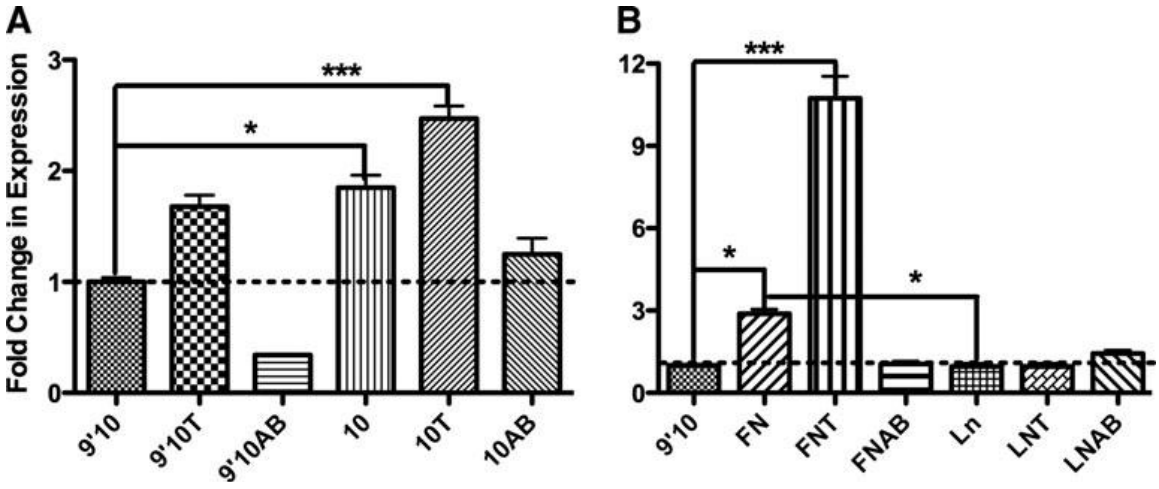

Figure 3.7: Pai-1 gene expression analysis. RLE-6TN cells were cultured for 48 hours on FnIII9'10, FnIII10 (**A**), Fn, or Ln (**B**) in the absence or presence of 5ng/mL active TGFβ. Levels of expression of the TGFβ responsive gene Pai-1 was determined by q-PCR. Fold changes in gene expression were determined by ΔΔCT analysis using GAPDH as the endogenous control and comparing expression to cells cultured on FnIII9'10. Reactions were performed in triplicate. *** denotes $p < 0.001$, * denotes $p < 0.05$ From (31)

Epithelial cells cultured on FnIII9'10 close wound-gap better than cells cultured on FnIII10 in an *in vitro* wound-healing assay

To determine the effect of the Fn synergy sequence on promoting wound healing and the utility of the engineered Fn fragments in directing epithelial cell physiology, a functional wound-healing assay was performed on FnIII9'10 (**Figure 3.8A, C**) or FnIII10 (**Figure 3.8B, D**) coated plates in the absence (**Figure 3.8A-B**) or presence (**Figure 3.8C-D**) of 5ng/mL of active TGFβ. Controls included RLE-6TN cells on Fn and Ln (**Figure 3.8E-F**). Percent wound closure was quantified for each condition (**Figure 3.8G**). FnIII9'10, resulting in 62% closure, promoted significantly greater wound closure at 15 hours than FnIII10 (25%; $p<0.001$). The addition of TGFβ resulted in decreased wound closure on both FnIII9'10 and FnIII10, but FnIII9'10 continued to promote significantly greater wound closure compared to FnIII10 (36% and 15% respectively; $p<0.001$). As expected, cells on Fn exhibited a high percentage of wound closure (70%), which was significantly higher than cells cultured on FnIII9'10 ($p<0.05$). Cells cultured on Ln displayed 51% wound closure, which was significantly less than cells cultured on FnIII9'10 ($p<0.001$).

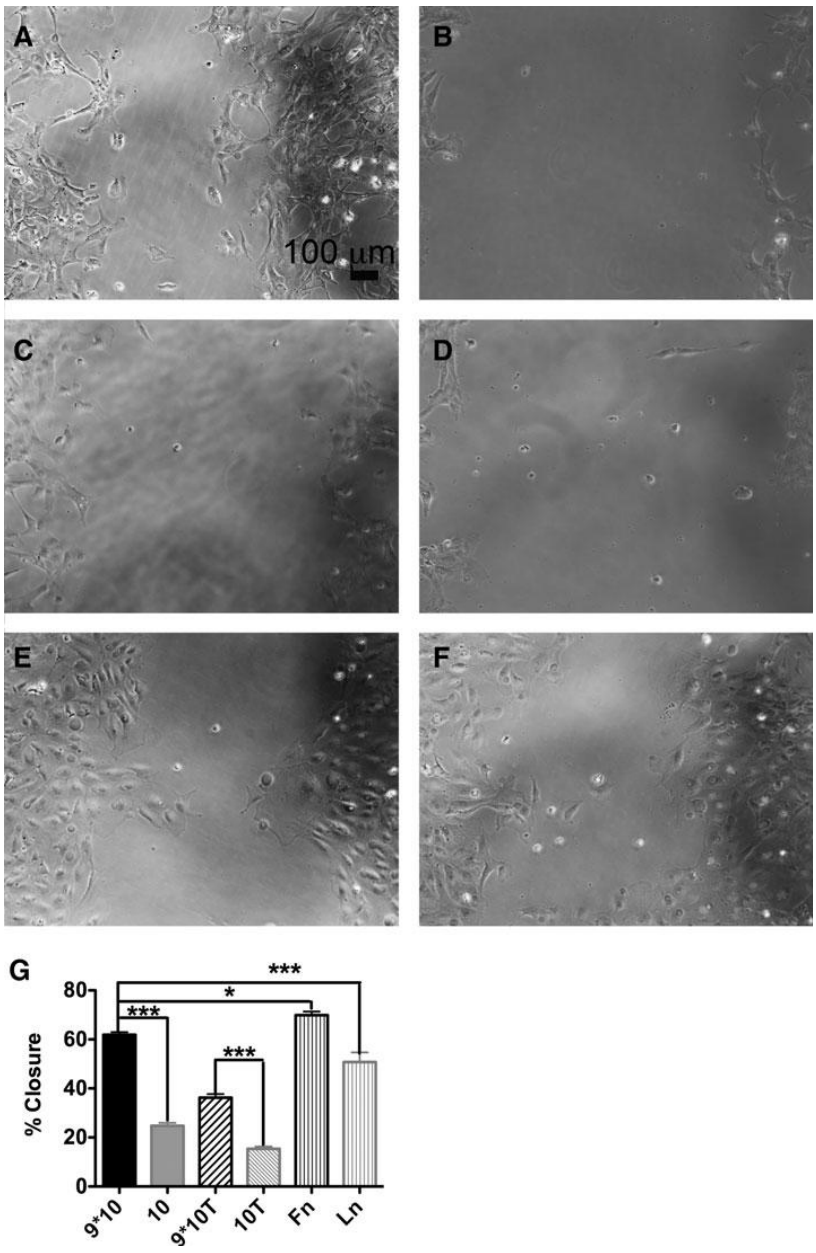

Figure 3.8: Wound healing responses on Fn fragments. A wound healing assay was performed with RLE-6TN cells plated on FnIII9'10 (**A, C**), FnIII10 (**B, D**) in the absence (**A**-**B**) or presence (**C**-**D**) of 5ng/mL active TGFβ. Controls included cells plated on Fn (**E**) and Ln (**F**). Cells were allowed to form a monolayer around a wound field insert, which was removed 5 hours post-seeding. Cells were allowed to migrate and close the wound field for 15 hours, then fixed and their nuclei stained. Cells were imaged at 10X magnification. Percent wound closure was determined (**G)** by measuring the wound gap area and dividing by original wound area and multiplying by 100%. At least 3 images were taken per condition, and conditions were run in triplicate. ******* denotes $p<0.001$, * denotes $p<0.05$. From (31)

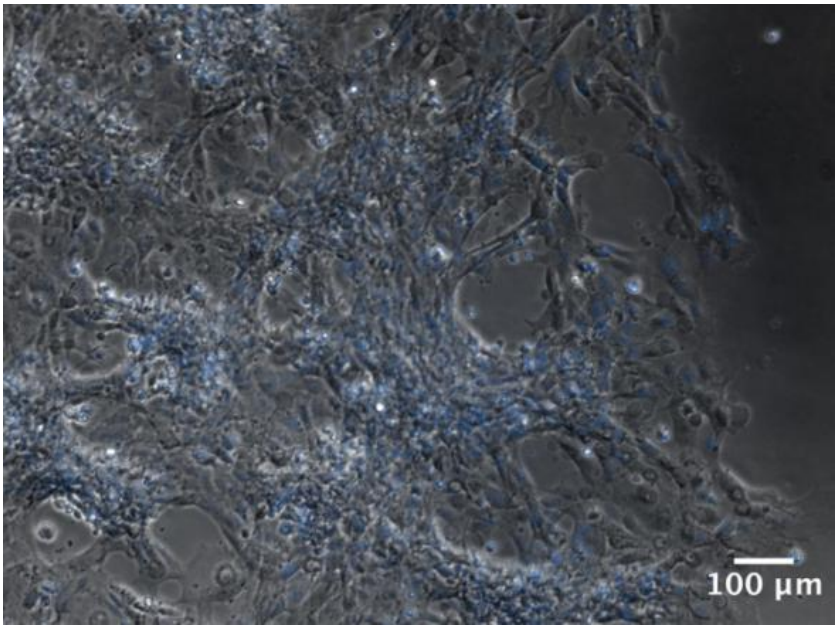

Figure 3.9: Formation of multicellular aggregate structures along the wound edge of RLE-6TN cells cultured on FnIII10. A wound healing assay was performed with RLE-6TN cells plated on FnIII10. Cells were allowed to form a monolayer around wound field inserts, which were removed 5 h post-seeding. Cells were allowed to migrate and close wound field for 15 h and then fixed, and nuclei stained. Cells were imaged at 10X magnification to the immediate left of the wound field. Image is representative. From (31)

Discussion

Cell-integrin interactions play a critical role in directing cellular processes that contribute to wound healing and tissue regeneration. Understanding these interactions in cellular environments with dynamic and rapidly changing ECMs, as in the case of wound healing, is important in understanding pathological progression of fibrotic pathologies, as well as for tissue engineering applications that aim to promote normal healing after removal of scar tissue, directing cell fate *in vitro*, or directing epithelial wound healing after injury (e.g. to the lung, mucosal lining, skin, etc.). Directing alveolar epithelial wound healing after lung injury, such as injury caused by particulate matter inhalation, is of particular interest because abnormal wound repair/EMT has been identified as one of the key pathologies in the development of pulmonary fibrosis (PF), a progressive and fatal lung disorder. (38) While significant effort has been made to prevent pathology-associated epithelial cell behaviors, such as EMT, these fundamental epithelial transitions are central to proper repair and regeneration of most, if not all, epithelial tissues. Cell-integrin interactions have been shown to play a significant role in directing EMT events, which if uncontrolled can have deleterious consequences such as fibrotic progression seen in PF. On the contrary, if controlled, directed EMT could have great potential for regenerative medicine purposes, for example in directing complex tissue formation from a single stem cell population. In this aim, it is demonstrated that epithelial cell integrin binding can be controlled through engineered Fn fragments displaying a synergy and RGD (FnIII9’10), or RGD alone (FnIII10) which in turn leads to differences in EMT-related cellular responses. Upon further investigation these fragments can be utilized to direct complex epithelial responses related to wound healing

and/or EMT.

First, it was confirmed that engineered Fn fragments can direct specific epithelial cell-integrin interactions; specifically, it was found that epithelial cell attachment to FnIII9'10 is blocked significantly by integrin α3, α5, and β1 function-blocking antibodies, while binding to FnIII10 is less specific but is affected most notably by integrin αv function blocking antibodies (**Figure 3.2A-B**). These data suggest that epithelial cells bind to FnIII9'10 via α3 and α5 integrins and that both of these integrins may interact with Fn in a synergy dependent manner, an interpretation further supported by inhibition of epithelial cell attachment with soluble RGD and synergy mimetic peptides. Because FnIII10 contains only the RGD site, known as a promiscuous partner to many integrins, it is not surprising that epithelial cell attachment to this fragment is less specific. Although a multi-variate ANOVA showed no significant inhibition of adhesion to FnIII10 by any one function-blocking antibody, a simple Student's t-test between cells incubated with integrin αv antibodies and the IgG control showed a significant difference between these two groups ($p<0.05$). FACS analysis of initial integrin expression confirmed previous reports that the epithelial cells utilized in these studies (alveolar epithelial cells) express αv integrins to a lesser extent than α3 or α5 (21); therefore, the observation that αv function blocking antibodies blocked attachment to FnIII10 to any observable degree suggests that this integrin likely plays an important role in binding to Fn's cell-binding domain when only the RGD site is available for binding, a result reported in numerous other studies. (30, 39, 40) The synergy-site dependence of α5 integrin has been well studied and was expected; however, the finding that α3 integrin binding to Fn may potentially be significantly enhanced by the presence

and spatial stabilization of the synergy site is a novel finding that will require additional studies to fully establish. Integrin α3β1, typically thought of as a laminin receptor, has been shown to bind Fn (in an RGD-dependent fashion) as well as collagen, yet these reported binding events are still somewhat controversial. (18, 41) Studies here with both soluble RGD and synergy mimetics, while not conclusive evidence for the synergy-dependence of α3 and α5 integrins, when taken together with the function-blocking antibody data is suggestive that these integrins require the presence of synergy.

Epithelial cell integrin clustering to Fn fragments was further demonstrated through immunofluorescence staining for α3, α5, and αv subunits. The clustering of integrins is one of the first events that triggers integrin-specific signaling cascades and the staining for α3 and α5 integrins in epithelial cells cultured on FnIII9'10 were indicative of integrin clustering and focal contact formation, (**Figure 3.3A, E**) whereas αv integrin staining demonstrated much less pronounced staining (**Figure 3.3C**) in epithelial cells cultured on FnIII9'10. This staining pattern suggests that although the cells express α3 and α5 integrins and that these integrins may be displaying some slight promiscuity, epithelial cells are not capable of engaging α3 or α5 integrins to any appreciable degree when interacting with RGD only (FnIII10). In contrast, cells cultured on FnIII10 exhibited a stronger staining pattern for αv integrins (**Figure 3.3E**) compared to epithelial cells cultured on FnIII9'10. Together, these data suggest that epithelial cells engage Fn with integrins differentially depending on the presentation of the RGD and synergy sequences.

Investigating epithelial cell phenotypic markers, specifically EMT related genes and proteins, it was observed that cells displayed a more mesechymal phenotype when

cultured on FnIII10 compared to cells cultured on FnIII9'10 (**Figures 3.4-5**). The observed shift towards a mesenchymal phenotype on FnIII10 was further evidenced by stress fiber formation, a significant decrease in circularity (**Figure 3.6**), and an elongated, fibroblast-like morphology that was accompanied by the loss of cell-cell contacts as observed through E-cadherin staining. In contrast, cells cultured on FnIII9'10 maintained expression of epithelial markers, cell-cell contacts, and displayed an epithelial-like morphology after 48 hours, suggesting that epithelial cell engagement of the synergy site of Fn may play an important role in the spatiotemporal control of EMT.

TGFβ signaling has been strongly linked to EMT and thus TGFβ responses were investigated through the analysis of Pai-1 mRNA expression, the up-regulation of which is primarily mediated through the TGFβ receptor/Smad signaling pathway. (42) Data indicate a substrate dependent TGFβ response (**Figure 3.7**) confirming previous reports that Fn and Ln instruct altered TGFβ responses. (10) As expected, the addition of exogenous active TGFβ further enhanced the expression of Pai-1 while the addition of a TGFβ inhibiting antibody resulted in a loss of substrate dependent difference. These data indicate that the differences in epithelial cell phenotype on Fn fragments are potentially due, in part, to differences in TGFβ activation or signaling or both.

Finally, the functional/physiological consequences of epithelial cell integrin-specific engagement to Fn fragments was demonstrated through an *in vitro* wound healing assay (**Figure 3.8**), which allow for the investigation of cell behavior indicative of enhanced wound repair, such as the ability to close cell monolayer gaps. Integrin α5β1's role in promoting wound healing has been well characterized (12, 13); therefore, it was expected that cells engaging α5β1 on FnIII9'10 would have a greater capacity to

heal monolayer wounds than cells engaging αv integrins on FnIII10. One observation requiring significant additional characterization is that epithelial cells cultured on FnIII10, rather than displaying the expected migratory phenotype associated with EMT, displayed at least a partial loss of contact inhibition as evidenced by the formation of multicellular aggregate structures along the wound edge (**Figure 3.9**). Interestingly, the addition of TGFβ resulted in a decrease in wound gap closure. TGFβ's role in wound healing is complex, both inhibiting proliferation and inducing EMT. Previous reports indicate that TGFβ inhibits epithelial wound closure, (43) yet TGFβ antagonists result in reduced *in vivo* scar/fibrosis. (44)

While Fn fragments displaying RGD or RGD and synergy have previously been used to direct mesenchymal stem cell fate, (29) these results illustrate the utility of these fragments in directing epithelial integrin-specific attachment, integrin clustering, and, in-turn, differences in cellular phenotype. In addition, these studies demonstrate the physiological relevance of the synergistic activity of Fn's 9^{th} type III repeat (synergy site) in concert with the 10^{th} type III repeat (RGD motif) in directing epithelial cell phenotypes of relevance to tissue repair and underscore the necessity of understanding not only the role of specific ECM molecules in directing cell fate, but also the role of particular molecular states, for example compact vs. extended, in directing cell fate. The use of Fn fragments modeling these two molecular states allows for greater control over integrin specificity and concomitant cell fate. This aim illustrates that altered biochemical states of Fn, as might be observed in response to extremely contractile fibrotic myofibroblasts, can contribute to altered integrin binding and perpetuation of aberrant cell phenotypes such as chronic EMT.

References

1. Harburger DS, Calderwood DA. Integrin signalling at a glance. J Cell Sci.122:159-63. 2009.

2. Carson AE, Barker TH. Emerging concepts in engineering extracellular matrix variants for directing cell phenotype. Regen Med.4:593-600. 2009.

3. Truong H, Danen EH. Integrin switching modulates adhesion dynamics and cell migration. Cell Adh Migr.3:179-81. 2009.

4. Madara JL, Dharmsathaphorn K. Occluding junction structure-function relationships in a cultured epithelial monolayer. The Journal of cell biology.101:2124-33. 1985.

5. Birchmeier C, Birchmeier W, Brand-Saberi B. Epithelial-mesenchymal transitions in cancer progression. Acta Anat (Basel).156:217-26. 1996.

6. Hay ED. An overview of epithelio-mesenchymal transformation. Acta Anat (Basel).154:8-20. 1995.

7. Elloul S, Vaksman O, Stavnes HT, Trope CG, Davidson B, Reich R. Mesenchymal-to-epithelial transition determinants as characteristics of ovarian carcinoma effusions. Clin Exp Metastasis.

8. Grunert S, Jechlinger M, Beug H. Diverse cellular and molecular mechanisms contribute to epithelial plasticity and metastasis. Nat Rev Mol Cell Biol.4:657-65. 2003.

9. Leroy P, Mostov KE. Slug is required for cell survival during partial epithelial-mesenchymal transition of HGF-induced tubulogenesis. Molecular biology of the cell.18:1943-52. 2007.

10. Kim KK, Kugler MC, Wolters PJ, Robillard L, Galvez MG, Brumwell AN, et al. Alveolar epithelial cell mesenchymal transition develops in vivo during pulmonary fibrosis and is regulated by the extracellular matrix. Proceedings of the National Academy of Sciences of the United States of America.103:13180-5. 2006.

11. Willis BC, Liebler JM, Luby-Phelps K, Nicholson AG, Crandall ED, du Bois RM, et al. Induction of epithelial-mesenchymal transition in alveolar epithelial cells by transforming growth factor-beta1: potential role in idiopathic pulmonary fibrosis. Am J Pathol.166:1321-32. 2005.

12. Herard AL, Pierrot D, Hinnrasky J, Kaplan H, Sheppard D, Puchelle E, et al. Fibronectin and its alpha 5 beta 1-integrin receptor are involved in the wound-

repair process of airway epithelium. The American journal of physiology.271:L726-33. 1996.

13. Margadant C, Sonnenberg A. Integrin-TGF-beta crosstalk in fibrosis, cancer and wound healing. EMBO Rep.11:97-105.

14. Annes JP, Chen Y, Munger JS, Rifkin DB. Integrin alphaVbeta6-mediated activation of latent TGF-beta requires the latent TGF-beta binding protein-1. The Journal of cell biology.165:723-34. 2004.

15. Fontana L, Chen Y, Prijatelj P, Sakai T, Fassler R, Sakai LY, et al. Fibronectin is required for integrin alphavbeta6-mediated activation of latent TGF-beta complexes containing LTBP-1. FASEB J.19:1798-808. 2005.

16. Wipff PJ, Hinz B. Integrins and the activation of latent transforming growth factor beta1 - an intimate relationship. Eur J Cell Biol.87:601-15. 2008.

17. Wipff PJ, Rifkin DB, Meister JJ, Hinz B. Myofibroblast contraction activates latent TGF-beta1 from the extracellular matrix. The Journal of cell biology.179:1311-23. 2007.

18. Elices MJ, Urry LA, Hemler ME. Receptor functions for the integrin VLA-3: fibronectin, collagen, and laminin binding are differentially influenced by Arg-Gly-Asp peptide and by divalent cations. The Journal of cell biology.112:169-81. 1991.

19. Humphries J, Byron, A, Humphries, M. Integrin ligands at a glance. J Cell Sci.119:3901-3. 2006.

20. Pankov R YK. Fibronectin at a glance. J Cell Sci.115:3861-3. 2002.

21. Sheppard D. Functions of pulmonary epithelial integrins: from development to disease. Physiological reviews.83:673-86. 2003.

22. Mao Y, Schwarzbauer JE. Fibronectin fibrillogenesis, a cell-mediated matrix assembly process. Matrix Biol.24:389-99. 2005.

23. Mardon HJ, Grant KE. The role of the ninth and tenth type III domains of human fibronectin in cell adhesion. FEBS letters.340:197-201. 1994.

24. Altroff H, Schlinkert R, van der Walle CF, Bernini A, Campbell ID, Werner JM, et al. Interdomain tilt angle determines integrin-dependent function of the ninth and tenth FIII domains of human fibronectin. The Journal of biological chemistry.279:55995-6003. 2004.

25. Burrows L, Clark K, Mould AP, Humphries MJ. Fine mapping of inhibitory anti-alpha5 monoclonal antibody epitopes that differentially affect integrin-ligand binding. Biochem J.344 Pt 2:527-33. 1999.

26. Grant RP, Spitzfaden C, Altroff H, Campbell ID, Mardon HJ. Structural requirements for biological activity of the ninth and tenth FIII domains of human fibronectin. The Journal of biological chemistry.272:6159-66. 1997.

27. Petrie TA, Capadona JR, Reyes CD, Garcia AJ. Integrin specificity and enhanced cellular activities associated with surfaces presenting a recombinant fibronectin fragment compared to RGD supports. Biomaterials.27:5459-70. 2006.

28. Petrie TA, Raynor JE, Reyes CD, Burns KL, Collard DM, Garcia AJ. The effect of integrin-specific bioactive coatings on tissue healing and implant osseointegration. Biomaterials.29:2849-57. 2008.

29. Krammer A, Craig D, Thomas WE, Schulten K, Vogel V. A structural model for force regulated integrin binding to fibronectin's RGD-synergy site. Matrix Biol.21:139-47. 2002.

30. Martino MM, Mochizuki M, Rothenfluh DA, Rempel SA, Hubbell JA, Barker TH. Controlling integrin specificity and stem cell differentiation in 2D and 3D environments through regulation of fibronectin domain stability. Biomaterials.30:1089-97. 2009.

31. Brown AC, Rowe JA, Barker TH. Guiding epithelial cell phenotypes with engineered integrin-specific recombinant fibronectin fragments. Tissue Eng Part A.17:139-50.

32. Humphries MJ. Cell-substrate adhesion assays. Current protocols in cell biology / editorial board, Juan S Bonifacino [et al.Chapter 9:Unit 9 1. 2001.

33. Altroff H, van der Walle CF, Asselin J, Fairless R, Campbell ID, Mardon HJ. The eighth FIII domain of human fibronectin promotes integrin alpha5beta1 binding via stabilization of the ninth FIII domain. The Journal of biological chemistry.276:38885-92. 2001.

34. Hsu YC, Chiu YT, Lee CY, Lin YL, Huang YT. Increases in fibrosis-related gene transcripts in livers of dimethylnitrosamine-intoxicated rats. J Biomed Sci.11:408-17. 2004.

35. Liu Q, Mao H, Nie J, Chen W, Yang Q, Dong X, et al. Transforming growth factor {beta}1 induces epithelial-mesenchymal transition by activating the JNK-Smad3 pathway in rat peritoneal mesothelial cells. Perit Dial Int.28 Suppl 3:S88-95. 2008.

36. Yang J, Blum A, Novak T, Levinson R, Lai E, Barasch J. An epithelial precursor is regulated by the ureteric bud and by the renal stroma. Dev Biol.246:296-310. 2002.

37. Smit MA, Geiger TR, Song JY, Gitelman I, Peeper DS. A Twist-Snail axis critical for TrkB-induced epithelial-mesenchymal transition-like transformation, anoikis resistance, and metastasis. Mol Cell Biol.29:3722-37. 2009.

38. Geiser T. Idiopathic pulmonary fibrosis--a disorder of alveolar wound repair? Swiss Med Wkly.133:405-11. 2003.

39. Mao Y, Schwarzbauer JE. Accessibility to the fibronectin synergy site in a 3D matrix regulates engagement of alpha5beta1 versus alphavbeta3 integrin receptors. Cell Commun Adhes.13:267-77. 2006.

40. Ochsenhirt SE, Kokkoli E, McCarthy JB, Tirrell M. Effect of RGD secondary structure and the synergy site PHSRN on cell adhesion, spreading and specific integrin engagement. Biomaterials.27:3863-74. 2006.

41. Hodivala-Dilke KM, DiPersio CM, Kreidberg JA, Hynes RO. Novel roles for alpha3beta1 integrin as a regulator of cytoskeletal assembly and as a trans-dominant inhibitor of integrin receptor function in mouse keratinocytes. The Journal of cell biology.142:1357-69. 1998.

42. Dong C, Zhu S, Wang T, Yoon W, Goldschmidt-Clermont PJ. Upregulation of PAI-1 is mediated through TGF-beta/Smad pathway in transplant arteriopathy. J Heart Lung Transplant.21:999-1008. 2002.

43. Wang XJ, Han G, Owens P, Siddiqui Y, Li AG. Role of TGF beta-mediated inflammation in cutaneous wound healing. J Investig Dermatol Symp Proc.11:112-7. 2006.

44. Singer AJ, Huang SS, Huang JS, McClain SA, Romanov A, Rooney J, et al. A novel TGF-beta antagonist speeds reepithelialization and reduces scarring of partial thickness porcine burns. J Burn Care Res.30:329-34. 2009.

CHAPTER 4

INTEGRIN α3β1 BINDS FIBRONECTIN AND IS DEPENDENT ON THE 9TH TYPE III REPEAT

Introduction

Cells interact with their surrounding extracellular matrix via transmembrane cell surface receptors, known as integrins. Integrins are heterodimeric proteins consisting of one α subunit and one β subunit, which are known to form at least 24 unique heterodimers. (1) Integrin interactions with their extracellular matrix (ECM) ligands facilitate a host of cellular responses, including cell spreading, migration, proliferation, and differentiation, and can contribute to more orchestrated cellular events, such as development and wound healing, by contributing to angiogenesis and epithelial to mesenchymal transitions. Integrin binding to ECM ligands occurs through specific binding sequences, the most notable of these sequences being Arg-Gly-Asp (RGD), which is found on a large number of ECM proteins, including fibronectin, vitronectin, osteoponin, laminin, thrombospondin, and several others. (2) Furthermore, integrin heterodimers can interact with multiple ECM ligands and bind to multiple binding sequences. (3, 4)

Fibronectin is a widely expressed extracellular matrix protein and is known to bind at least 16 integrins. Biochemically, Fn exists as a soluble dimeric glycoprotein composed of two nearly identical 230-270 kDa monomers linked covalently near their C-termini by a pair of disulfide bonds. (5, 6) Each monomeric subunit consists of three

types of repeating modules, type I, II, and III. These modules comprise functional domains that mediate interactions with other ECM components, cell surface receptors, and Fn itself. (6) Whereas type I and II repeats are structurally stabilized with two intrachain disulfide bonds in each repeat, type III repeats have no disulfide bonds and, therefore, are highly sensitive to force-mediated unfolding, resulting in alterations of conformation of the molecule. (5, 7, 8) Interestingly, a large number of Fn/integrin interactions occur through the RGD site, which is located on the 10th type III repeat. The recognition of this simple tripeptide sequence can be quite complex and greatly depends on flanking residues, its three dimensional presentation, and individual features of the integrin-binding pockets. This is most well characterized in α5β1 integrin binding to Fn, in which RGD in concert with a second recognition sequence (PHSRN), the so-called "synergy" site, in the adjacent 9th type III repeat is known to promote the specific interaction of α5β1 integrin binding to Fn through interactions with the α5 subunit. (9, 10) The synergy site is located approximately 32 Å from the RGD loop on the 10^{th} type III repeat. The type III repeats show great elasticity in the loops between their F- and G-β strands, known as the FG loop, which allows the 9^{th} and 10^{th} type III repeats to present multiple conformations. Under small applied forces (on the order of 10 pN) Fn's 10th type III repeat is susceptible to partial unfolding, resulting in an intermediate state in which the RGD loop within the 10^{th} type III repeats begins to translocate away from the 9^{th} type III repeat, resulting in an increase in the distance between the RGD and synergy sites from approximately 32 Å to approximately 55 Å. (11) This capacity to present multiple spatial orientations of the 9^{th} and 10^{th} type III repeats has great implications on cell binding because the relative positioning of these two domains has been shown to

influence integrin α5β1 binding. Integrin α5β1 binds by simultaneously engaging the RGD and synergy sites. As these sites translocate away from one another, they can no longer be bound simultaneously, and integrin α5β1 no longer binds. These findings suggest that an integrin "switch" can be mechanically induced by stretching and partially unfolding these two domains. Further evidence suggesting that a mechanically induced integrin switch exists within the 9^{th} and 10^{th} type III repeats of Fn was shown by studies in which conformational stability was conferred to the 9^{th} or 10^{th} type III repeats, resulting in modulation of integrin specificity. In these studies, the 9^{th} type III repeat was stabilized via a Leu-Pro mutation at amino acid 1408, (12, 13) or the 10^{th} type III repeat (14) was stabilized through stabilization of the hydrogen bonding within the repeat. In both cases, stabilization of the relative positions of the two repeats resulted in increased affinity for integrin α5β1 over integrin αvβ3. In addition, studies in which the linker region between the 9^{th} and 10^{th} type III repeats was increased in length showed reduction in α5β1 binding. (15)

As reported in the previous aim, α3β1 binding to Fn may also be promoted by the 9th type III repeat. (16) Using recombinant Fn fragments displaying the RGD and synergy sites with a stabilizing (L_{1408}-P) point mutation (FnIII9'10) or RGD alone (FnIII10), it was previously demonstrated that the presence of Fn's synergy site enhances epithelial cell integrin specificity; epithelial cell binding to FnIII9'10 was significantly inhibited by anti-α3 and anti-α5 antibodies ($p<0.01$), while their inhibition of cell binding to RGD only Fn fragments was negligible. Additionally, epithelial cells seeded on FnIII9'10, but not FnIII10, formed α3 and α5 integrin clusters.

Though the classical ligand for integrin α3β1 is laminin (Ln) (17, 18) it has been reported to bind collagen and Fn (6, 19, 20) and facilitate cell-cell interactions through both homophillic binding and binding to E-cadherin (21-23) Furthermore, integrin α3β1 binding to Fn has been shown to occur in an RGD dependent fashion, however, α3β1 binding to Ln and collagen does not occur through RGD sites. Integrin α3β1 is highly expressed by many epithelial cells, including alveolar epithelial cells, renal epithelial cells, and keratinocytes, and has been shown to be critical for regulation of epithelial phenotype. (24, 25) Integrin α3β1 plays a critical role in maintaining epithelial integrity and facilitating wound repair responses, and, if not bound to its extracellular matrix ligands, it can contribute to pathologies such as EMT. (24, 26) During wound healing responses, the ECM rapidly undergoes changes in composition from mostly Ln and elastin to higher concentrations of provisional matrix components, such as Fn. Understanding the ability of integrin α3β1 to bind to both its classical ligand Ln as well as Fn is important to understand cell interactions with these dynamic matrices observed in wound healing and may elucidate mechanisms involved in normal vs. pathological wound healing responses.

Based on results reported in the previous aim that α3β1 binding to Fn may be promoted by the 9th type III repeat and other's reports that α3β1 binding to Fn is RGD dependent, it was hypothesized that α3β1 binding to Fn is enhanced by the presence of the 9^{th} type III repeat. To explore this hypothesis, a variety of recombinant FnIII9'10 variants were created displaying i) a dominant negative R-A mutation in the synergy site ($FnIII^{9R-A}10$), ii) a 2xG insertion in the linker region ($FnIII9^{2G}10$), or iii) a 4xG insertion

in the linker region (FnIII9^{4G}10) and surface plasmon resonance (SPR) was utilized to determine binding kinetics of integrin $\alpha 3\beta 1$ to the Fn fragments.

Materials and Methods

Construction of mutant pGEX4T1-FnIII9-10 clones

Cloning of the wild type FnIII9-10 was performed as previously described. A Leu1408 to Pro mutation (FnIII9'10) was made using the pGEX4T-1-FN III9-10 plasmid as previously described. (12, 13, 16) FnIII9'10 variants displaying i) a dominant negative R-A mutation in the synergy site (FnIII^{9R-A}10), ii) a 2xG insertion in the linker region (FnIII9^{2G}10), or iii) a 4xG insertion in the linker region (FnIII9^{4G}10) were then created using the QuikChange® II-E Site-Directed Mutagenesis Kit (Stratagene, La Jolla, CA). Sequences are presented in **Table 4.1**. All plasmids were introduced to and maintained in the electro-competent XL-1 Blue *E.coli* strain provided and cultured in LB + ampicillin plates at 37°C. Plasmids were extracted from cultures using the QIAquick Spin Miniprep Kit (QIAGEN, Valencia, CA) and verified via sequencing (Johns Hopkins Synthesis & Sequencing Facility, Baltimore, MD).

Expression and purification of recombinant FnIII9'10 proteins

Recombinant Fn fragments were produced as previously described. (13, 16) Briefly, the expression vectors described above were transformed into BL21 *E.coli*, cells were grown to the exponential growth phase and treated with IPTG for 3 hours. Cells were then lysed by the addition of 10mg/ml lyzozyme and sonication, followed by incubation with 1% triton X-100 and 10U/ml of DNAse I. Fn fragments were purified by GST affinity chromatography (AKTA Purifier, GE Healthcare, Piscataway, NJ, USA).

GST tags were removed using bovine thrombin (Sigma–Aldrich, St. Louis, MO, USA). A second round of purification was performed using GST and serine protease affinity chromatography to remove cleaved GST tags and thrombin. Proteins were verified as >98% pure by SDS-PAGE.

Surface plasmon resonance studies

The Biacore 2000 (Biacore Lifesciences, GE Healthcare) was used to investigate kinetic binding constants (k_a and k_d) of Fn fragments variants for integrins α3β1, α5β1, and αvβ3. Briefly, integrins α3β1, α5β1, or αvβ3 (R&D Systems, Minneapolis, MN, USA) were covalently immobilized to gold-coated SPR sensor chips via self-assembled monolayer surface chemistry to generate a non-fouling surface with a controlled density of reactive carboxylic acid groups. Mixed self-assembled monolayers were generated on gold-coated chips as previously described (27, 28) by incubating with a 10:1 mixture of 1-mM of tri(ethylene glycol)–terminated alkanethiols (HS-(CH2)11–(OCH2CH2)3–OH (ProChimia, Gdansk, Poland) and carboxylic acid–terminated alkanethiols (HS-(CH2)11–(OCH2CH2)6–OCH2COOH) overnight. The senor chip was then loaded into the Biacore 2000 and the carboxylic acid–terminated alkanethiol surfaces was activated by flowing 200mM 1-ethyl-3-(3-dimethylaminopropyl) carbodiimide (Sigma-Aldrich) and 50mM N-hydroxysuccinimide (Sigma-Aldrich; 5µL/minute for 10 minutes). Immediately after activation, α3β1, α5β1, or αvβ3 integrins (100µg/ml) were immobilized at a flow rate of 5µL/minute for 10 minutes to achieve approximately 1500 resonance units (1 resonance unit ~ 1 pg/mm2). An additional channel was immobilized with BSA to serve as a reference channel; BSA (100ug/ml) was immobilized to achieve

approximately 1500 resonance units. Immobilization of integrins and BSA were performed in 0.1M sodium acetate, pH4.5. Unreacted N-hydroxysuccinimide groups were quenched in all flow cells with 1M ethanolamine, pH 8.5 (10 µL/minute for 10 minutes). Upon stabilization of the baseline signal, kinetic binding experiments were run in duplicate with Fn fragments, full length Fn, or Ln as the flow analytes. Various concentrations for each Fn fragment (10µM-1nM) were flowed at 30µL/minute for 5 minutes immediately followed by a 10-minute dissociation phase. Binding experiments were performed in 10mM HEPES, 150mM NaCl, 0.0001% Triton-X 100, and 2mM each $MgCl_2$ and $MnCl_2$, pH 7.4. Experiments to determine the role of divalent cations in Fn fragment/$\alpha 3\beta 1$ integrin interactions were performed in 10mM HEPES, 150mM NaCl, 0.0001% Triton-X 100, and 2mM EDTA. Between each injection, the surface was regenerated with two 30 second pulses (10µL/minute) of 20mM EDTA and 1M NaCl (pH6.0). At least two independent SPR experiments were performed with varying Fn fragment injection order to rule out binding trends associated with injection sequence.

SPR analysis and evaluation

SPR sensorgrams were analyzed with the aid of Scrubber 2 and ClampXP software (Center for Biomolecular Interactions Analysis, University of Utah). (29-31) Reference cell responses were subtracted from corresponding active response curves. Double-referenced curves were acquired by further subtracting the reference cell blank buffer injections from each reference-subtracted response curve. (32) The resulting curves were then analyzed and fitted to the kinetic models. Kinetic modeling and simulations were performed with ClampXP software with the Langmuir 1:1 model or the heterogeneous surface model; globally fitted parameters were determined for each kinetic dataset per Fn

fragment. Equilibrium binding constants were calculated from fitted kinetic constants. Goodness of fit for each model was determined by evaluating the residual plots and residual sum of squares.

Cell spreading and α3β1 integrin binding

In order to determine the role of Fn fragments in epithelial cell spreading, RLE-6TN cells were cultured on FnIII9'10 (2μM), FnIII^{9R-A}10 (2μM), FnIII9^{2G}10 (2μM), FnIII9^{4G}10 (2μM), Fn (0.1μM), or Ln (0.1μM) coated, hd-BSA blocked coverslips in serum-free DMEM/F12 media for 3 hours and fixed with 4% formaldehyde. The concentration of Fn was chosen based on previous studies showing similar binding of an antibody specific to the 7-10 type III repeats of Fn (clone HFN7.1a1) (13) to Fn coated at 0.1μM and the Fn fragments at 2μM concentrations. The concentration of Ln was chosen based on ELISAs showing saturation of the surface using 0.1μM. Cells were washed with PBS, fixed with 4% formaldehyde, permeabilized with 0.2% Triton-X 100 and then blocked with 10% goat serum. Integrin α3 (Ralph 3.2) antibodies were incubated overnight at 4°C then washed thoroughly with PBS + 0.2% Tween-20. Secondary antibodies (Alexa-Fluor-488 goat-anti-mouse, Invitrogen; FITC-conjugated goat anti-Armenian hamster, Santa-Cruz Biotech) were incubated for 1 hour then washed thoroughly with PBS + 0.2% Tween-20. Actin was stained with Texas-red phalloidin (Invitrogen) and nuclei were stained with Hoescht stain (Invitrogen). Coverslips were mounted and images acquired with a Nikon Eclipse (TiE) inverted fluorescence microscope at 100X magnification (PlanApo 100X, 1.4 NA oil-immersion objective) with a CoolSNAP HQ2 Monochromatic CCD camera. Representative images are presented. Area and perimeter of individual cells was determined for each condition

using Image J (NIH Freeware) image processing software, and circularity was determined using the equation circularity = 4π(area/perimeter^2). Three independent images were analyzed for each condition, and at least 10 cells were analyzed per image. Data is pooled from all 3 images analyzed per condition. **S**tatistical analysis was performed by multi-variate ANOVA using Prism (Graphpad Software Inc., La Jolla, CA, USA). Statistical significance was achieved for $p<0.05$.

Results

Kinetic binding models

SPR with soluble recombinant integrin immobilized to the surface of the sensor chip was utilized to determine the role of FnIII9 in integrin $\alpha3\beta1$ interactions with Fn. (**Figure 4.1**) The experimental data was fit with the use of both a Langmuir 1:1 model and a heterogeneous surface model to account for variable conformational state of immobilized integrin that can result from amine coupling.

Table 4.1: FnIII9'10 variants produced and function

Fragment	**Sequence 1373-1423 of FnIII9-10**	**Role**
FnIII9'10	DRVPHSRNSITLTNLTPGTEYVVSIVALN GREESP**P**LIGQQSTVSDVRPD	Leu1408 to Pro; Stabilizes relative positions of FnIII9 and FnIII10
FnIII$^{9R\text{-}A}$10	DRVPHS**A**NSITLTNLTPGTEYVVSIVALN GREESP**P**LIGQQSTVSDVRPD	Arg to Ala point mutation in PHSRN site
FnIII^{2G}10	DRVPHSRNSITLTNLTPGTEYVVSIVALN GREESP**P**LIGQQSTVS**GG**DVRPD	Increased distance between FnIII9 and FnIII10
FnIII^{4G}10	DRVPHSRNSITLTNLTPGTEYVVSIVALN GREESP**P**LIGQQSTVS**GGGG**DVRPD	Increased distance between FnIII9 and FnIII10

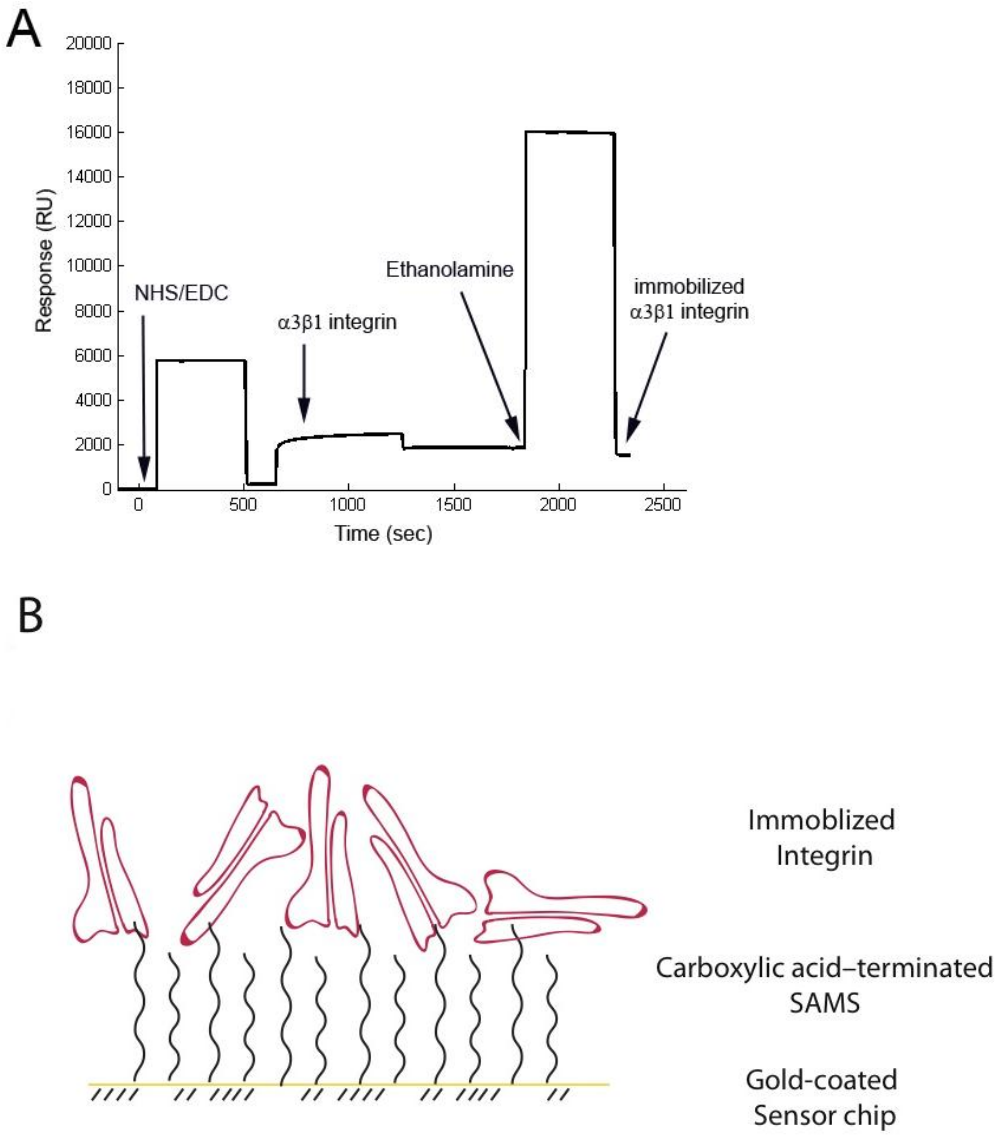

Figure 4.1: Integrin α3β1 immobilization: To analyze integrin binding to FnIII9'10 variants, recombinant soluble integrin was immobilized onto a Biacore sensor chip to achieve approximately 1500 resonance units. (**A**) Schematic of immobilized integrins on surface. Amine coupling can result in random orientation of immobilized integrins (**B**)

In comparing model simulation results, the heterogeneous ligand model fit the experimental binding data better than the Langmuir 1:1 model. Response, simulation curves, and residual plots for a single set of experimental data are presented here (FnIII9'10 binding to integrin α3β1; **Figure 4.2**). The range for the 1:1 Langmuir model (5.85-0.23; **Table 4.1**) was higher than the heterogeneous ligand model (1.5-0.18; **Table 4.2**), suggesting that the fitted heterogeneous ligand model deviated less from the experimental data. In addition, graphically plotting the residuals, which are defined as the difference between experimental data and fitted curves, over time showed that the residuals for 1:1 Langmuir model followed a systematic trend (**Figure 4.2C**), indicative of fitting an inappropriate model to the experimental data. (33) In contrast, the residuals for the heterogeneous model were lower and more randomly distributed (**Figure 4.2D**), indicating that this model more adequately describes the binding response curves. (29, 33)

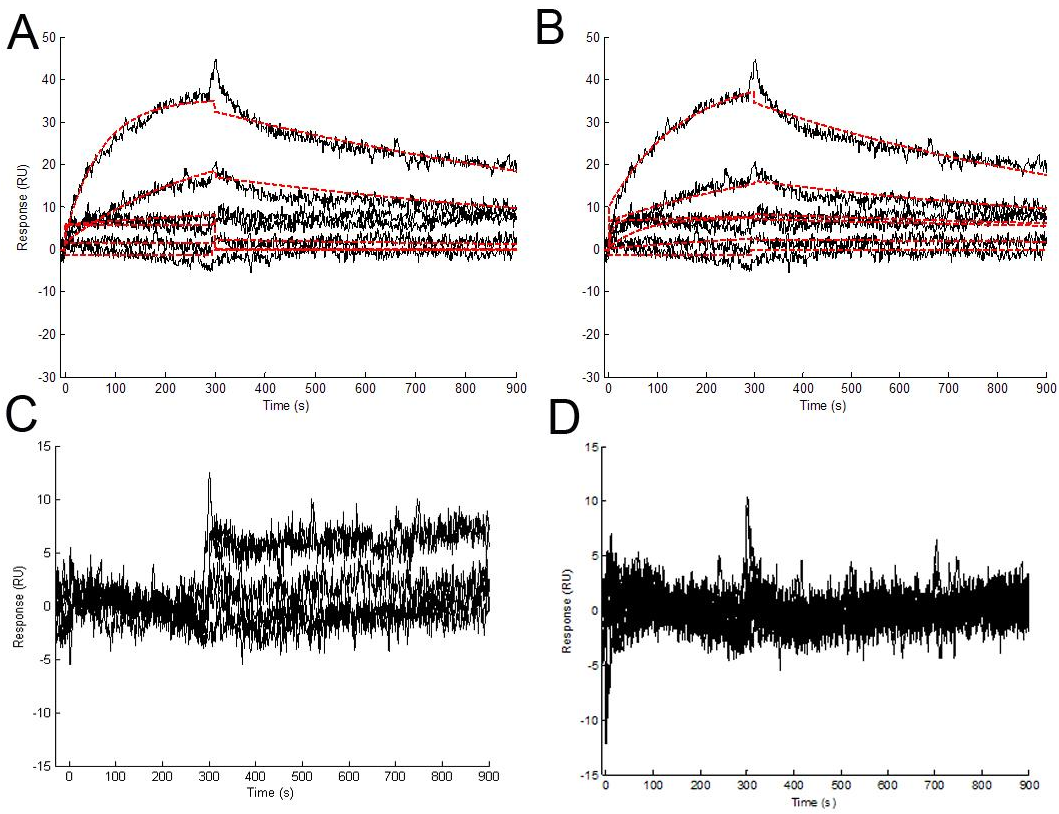

Figure 4.2: Determination of kinetic binding model: Experimental SPR sensorgrams were fit to both a 1:1 Langmuir binding model (**A**) and a heterogeneous surface model (**B**). Representative fits of sensorgrams obtained from FnIII9'10 binding to integrin α3β1 and resulting residuals (**C-D**) are shown. Solid lines indicate experimental SPR response curves, and dashed red curves indicate fitted models.

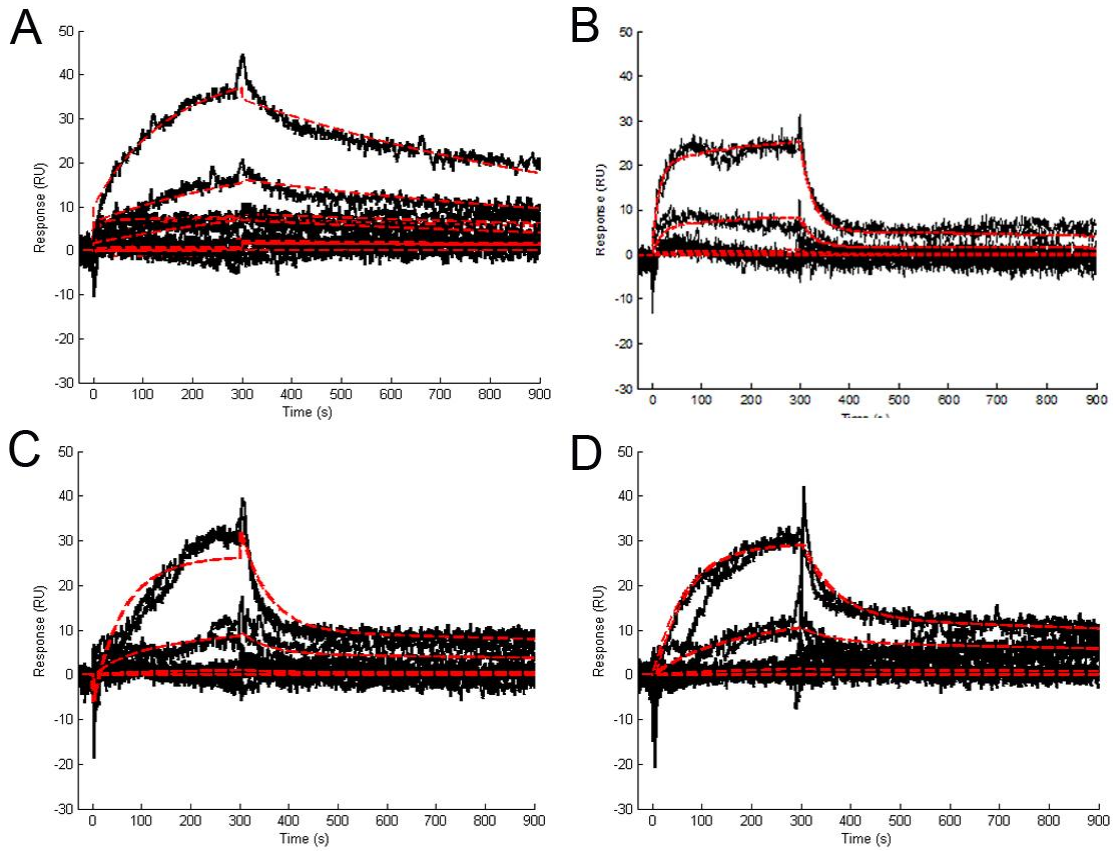

Figure 4.3: FnIII9'10 variant binding to immobilized integrin α3β1: Response curves obtained from FnIII9'10 variants binding to immobilized integrin α3β1 were fit to a heterogeneous surface model. Experimental response curves and resulting fits are shown for FnIII9'10 (**A**), FnIII$^{9R\text{-}A}$10 (**B**), FnIII^{2G}10 (**C**), and FnIII^{4G}10 (**D**). Solid lines indicate experimental SPR response curves and dashed curves indicate fitted models.

Fitted α3β1 binding affinity parameters: Langmuir 1:1 model

Response curves obtained from all FnIII9'10 variants binding to integrin α3β1 were fit to both a 1:1 Langmuir binding model and a heterogeneous surface model; experimental response curves and heterogeneous surface fits are shown in **Figure 4.3**. The fitted parameters k_a ("on rate") and $k_{d,}$ ("off rate"), calculated Kd and residual sum of squares of the fit of each FnIII9'10 variant, Fn, and Ln using a Langmuir 1:1 model are displayed in **Table 4.2**. Comparing k_d values obtained from a Langmuir 1:1 model, FnIII9'10 was

found to have the lowest k_d of all FnIII9'10 variants analyzed at 7.1 x 10^{-4} s^{-1}. Increasing the linker region between the 9th and 10th type III repeats with either 2 Gly residues or 4 Gly residues resulted in an increase in the k_d to 10.8 x 10^{-4} s^{-1} and 27.5 x 10^{-4} s^{-1}, respectively, indicating that increasing the space between the PHSRN and RGD sites disrupts the interactions between FnIII9-10 domains and integrin α3β1. Furthermore, an Arg to Ala point mutation within the PHSRN site results in an eight-fold increase in k_d to 59 x 10^{-4} s^{-1}. Equilibrium dissociation constants, which take k_d and k_a values into account, were calculated for each analyte. FnIII9'10 was found to have the lowest K_d, 32nM. Direct disruption in the PHSRN site resulted in a fivefold increase in K_d to 172nM, while increasing the spacing between the 9th and 10th type III repeats by either 2 or 4 Gly residues resulted in a three and 26-fold increase to 97nM and 855nM, respectively. The K_d value for Ln was the lowest for all analytes, 14nM, which was expected, as Ln is thought of as the dominant ligand for integrin α3β1; however, Fn was found to have a high affinity for the integrin, with a K_d of 24nM. These results indicate that Fn does bind integrin α3β1 with a high affinity, and this binding is dependent on the positioning and spatial orientation of the PHSRN and RGD sites.

Table 4.2: K_d values: α3β1: Langmuir 1:1 model

Analyte	k_a*10^{-4}	k_d*10^4	$Kd*10^9$	RSS
FnIII9'10	4.3+/- 0.3	7.1+/- 0.29	**32**	1.7
$FnIII^{9R-A}10$	0.49+/- 0.44	59+/- 8.4	**172**	2.56
$FnIII^{2G}10$	1.12+/- 1.12	10.8+/- 5.2	**97**	2.52
$FnIII^{4G}10$	0.311+/- 0.19	27.5+/- 1.7	**855**	5.85
Fn	1.0+/- 0.81	2.5+/- 0.9	**24**	2.5
Ln	3.47+/- 1.8	4.87+/- 2.46	**14**	0.223

Fitted α3β1 binding affinity parameters: heterogeneous surface model

Crystal structures of integrins binding to their ligand show that 1 integrin binds to 1 ligand. Therefore, it was expected that the data would be modeled best by a simple Langmuir 1:1 interaction. However, examination of the residual plots obtained from the Langmuir 1:1 fit showed that the residuals followed a systematic trend (**Figure 4.2C**), indicating an inappropriate model for the experimental data. The observed lack of fitting of the Langmuir 1:1 model could be the result of the presence of both high and low affinity states of the receptor on the surface. Integrins inherently can present both high and low affinity states, which can result in a heterogeneous surface displaying complex binding kinetics. Furthermore, the amine coupling procedure utilized for immobilization of integrin onto the surface can result in a random receptor orientation (**Figure 4.1B)** and heterogeneous surface, also presenting both high and low affinity states of receptor. In order to account for the possibility of both high and low affinity states of the integrin, a heterogeneous surface model was utilized to fit the response curves. As shown in **Figure 4.2**, the heterogeneous surface model results in a better fit to the experimental response curves than a simple Langmuir 1:1 model, as demonstrated by lower and more randomly distributed residual plots (**Figure 4.2.D**). The fitted parameters k_{a1}, k_{d1}, k_{a2}, k_{d2}, calculated K_{d1} and K_{d2}, and residual sum of squares of the fit of each FnIII9'10 variant, Fn, and Ln using a heterogeneous surface model are displayed in **Table 4.3.** As expected, examination of the fitted parameters obtained from a heterogeneous surface model demonstrates a high affinity binding event and a secondary low affinity binding event. The respective contribution of high affinity and low affinity binding to total binding using the heterogeneous surface model can be seen graphically in **Figure 4.3**, which

shows simulation sensorgrams generated by the heterogeneous surface model for FnIII9'10 binding to integrin α3β1. Lower affinity states of the integrin result in a series of lower affinity binding events, described collectively by k_{a2}, k_{d2}, and the resulting calculated K_{d2}.

Table 4.3: K_d values: α3β1: Heterogeneous surface model

Analyte	$k_{a1}*10^{-4}$	$k_{d1}*10^{4}$	$K_{d1}*10^{9}$	$k_{a2}*10^{-4}$	$k_{d2}*10^{4}$	$K_{d1}*10^{9}$	RSS
FnIII9'10	211+/- 365	128+/- 194	**6.06**	31.4+/-34.9	192+/- 32.1	**61.0**	1.5
$FnIII^{9R-A}10$	48.2+/- 43.3	757+/-93.9	**157**	0.63+/- 0.78	125+/- 20.8	**1978**	2.38
$FnIII^{2G}10$	69.3+/- 117	596+/- 102	**85.9**	46.4+/- 79.3	54.3+/- 86.4	**11.7**	2.50
$FnIII^{4G}10$	15.1+/- 23.8	748+/- 123	**495**	180.2+/- 30	45.4+/- 72.7	**24.9**	4.1
Fn	1.62+/- 0.6	2.43+/- 0.66	**13.1**	21.8+/-30.6	1341+/- 178	**615**	2.0
Ln	3.1+/- 1.78	2.27+/- 2.62	**7.85**	225+/-318	304+/-178	**13.5**	0.18

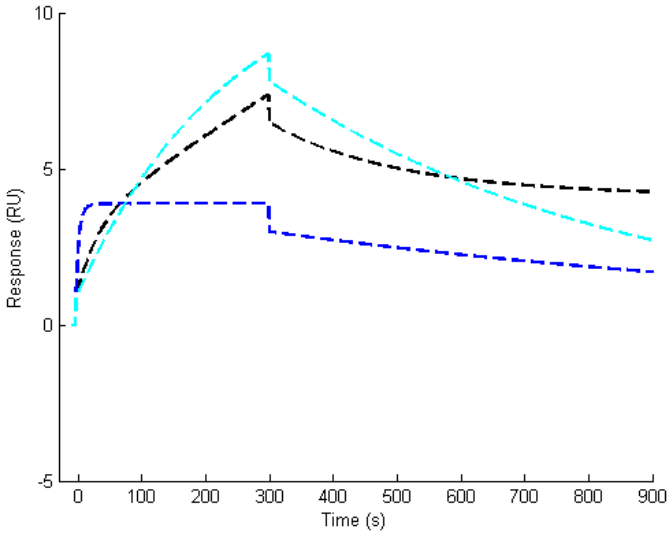

Figure 4.4: Contribution of high affinity and low affinity binding in heterogeneous surface model. Simulation sensorgrams generated by the heterogeneous surface model for FnIII9'10 to integrin α3β1. The combined response, denoted by the black line, is a sum of analyte-ligand complexes AB (cyan line) and AB* (blue line).

Evaluation of the fitted parameters for the high affinity binding events demonstrates trends similar to those obtained through the Langmuir 1:1 fitting. Once again, it was found that FnIII9'10 had the lowest k_{d1} of all FnIII9'10 variants analyzed, with a value of 128 x 10^{-4} s^{-1}. Increasing the linker region between the 9th and 10th type III repeats with either 2 Gly residues or 4 Gly residues, resulted in an increase in the k_d to 596 x 10^{-4} s^{-1} and 748 x 10^{-4} s^{-1} respectively, indicating increasing the space between the PHSRN and RGD sites disrupts the interactions between FnIII9-10 domains and integrin α3β1. Furthermore, the disrupting Arg to Ala point mutation within the PHSRN site resulted in an increased k_d of 757 x 10^{-4} s^{-1}. Equilibrium dissociation constants, which takes k_{d1} and k_{a1} values into account, were calculated for each analyte for the high affinity binding state, and FnIII9'10 was again found to have the lowest K_{d1} of all FnIII9'10 variants, with a value of 6.06nM. Direct disruption in the PHSRN site resulted in a 26-fold increase in K_d to 157nM, while increasing the spacing between the 9th and 10th type III repeats by either 2 or 4 Gly residues resulted in a 14- and 82-fold increase to 85.9nM and 495nM, respectively. The K_d value for Ln was the lowest for all analytes, 7.85nM, while Fn was also found to have a high affinity for the integrin, with a K_d of 13.1nM. Focusing on the high affinity binding parameters obtained from the heterogeneous surface model shows similar trends to those observed through the Langmuir 1:1 model, and demonstrates that stabilization of the 9th and 10th type III domains of Fn results in affinities for integrin α3β1 similar to those observed for the classical α3β1 ligand Ln.

<u>FnIII9'10 binding to integrin α3β1 is dependent on the presence of divalent cations</u>

Integrin binding is typically dependent on the presence of divalent cations, (19, 34) and as such all SPR experiments were performed in the presence of 2mM each $MgCl_2$ and

$MnCl_2$. To confirm that integrin binding to FnIII9'10 variants is dependent on the presence of divalent cations, binding events were characterized in the presence of 2 mM EDTA. Experimental response curves for FnIII9'10 variants in the presence of 2mM each $MgCl_2$ and $MnCl_2$ are shown in **Figure 4.4A**, and experimental response curves in the presence of EDTA are shown in **Figure 4.4B**. In the presence of EDTA, minimal binding to integrin α3β1 was observed, indicating as expected, that FnIII9'10 binding is dependent on the presence of divalent cations.

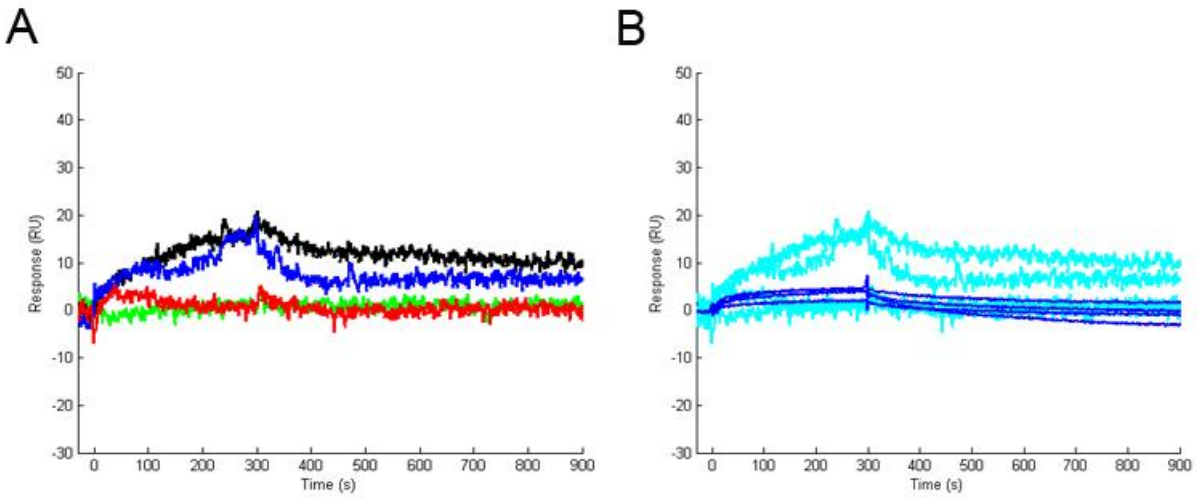

Figure 4.4: FnIII9'10 variant binding to integrin α3β1 is dependent on the presence of divalent cations. Experimental response curves for FnIII9'10, FnIII$^{9R\text{-}A}$10, FnIII^{2G}10, and FnIII$^{9R\text{-}A}$10 binding to integrin α3β1 are shown in the absence (**A**) or presence (**B**) of 2 mM EDTA. FnIII9'10, FnIII$^{9R\text{-}A}$10, FnIII^{2G}10, and FnIII^{4G}10 responses in the absence of EDTA are shown in black, red, blue, and green lines respectively (**A**). The same response curves are shown in cyan (**B**) superimposed with response curves in the presence of EDTA shown in blue.

<u>K_d values for control integrins</u>

The role of the PHSRN site, as well as the relative orientation with respect to the RGD site, is critical for α5β1 binding to Fn, while binding to αvβ3 only requires the RGD site.

To confirm these previous reports, binding of FnIII9'10, FnIII^{9R-A}10, FnIII9^{2G}10, FnIII9^{4G}10, Fn, and Ln to immobilized integrin α5β1 and αvβ3 was investigated. Curves were fit to a simple Langmuir 1:1 model. Experimental curves and calculated K_d values are shown in **Figure 4.5**. As expected, α5β1 binding was found to depend on the presence and spatial orientation of the PHSRN site. Equilibrium dissociation constants were calculated for each analyte, and FnIII9'10 was found to have the lowest K_d of all FnIII9'10 variants, with a value of 12.9 nM. FnIII^{9R-A}10, FnIII9^{2G}10 , FnIII9^{4G}10 were found to have K_d values of 3100 nM, 417 nM, and 2530 nM, respectively. Fn and Ln were found to have K_d values of 44 nM and 519 nM, respectively. Though Ln is not typically regarded as a ligand for α5β1, there have been previous reports demonstrating interactions between these molecules. (35) Analysis of binding parameters using the heterogeneous surface model demonstrates that these interactions are largely due to the secondary binding events.

Evaluation of FnIII9'10 binding to integrin αvβ3 was not dependent on the presence or spatial orientation of the PHSRN site, which was expected as αvβ3 interactions occur through the RGD site alone. Equilibrium dissociation constants were calculated for each analyte, and K_d values were within the same range for all FnIII9'10 variants. FnIII9'10, FnIII^{9R-A}10, FnIII9^{2G}10, and FnIII9^{4G}10 were found to have K_d values of 59.6 nM, 25.9 nM, 44.5 nM, and 21.5nM, respectively. Though all values were comparable, minor differences in binding were observed, and, interestingly, an opposite trend from α5β1 binding was observed, such that affinity for FnIII9'10 < FnIII9^{2G}10 < FnIII^{9R-A}10 < FnIII9^{4G}10. Fn was found to have a K_d value of 9.59 nM, while only minimal binding was observed to Ln.

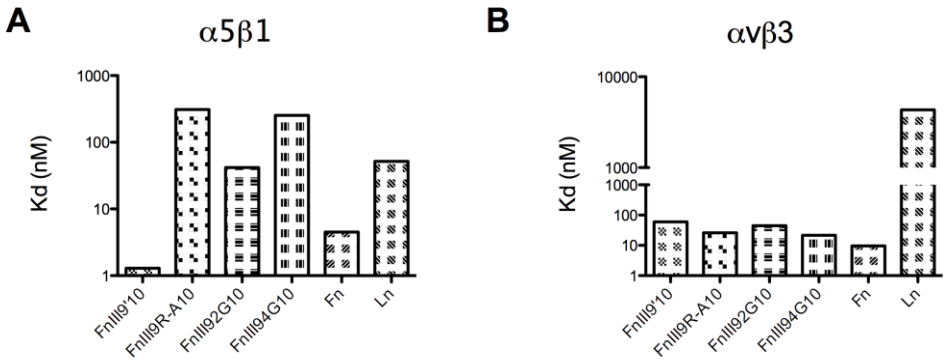

Figure 4.6: FnIII9'10 variants bind to control integrins α5β1 and αvβ3 as previously described. K_d values for FnIII9'10 variants, Fn, and Ln interactions with immobilized integrin α5β1 (**A**) or αvβ3 (**B**) were determined using a Langmuir 1:1 model.

Epithelial cell spreading on FnIII9'10 variants

To characterize α3β1 binding to FnIII9'10 variants in a cell system and subsequent changes in cell spreading, RLE-6TN cells, an alveolar epithelial cell line, were cultured on Fn fragments, Fn, and Ln for a period of 3 hours and then stained for integrin subunits α3 and actin. This cell type highly expresses α3β1 and also expresses α5β1 and several αv integrins. Cells cultured on Ln and FnIII9'10 displayed staining for α3, while cells cultured on Fn and all other FnIII9'10 variants displayed minimal staining for α3 integrins (**Figure 4.6**). Cells cultured on FnIII9'10 displayed a rounded, cuboidal morphology and diffuse staining for actin, which was similar to cellular responses on Ln.

Cells cultured on Fn and all other FnIII9'10 variants displayed were more spread and began to display aligned actin filaments. Cell shape was further characterized through analysis of circularity, with values closer to 1 indicating a more rounded cell. Cells cultured on FnIII9'10 exhibited a circularity value of 0.79, which was similar to cells cultured on Ln, with a circularity value of 0.73. Cells cultured on Fn and all other FnIII9'10 variants were found to have significantly lower circularity values compared to cells cultured on FnIII9'10 and Ln ($p < 0.001$), with values ranging from 0.65 to 0.61.

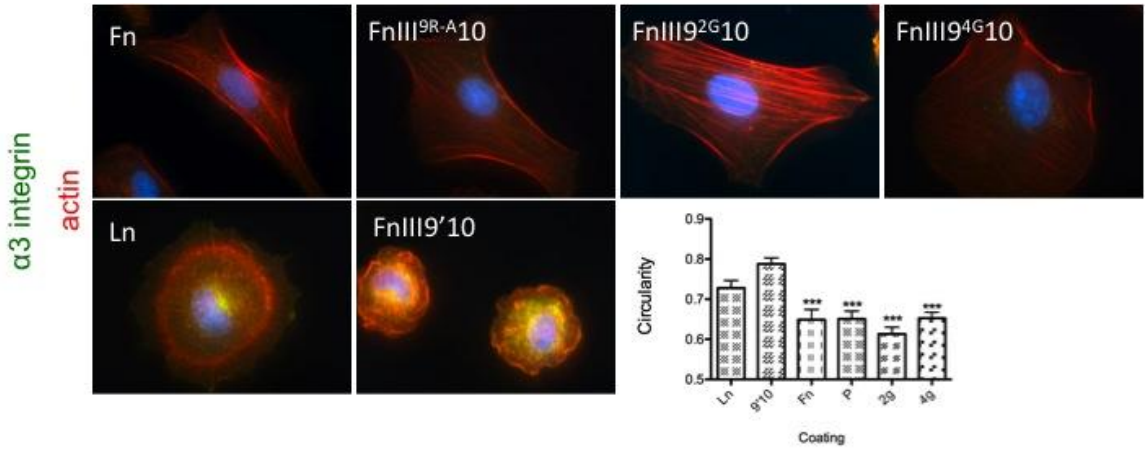

Figure 4.7: Cell spreading on Fn mutants. To evaluate cell-surface α3β1 integrin binding to FnIII9'10 variants and control surfaces and cell spreading responses, RLE-6TN cells were cultured on FnIII9'10, FnIII^{9R-A}10, FnIII^{2G}10, FnIII^{9R-A}10, Fn, or Ln coated surfaces for 3 hours. α3β1 integrin binding was visualized through immunofluorescence staining (green), and actin (red) was visualized through staining with Texas-red-X conjugated phallodin. Circularity was calculated to measure differences in cell spreading/shape. *** represents $p<0.001$ compared to FnIII9'10.

Discussion

These studies show that Fn binds integrin α3β1 in cell-free system, and this binding is dependent on the presence of the PHSRN site and is dependent on the spacing relative to the RGD site. The results from this study provide significant insights into the role of changes in Fn conformation, such as those resulting from molecular unfolding, in interactions between the central cell binding domain of Fn, i.e. the 9^{th} and 10^{th} type III repeats, and what is classically considered a Ln receptor, integrin α3β1. These findings have implications in dynamic epithelial tissue wound healing responses since integrin α3β1 is highly expressed by many epithelial cells, which interact with Fn predominantly during wound healing.

The role of the PHSRN sites in α5β1 integrin binding to Fn is well characterized, and in addition, this site has been shown to enhance binding of additional integrins, as illustrated by its role in facilitating strong interactions between Fn and the platelet integrin αIIbβ3. (36) Studies suggest that the PHSRN site acts to stabilize the high affinity conformation of the RGD site required for α5β1 integrin binding. The results presented in this aim show that α3β1 integrin binding to Fn is also dependent on the relative positioning of the RGD and PHSRN sites. Previous investigations to elucidate potential ligands for integrin α3β1 have been conflicting regarding interactions with Fn. Many of these studies involve cell based attachment assays, which are at times difficult to interpret, especially in the case of integrin α3β1, in which binding affinity to ECM ligands is influenced by the presence of additional integrins. (37) Studies utilizing soluble integrins in cell free systems are also conflicting. For example, studies by Eble *et al.* showed minimal α3β1 binding to Fn. (18) Interestingly, these studies showing

minimal binding were performed on tissue culture plastic, while several studies confirming Fn/α3β1 interactions utilized ECM affinity columns. (19, 38) Furthermore, the studies presented here exploring ATII cell binding to full length Fn show minimal staining for α3β1. The findings of this aim possibly bridge these discrepancies. Fn has been shown to undergo unfolding upon adsorption as a consequence of the hydrophobic effect and the protein adopting its lowest energy state. (39-42) Such unfolding events likely disrupt the relative positioning of the RGD and PHSRN sites, and according to the SPR studies presented here, would disrupt α3β1 binding. This conclusion is further supported by the fact that full length Fn in solution binds α3β1 exceptionally well, as indicated by the presented SPR results.

Because α3β1 and α5β1 integrin are involved in epithelial wound repair, these findings that α3β1 integrin, like α5β1 integrin, binds to Fn in a synergy dependent manner have implications in cell interactions during wound healing. Alveolar epithelial type II cells (ATII) only express α5β1 integrin in response to injury; (43) therefore, it is likely that integrin α3β1 binds Fn with great affinity in this cell type in early wound repair before α5β1 integrin is highly expressed. Though α5β1 appears to be the main Fn receptor during alveolar wound repair, integrin blocking experiments with airway epithelial cells showed that in addition to α5, β1, and Fn blocking antibodies, α3 blocking antibodies also resulted in a significant decrease in wound repair. (43) Interestingly, it has been shown that integrin α3β1 binding to Fn can be affected by the presence of α5β1 integrin such that α3β1 binding is low in cells expressing α3β1 and α5β1 at comparable levels, but α3β1 binding to Fn is greatly enhanced in H69 cells that highly express α3β1 compared to other integrins. (19) These reports, taken along with

the findings of this aim, suggest that α3β1 binding to Fn may modulate wound repair by facilitating binding to ECM in a wound healing environment as the ECM composition transitions from predominantly Ln to high levels of Fn.

Control SPR experiments demonstrate similar affinities of all FnIII9'10 variants for integrin αvβ3, with all FnIII9'10 variants showing affinities in the 10s of nM range. However, small variations were observed, with a trend of increasing affinity opposite of those observed with PHSRN-dependent integrins α3β1 and α5β1, such that affinity of FnIII9'10 < FnIII9^{2G}10 < FnIII^{9R-A}10 < FnIII9^{4G}10. This indicates that increasing the linker region between the 9th and 10th type III repeats or mutations in the PHSRN site may make the RGD site more accessible to αvβ3, but more rigorous studies would be required to confirm this interpretation. The RGD and PHSRN sites have previously been described as an on/off "switch" for α5β1 binding to Fn. These findings shown that in the context of epithelial cells, destabilizing the PHSRN and RGD sites may turn the switch off for α3β1/α5β1 binding and on for αv integrin binding. Highlighting the significance of such an integrin switch, binding of α3β1/α5β1 integrins have markedly different effects on epithelial phenotype compared to αv integrin binding. Integrin α3β1 epithelial cell interactions are associated with maintenance of epithelial phenotype and wound healing, while interactions with αv integrins have been associated with abhorrent wound healing, scar tissue formation, epithelial to mesenchymal transitions, and even tumor metastasis. (17, 24, 26, 44)

Using SPR, these results show for the first time that integrin α3β1 binds FnIII9'10 with high affinity, similar to affinity seen for the classical α3β1 ligand Ln, in a PHSRN-dependent manner. Furthermore, the physiological relevance of these interactions are

confirmed by demonstrating differences in cell spreading in epithelial cells cultured on FnIII9’10 compared to cells cultured on FnIII9’10 with mutation in the PHRSN site or alterations in the spatial orientation of RGD and PHSRN. These studies provide insights into how Fn interactions can contribute to normal vs. pathological wound healing.

References

1. Humphries J, Byron, A, Humphries, M. Integrin ligands at a glance. J Cell Sci.119:3901-3. 2006.

2. Ruoslahti E. RGD and other recognition sequences for integrins. Annu Rev Cell Dev Biol.12:697-715. 1996.

3. Humphries MJ. The molecular basis and specificity of integrin-ligand interactions. J Cell Sci.97 (Pt 4):585-92. 1990.

4. Plow EF, Haas TA, Zhang L, Loftus J, Smith JW. Ligand binding to integrins. The Journal of biological chemistry.275:21785-8. 2000.

5. Mao Y, Schwarzbauer JE. Fibronectin fibrillogenesis, a cell-mediated matrix assembly process. Matrix Biol.24:389-99. 2005.

6. Pankov R YK. Fibronectin at a glance. J Cell Sci.115:3861-3. 2002.

7. Baneyx G, Baugh L, Vogel V. Fibronectin extension and unfolding within cell matrix fibrils controlled by cytoskeletal tension. Proc Natl Acad Sci U S A.99:5139-43. 2002.

8. Barker TH, Baneyx G, Cardo-Vila M, Workman GA, Weaver M, Menon PM, et al. SPARC regulates extracellular matrix organization through its modulation of integrin-linked kinase activity. The Journal of biological chemistry.280:36483-93. 2005.

9. Mardon HJ, Grant KE. The role of the ninth and tenth type III domains of human fibronectin in cell adhesion. FEBS letters.340:197-201. 1994.

10. Mould AP, Askari JA, Aota S, Yamada KM, Irie A, Takada Y, et al. Defining the topology of integrin alpha5beta1-fibronectin interactions using inhibitory anti-alpha5 and anti-beta1 monoclonal antibodies. Evidence that the synergy sequence of fibronectin is recognized by the amino-terminal repeats of the alpha5 subunit. The Journal of biological chemistry.272:17283-92. 1997.

11. Krammer A, Craig D, Thomas WE, Schulten K, Vogel V. A structural model for force regulated integrin binding to fibronectin's RGD-synergy site. Matrix Biol.21:139-47. 2002.

12. Altroff H, Schlinkert R, van der Walle CF, Bernini A, Campbell ID, Werner JM, et al. Interdomain tilt angle determines integrin-dependent function of the ninth and tenth FIII domains of human fibronectin. The Journal of biological chemistry.279:55995-6003. 2004.

13. Martino MM, Mochizuki M, Rothenfluh DA, Rempel SA, Hubbell JA, Barker TH. Controlling integrin specificity and stem cell differentiation in 2D and 3D environments through regulation of fibronectin domain stability. Biomaterials.30:1089-97. 2009.

14. Khew ST, Zhu XH, Tong YW. An integrin-specific collagen-mimetic peptide approach for optimizing Hep3B liver cell adhesion, proliferation, and cellular functions. Tissue engineering.13:2451-63. 2007.

15. Grant RP, Spitzfaden C, Altroff H, Campbell ID, Mardon HJ. Structural requirements for biological activity of the ninth and tenth FIII domains of human fibronectin. J Biol Chem.272:6159-66. 1997.

16. Brown AC, Rowe JA, Barker TH. Guiding epithelial cell phenotypes with engineered integrin-specific recombinant fibronectin fragments. Tissue Eng Part A.17:139-50.

17. Sheppard D. Functions of pulmonary epithelial integrins: from development to disease. Physiological reviews.83:673-86. 2003.

18. Eble JA, Wucherpfennig KW, Gauthier L, Dersch P, Krukonis E, Isberg RR, et al. Recombinant soluble human alpha 3 beta 1 integrin: purification, processing, regulation, and specific binding to laminin-5 and invasin in a mutually exclusive manner. Biochemistry.37:10945-55. 1998.

19. Elices MJ, Urry LA, Hemler ME. Receptor functions for the integrin VLA-3: fibronectin, collagen, and laminin binding are differentially influenced by Arg-Gly-Asp peptide and by divalent cations. The Journal of cell biology.112:169-81. 1991.

20. Kaufmann R, Frosch D, Westphal C, Weber L, Klein CE. Integrin VLA-3: ultrastructural localization at cell-cell contact sites of human cell cultures. The Journal of cell biology.109:1807-15. 1989.

21. Sriramarao P, Steffner P, Gehlsen KR. Biochemical evidence for a homophilic interaction of the alpha 3 beta 1 integrin. The Journal of biological chemistry.268:22036-41. 1993.

22. Kim KK, Wei Y, Szekeres C, Kugler MC, Wolters PJ, Hill ML, et al. Epithelial cell alpha3beta1 integrin links beta-catenin and Smad signaling to promote myofibroblast formation and pulmonary fibrosis. J Clin Invest.119:213-24. 2009.

23. Kim Y, Kugler MC, Wei Y, Kim KK, Li X, Brumwell AN, et al. Integrin alpha3beta1-dependent beta-catenin phosphorylation links epithelial Smad signaling to cell contacts. The Journal of cell biology.184:309-22. 2009.

24. Lubman RL, Zhang XL, Zheng J, Ocampo L, Lopez MZ, Veeraraghavan S, et al. Integrin alpha(3)-subunit expression modulates alveolar epithelial cell monolayer formation. American journal of physiology.279:L183-93. 2000.

25. Kreidberg JA, Donovan MJ, Goldstein SL, Rennke H, Shepherd K, Jones RC, et al. Alpha 3 beta 1 integrin has a crucial role in kidney and lung organogenesis. Development.122:3537-47. 1996.

26. Kim KK, Kugler MC, Wolters PJ, Robillard L, Galvez MG, Brumwell AN, et al. Alveolar epithelial cell mesenchymal transition develops in vivo during pulmonary fibrosis and is regulated by the extracellular matrix. Proc Natl Acad Sci U S A.103:13180-5. 2006.

27. Stabenfeldt SE, Gossett JJ, Barker TH. Building better fibrin knob mimics: an investigation of synthetic fibrin knob peptide structures in solution and their dynamic binding with fibrinogen/fibrin holes. Blood.116:1352-9.

28. Petrie TA, Capadona JR, Reyes CD, Garcia AJ. Integrin specificity and enhanced cellular activities associated with surfaces presenting a recombinant fibronectin fragment compared to RGD supports. Biomaterials.27:5459-70. 2006.

29. Morton TA, Myszka DG. Kinetic analysis of macromolecular interactions using surface plasmon resonance biosensors. Methods Enzymol.295:268-94. 1998.

30. Joss L, Morton TA, Doyle ML, Myszka DG. Interpreting kinetic rate constants from optical biosensor data recorded on a decaying surface. Anal Biochem.261:203-10. 1998.

31. Myszka DG, Morton TA. CLAMP: a biosensor kinetic data analysis program. Trends Biochem Sci.23:149-50. 1998.

32. Myszka DG. Improving biosensor analysis. J Mol Recognit.12:279-84. 1999.

33. Cornish-Bowden A. Detection of errors of interpretation in experiments in enzyme kinetics. Methods.24:181-90. 2001.

34. Mould AP, Akiyama SK, Humphries MJ. Regulation of integrin alpha 5 beta 1-fibronectin interactions by divalent cations. Evidence for distinct classes of binding sites for Mn2+, Mg2+, and Ca2+. The Journal of biological chemistry.270:26270-7. 1995.

35. Rao SP, Gehlsen KR, Catanzaro A. Identification of a beta 1 integrin on Mycobacterium avium-Mycobacterium intracellulare. Infect Immun.60:3652-7. 1992.

36. Chada D, Mather T, Nollert MU. The synergy site of fibronectin is required for strong interaction with the platelet integrin alphaIIbbeta3. Ann Biomed Eng.34:1542-52. 2006.

37. Hodivala-Dilke KM, DiPersio CM, Kreidberg JA, Hynes RO. Novel roles for alpha3beta1 integrin as a regulator of cytoskeletal assembly and as a trans-dominant inhibitor of integrin receptor function in mouse keratinocytes. The Journal of cell biology.142:1357-69. 1998.

38. Elices MJ, Hemler ME. The human integrin VLA-2 is a collagen receptor on some cells and a collagen/laminin receptor on others. Proc Natl Acad Sci U S A.86:9906-10. 1989.

39. Underwood PA, Steele JG, Dalton BA. Effects of polystyrene surface chemistry on the biological activity of solid phase fibronectin and vitronectin, analysed with monoclonal antibodies. J Cell Sci.104 (Pt 3):793-803. 1993.

40. Pitt WG, Weaver DR, Cooper SL. Fibronectin adsorpton kinetics on phase segregated polyurethaneureas. J Biomater Sci Polym Ed.4:337-46. 1993.

41. Narasimhan C, Lai CS. Conformational changes of plasma fibronectin detected upon adsorption to solid substrates: a spin-label study. Biochemistry.28:5041-6. 1989.

42. Wolff C, Lai CS. Fluorescence energy transfer detects changes in fibronectin structure upon surface binding. Arch Biochem Biophys.268:536-45. 1989.

43. Herard AL, Pierrot D, Hinnrasky J, Kaplan H, Sheppard D, Puchelle E, et al. Fibronectin and its alpha 5 beta 1-integrin receptor are involved in the wound-repair process of airway epithelium. The American journal of physiology.271:L726-33. 1996.

44. Seftor, RE, Seftor, EA, Gehlsen, KR, Stetler-Stevenson, WG, Brown, PD, Ruoslahti, E, et al. Role of the alphavbeta3 integrin in human melanoma cell invasion. Proc Natl Acad Sci USA. 89:1557-1561. 1992.

CHAPTER 5

FIBRONECTIN-INDUCED EPITHELIAL TO MESENCHYMAL TRANSITION IS DEPENDENT ON INCREASED TISSUE STIFFNESS

Introduction

Epithelial to mesenchymal transition (EMT) is a fundamental hallmark of invasive pathologies such as cancer and fibrosis. EMT is also vital for proper development, whereas dysregulation of EMT leads to significant tissue and organ defects. As a consequence, a significant amount of effort has been devoted to understanding the mechanisms driving these drastic phenotypic shifts. EMT, the phenotypic transdifferentiation of cells from epithelial to mesenchymal lineages, is a highly orchestrated process involving the integration of biochemical signals from ECM receptors (integrins) and growth factor receptors like transforming growth factor-β (TGF-β) receptor and receptor tyrosine kinases. (1)

The contribution of biochemical components of the ECM in directing cell fate, and in particular EMT, is becoming more established through traditional cell biological studies. In particular, the ECM-associated growth factor TGF-β is highly implicated in EMT, (2-10) but only in the context of provisional matrices like fibrin and fibronectin (Fn). Epithelial cells cultured on laminin (Ln) substrates selectively undergo apoptosis in the presence of active TGFβ (4) and these responses appear to be a consequence of integrin specific engagement of the ECM. (11) Furthermore, there are several reports that suggest

epithelial cells will spontaneously undergo EMT when cultured on Fn. Potentially adding to the complexity, recent publications suggest that the physical/mechanical properties of the ECM, such as matrix stiffness, can in part regulate a host of cellular processes and phenotypes, from regulation of stem cell differentiation to malignant phenotypes. (12-17) Specifically, cells are able to sense the underlying mechanical properties of the ECM, such as compliance. (18, 19) In the case of compliance sensing, cells engage their actinomyosin contractile machinery in a manner that facilitates cell-ECM compliance matching. In other words, a cell may adjust its internal stress through contraction to "match" its external environment. (19) As a consequence of this mechano-homeostasis between the cell and its ECM, cells in increasingly rigid, or stiff, environments display increased activation of contractile signals like Rho and Rho associated kinase (ROCK), resulting in multiple and diverse secondary effects. An elegant example of this is shown by Wipff *et. al.* who demonstrated that fibroblast activation of TGFβ increases on increasingly rigid substrates, leading to greater myofibroblast differentiation on stiff, but not compliant substrates. (20) These data call into question what is currently known about EMT. The vast majority of published accounts describing EMT mechanisms *in vitro* are based on studies performed on tissue culture plastic or glass, both of which have stiffness values in the gigapascal (GPa; 10^9 Pa) range. For reference, native tissues rarely exceed 100 kPa (10^5 Pa).

Idiopathic pulmonary fibrosis (IPF), the experimental disease model utilized here, is a currently untreatable and ultimately fatal condition with 3 and 5 year mortality rates of 50% and 80%, respectively. (21) IPF is characterized by excessive extracellular matrix (ECM) deposition, resulting in interstitial scar tissue and loss of tissue compliance, (22)

not unlike the characteristics of tumor stroma. (14) Very recent mesoscale (10-100s of μm) characterization of fibrotic tissue from bleomycin treated mouse lungs indicates that tissue stiffness is highly variable within the fibrotic lung and that on average the tissue stiffness is increased six-fold compared to healthy tissue. (23) Although the exact mechanisms initiating lung fibrosis are poorly understood, recent studies implicate alveolar epithelial type II (ATII) cell EMT in the onset and progression of pulmonary fibrosis. (3, 4, 8-10) EMT has been theorized to increase the number of ECM secreting mesenchymal cells perpetuating the fibrotic condition and resulting in the observed increase in lung stiffness. In other words, tissue stiffness is presumed to be a consequence of EMT. Despite recent evidence highlighting the effect of matrix stiffness on cell phenotype, it is perhaps surprising that it has not been asked whether the converse is true: that alterations in tissue stiffness lead to the observed EMT in fibrosis. If the later is true then it has major implications in therapeutic approaches towards EMT-related diseases, like cancer and fibrosis.

In this aim, it was hypothesized that as epithelial cells engage increasingly rigid environments/substrates, they will become increasingly contractile leading to enhanced TGFβ activation and EMT. In this study the elastic moduli of fibrotic and non-fibrotic regions were characterized in an *in vivo* model of pulmonary fibrosis and subsequently, the observed range of matrix/substrate rigidities were utilized to investigate the potential for stiffness-mediated EMT events *in vitro*.

Materials and Methods

Animals and bleomycin-induced fibrosis

8-10 week old C57/Bl6 mice (Charles River, MA) were intubated and 3.2 U/kg bleomycin (EMD Chemicals, NJ) was instilled intratracheally in 50 μL of sterile saline. Mice were sacrificed after 14 days for tissue harvesting. All experiments were performed in accordance with guidelines set forth by the National Institutes of Health and Georgia Institute of Technology Institutional Animal Care and Use Committee-approved protocols.

Lung tissue preparation for fluorescence microscopy and AFM force mapping

Lungs were inflated using 2% ultra low-melting temperature agarose (SeaPrep, Lonza Inc.) warmed to 37°C and subsequently allowed to solidify on ice. The left lobe was dissected into approximately 1 cm^3 blocks, and 100 μm thick slices were generated using a VT100S vibratome (Leica, IL). Samples were kept in 10% FBS, 1% penicillin & streptomycin-supplemented DMEM after harvesting and during mechanical analysis. To allow for visualization of tissue architecture and type, lung slices were stained with fluorescein-labeled lectin from the Cry-Baby Tree, *Erythrina crystagalli* (ECL; Vector Laboratories) to label alveolar type I epithelial cells (ATI) and LysoTracker Red (Invitrogen) to label the lamellar bodies of alveolar type II epithelial cells (ATII). Cell nuclei were stained Hoechst 33258 (Invitrogen). Slices were incubated at 37^oC for 30 minutes before washing with warm DMEM.

AFM force spectroscopy analysis

Vital stains for ATI, ATII cells and cell nuclei were used to direct measurements to peri-alveolar regions of interest. For fibrotic regions, areas of enhanced cellularity distinct

from larger airways were chosen. Using a MFP-3D-BIO AFM (Asylum, ST) with a 4.74 μm diameter silica glass bead customized-silicon nitride AFM tip (Veeco), peri-alveolar regions were located and probed by contact mode force spectroscopy at a scan rate of 1.0 Hz. Cantilever spring constants were determined using the thermal resonance frequency method with values ranging from 0.06-0.08 N/m. Force-indentation profiles were measured in 10x10 um grids with approximately 600 nm spacing between points. A minimum of 8 regions were selected for each tissue slice and a minimum of 3 slices used per mouse. Force-indentation profiles were fit to a Hertz model for elastic deformation between spheres to calculate the Young's modulus for each point, assuming a Poisson's ratio of 0.4. For single cell analysis, single force points were taken from ~5 locations about the cell body in regions that were greater than 300 nm in height and not directly above the nucleus. Similarly, regions of the gel substrate surrounding measured cells were probed. At least 10 cells were measured per substrate and averages of cell stiffness and gel stiffness for each gel fabrication mixture are presented.

LIVE/DEAD assay of tissue cell viability

To study viability of resident tissue cells over the time course of mechanical characterization, the LIVE/DEAD Viability Kit for mammalian cells was used (L-3224, Invitrogen). Lung slices were incubated with 10 μM calcein AM and 5 μM EthD-1 for 1 hour prior to their corresponding time point. Samples were then fixed with 4% formaldehyde and mounted. Additionally, a dead control group was included by incubating samples with 70% methanol for 30 minutes prior to dye incubation. Samples were imaged with a laser scanning confocal microscope (LSM 510 META, Carl Zeiss Inc.) at 63x.

Poly-acrylamide gel production

To determine the role of substrate stiffness on EMT events, poly-acrylamide (PA) gels of varying bisacrylamide concentrations were created on amino-silanated coverslips as previously described.(24) PA gel solutions were produced by combining acrylamide and bisacrylamide to final concentrations of 8% acrylamide (Biorad, Hercules, CA, USA) and 0.048%, 0.117%, 0.208%, 0.296%, or 0.391% bis (Biorad) to obtain gels with final elastic moduli of 2 kPa, 8 kPa, 16 kPa, 24 kPa, or 32 kPa respectively. 50 µl of each solution was polymerized by the addition of ammonium persulfate (VWR, West Chester, PA, USA) and N,N,N',N'-tetramethylethylenediamine (Biorad, Hercules, CA, USA) (1% and 0.1% final concentration respectively). The gels were allowed to polymerize for approximately 20 minutes, then washed extensively with PBS. Human plasma fibronectin (Fn) (BD Bioscience, San Jose, California, USA) was covalently attached to the surface using the heterobifunctional crosslinker sulfosuccinimidyl-6-(4'-azido-2' nitrophenyl-amino)hexanoate (sulfo-SANPAH; Pierce Chemical Co., Rockford, IL., USA). Following an overnight incubation with 20 µg/ml Fn, gels were then washed with PBS.

To confirm equivalent amounts of Fn were cross-linked to each surface regardless of stiffness, gels were incubated with 5% Alexa-488 Fn/ 95% unlabeled Fn. Fluorescence was quantified using a plate reader and normalized to gels with no cross-linked Fn. No statistical difference in fluorescence was observed between gels (**Appendix A.1**).

Cell culture

RLE-6TN cells, an alveolar epithelial cell line were purchased from ATCC, and grown in DMEM/F12 media supplemented with 10% FBS, 1% P/S. To determine the effect of substrate stiffness on epithelial cell fate, cells were plated on PA gels with Fn cross-

linked on the surface with the following rigidities: E=2 kPA, 8 kPa, 16 kPA, 24 kPA, 32 kPA, or on glass coverslips coated with Fn or Ln as controls. Cells were plated in growth media in the absence or presence of 10 μM Y-27632 (EMD Biosciences, Gibbstown, NJ, USA). To determine the role of TGFβ in substrate mediated EMT, cells were cultured on the lowest stiffness substrate (2kPa) in the absence or presence of 5 ng/mL active TGFβ (R&D Systems, Minneapolis, MN, USA) and cells cultured on the highest stiffness substrate (32 kPa) were cultured in the absence or presence of 10 ug/mL TGFβ neutralizing antibody (9016, R&D Systems). Media was changed every 48 hours.

Immunofluorescence staining and circularity analysis

Following culture for 5 days, cells were washed with PBS, fixed with 4% formaldehyde, permeabilized with 0.2% Triton-X 100 and then blocked with 10% goat serum. Primary anti-α-SMA (1A4, Sigma-Aldrich) or anti-E-cadherin (36/E-cadherin, BD Transduction Laboratories) antibodies were incubated overnight then washed thoroughly with PBS + 1.5% goat serum. Alexa-Fluor-488-conjugated goat-anti-mouse (Invitrogen) was used as the secondary antibody. To characterize cell shape, actin was stained with Texas-red phalloidin (Invitrogen) and nuclei were stained with Hoescht stain (Invitrogen). Images were acquired with a Nikon Eclipse (TiE) inverted fluorescence microscope at 20X magnification (PlanFluor 20X, 0.5 NA objective) with a CoolSNAP HQ2 Monochromatic CCD camera. Experiments were performed in triplicate, and images presented are representative from 5-10 random fields for each independent experiment. To characterize circularity, area and perimeter of individual cells stained for actin were determined for each condition using Image J (NIH Freeware) image processing software, then circularity was determined using the equation circularity = $4\pi(\text{area}/\text{perimeter}^2)$.

Three independent images were analyzed for each condition, and at least 10 cells were analyzed per image. Data is pooled from all 3 images analyzed per condition.

Immunoblot

RLE-6TN cells were cultured for 5 days then washed with PBS and cells lysed directly in Lamelli buffer containing protease and phosotase inhibitors (Roche Applied Sciences). Total protein concentration was determined using the BCA protein quantification kit (Pierce Chemical Co.). 40 ug of total protein was separated electrophoretically on a 4-15% gel, then transferred to a nitrocellulose membrane using a semi-dry transfer system, blocked with 5% nonfat dry milk in TBS, then incubated with E-cadherin (36/E-cadherin), pan cytokeratin (5D3 + LP34, abcam, Cambridge, MA, USA), α-SMA (1A4), prolyl-4-hydroxylase (P4H; 1D3, Santa Cruz Biotechnology, Santa Cruz, CA, USA), or GAPDH (14C10, Cell Signaling Technologies, Boston, MA, USA) antibodies overnight at 4° C. Following washing with TBS + 0.1% Tween 20, membranes were incubated for 2 hours with IR secondary antibody (Licor), washed, and then imaged using the Odyssey IR scanner. Western blots were quantified using Image J image processing software, using GAPDH as the endogenous control.

Analysis of pai-1 mRNA expression

Cells were trypsinized, mRNA isolated (RNAeasy Mini Kit, Qiagen, Valencia, CA, USA) and c-DNA generated (High Capacity cDNA Reverse Transcription Kit, Applied Biosystems, Foster City, CA, USA). Primers (Invitrogen, Carlsbad, CA, USA) used for q-PCR reactions were as follows: β-actin forward ACCCGCCACCAGTTCGCCAT; β-actin reverse CTTGCTCTGGGCCTCGTCGC; Plasminogen activator inhibitor-1 (Pai-1) forward CACAGTGCTGGGTGTAATGG; Pai-1 reverse

GTTTGTGGGGCAGCTATTGT (designed using Primer3Plus software). Q-PCR was performed on a Step One Plus ABI thermocycler (Applied Biosystems) using Power SYBR Green Master Mix (Applied Biosystems). Data was analyzed using the $\Delta\Delta C_t$ method taking reaction efficiency into account (25) using β-actin as the endogenous control and comparing expression levels to cells cultured on the lowest stiffness substrate (E=2 kPA). Q-PCR reactions were run in triplicate and performed for 3 independent experiments. Data shown was pooled from 3 independent experiments.

Statistical Analysis: All statistical analysis for 3 or more experimental groups was performed by multi-variate ANOVA using Prism (Graphpad Software Inc., La Jolla, CA, USA). Statistical significance is achieved for $p<0.05$.

Results

Epithelial cells experience significantly greater stiffness in fibrotic versus normal lung.

Given that one of the hallmarks of fibrotic diseases is an increase in tissue stiffness, the mechanical environment of the alveolus in normal and pathological conditions was characterized to determine the range of stiffness encountered by ATII epithelial cells *in vivo*. Bleomycin-treated mice were utilized to model pulmonary fibrosis, and as previously demonstrated, fixed lung sections isolated from the fibrotic lung displayed increased cellularity and alveolar wall expansion as observed through H&E staining compared to non-treated mice (**Figure 5.1A**). Because it has been shown that cells contribute significantly to the mechanical properties of tissues, and in addition fixing tissue can alter tissue mechanics, living lung slices were utilized for AFM analysis

of tissue elasticity. Lung tissue from either normal or bleomycin-treated mice was tested within 6 hours of harvest to ensure tissue integrity and resident cell viability. Lung architecture observed in fixed tissue is recapitulated in thick (~100 μm) living lung slices as observed by widefield fluorescence microscopy using vital stains for ATI and ATII cells, and cell nuclei (**Figure 5.1B**). The average Young's modulus of lung tissue was characterized through AFM analysis. To ensure correct spatial and anatomical location within the lung, peri-alveolar regions were located based on vital staining for ATI and ATII epithelial cells; representative DIC-fluorescence overlay, fluorescence-only image, and a force-indentation profile are depicted (**Figure 5.1C-E)**. Mean and standard deviation values are reported for samples obtained from individual mice (**Figure 5.1F**) and as mean values of all samples (**Figure 5.1G**). The average Young's modulus of normal lung tissue was 1.96 kPa (+/- 1.21), and in the bleomycin treated mouse, the average Young's modulus increased to 17.25 kPa (+/- 11.06). This is in good agreement with previously published work exploring the micro-scale bulk tissue mechanics of lung.(23) Cell viability within prepared tissue slices was verified using calcein AM and EthD-1. Predominately viable cells/tissue were detected as long as 24 hours post harvest (**Figure 5.1H, I**).

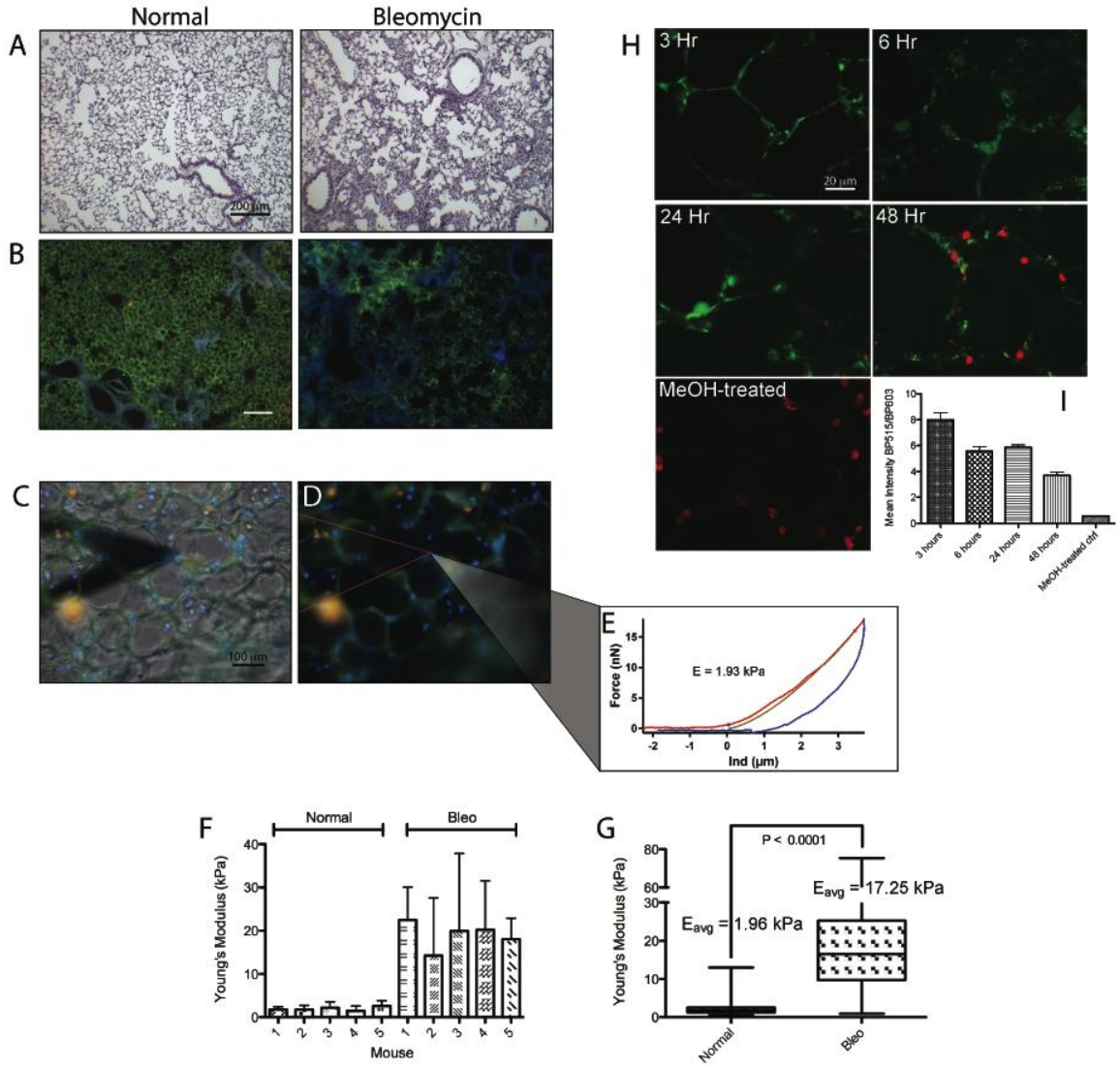

Figure 5.1: Alveolar epithelial cells undergo EMT when cultured on substrates of increasing stiffness Lung slices from mice exposed to bleomycin display higher Young's modulus than those obtained from healthy mice. The *in vivo* mechanical environment of the alveolus was investigated at cellular length scales to determine the range of stiffness encountered by ATII cells under normal and pathologic conditions. H&E staining was performed on normal and treated lung sections (**A**) and thick living lung slices were imaged with widefield fluorescence using vital stains for ATI, ATII cells, and cell nuclei (**B**). The average Young's modulus of lung tissue was characterized through AFM analysis, with a representative DIC-fluorescence overlay (**C**), fluorescence-only image (**D**), and force-indentation profile for the depicted region shown (**E**). Mean and standard deviation values are reported for samples obtained from individual mice (**F**) and as mean values of all samples (**G**). The time course of cell viability within tissue slices was assayed using calcein AM and EthD-1, and mostly viable cells were detected after 24 hours post harvest (**H, I**).

Alveolar epithelial cells undergo EMT when cultured on substrates of increasing stiffness

EMT has previously been observed *in vivo* in fibrotic lung regions of both human IPF patients and bleomycin-treated mice.(4) Because a range of stiffness was observed *in vivo* in fibrotic lung regions, it was interrogated if increases in matrix/substrate stiffness alone would be sufficient to induce EMT. Utilizing polyacrylamide (PA) gels with surface immobilized Fn and varying stiffness from 2 kPa to 32 kPa, epithelial cells were cultured for 5 days and then analyzed for EMT events. EMT was characterized through analysis of expression of various epithelial and mesechymal markers by immunofluorescence staining and western blotting. Cells cultured on 2 kPa and 8 kPa surfaces maintained an epithelial phenotype with positive staining for E-cadherin at cell-cell contacts and minimal staining for α-SMA, while cells cultured on 16 kPa-32 kPa surfaces exhibited increasing EMT with minimal staining for E-cadherin at cell-cell contacts and positive staining for α-SMA (**Figure 5.2A-N**). The shift from epithelial to mesenchymal phenotypes as stiffness increased was further verified with western blots for E-cadherin and cytokeratin (epithelial) and α-SMA and prolyl-4 hydroxylase (P4H; mesenchymal, **Figure 5.2O**). Western blots were quantified and expressed as fold change compared to expression on 2 kPa, normalizing to GAPDH expression (**Figure 5.2P**). Higher expression of cytokeratin was observed on 2 kPa and 8 kPa substrates compared to the higher stiffness substrates, while expression of α-SMA and P4H was higher on 16kPa-32kPa substrates than on the lower stiffness substrates. While E-cadherin was lost from cell-cell contacts as stiffness increased, total protein expression was similar in cells on all surfaces, although there was a slight decrease in expression as stiffness increased. These observations are in agreement with reports describing the loss of E-cadherin at

cell-cell contacts at early time points during EMT while maintaining intracellular localization of E-cadherin. Loss of E-cadherin expression during EMT often requires up to two weeks.(1, 26, 27) ATII epithelial cells have previously been shown to undergo EMT on Fn-coated glass surfaces (~ 30 GPa stiffness) but maintain epithelial phenotypes on Ln-coated glass.(4) Using these conditions as control experiments it was observed, as expected, EMT of cells on Fn-coated glass as indicated by significantly increased expression of α-SMA and P4H and a concomitant decrease in expression cytokeratin and a loss of E-cadherin at cell-cell contacts. Conversely, cells cultured on Ln-coated glass surfaces maintained their epithelial nature exhibiting high levels of cytokeratin expression, low levels of α-SMA and P4H, and maintaining E-cadherin containing cell-cell contacts. These results indicate that both the biochemical and mechanical microenvironment of the ECM are important contributing factors in driving EMT.

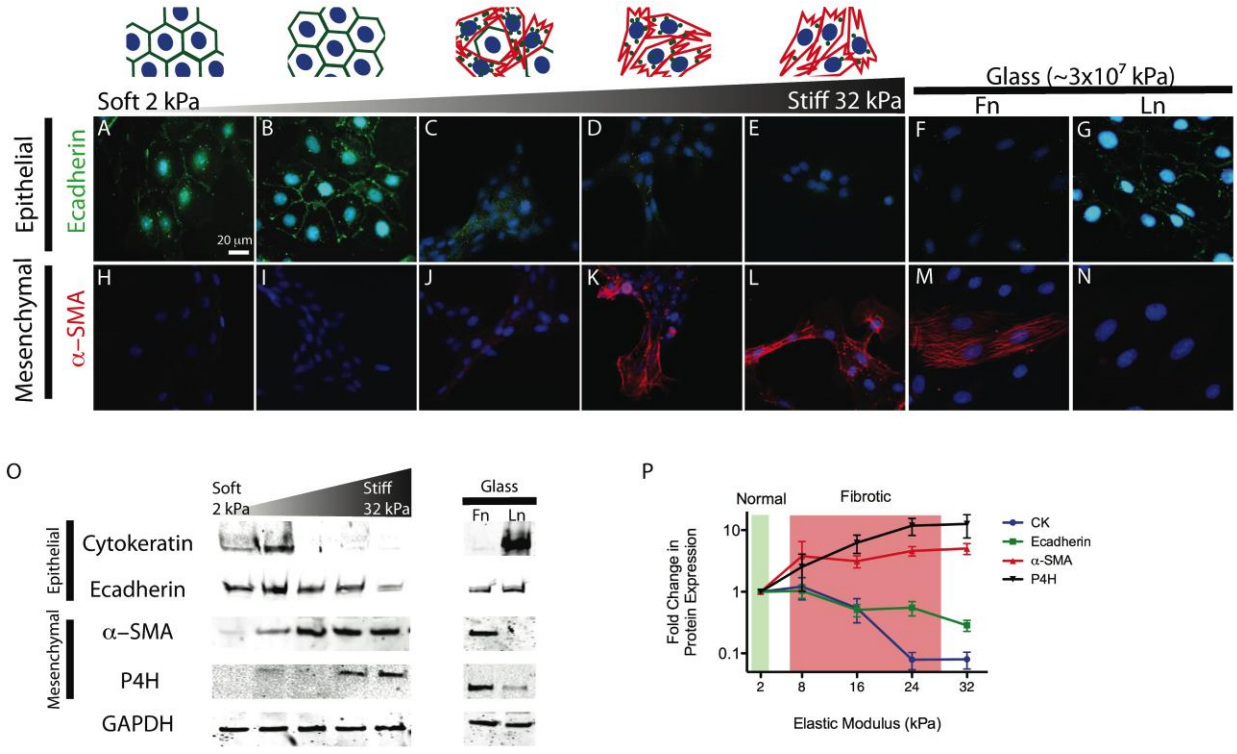

Figure 5.2: Analysis of epithelial and mesenchymal gene and protein expression of RLE-6TN cells cultured on substrates of varying stiffness. RLE-6TN cells were cultured on substrates of varying rigidities for 5 days then analyzed for epithelial and mesenchymal protein expression through immunofluorescence staining for E-cadherin (**A-G**) and α-SMA (**H-N**) and western blotting for E-cadherin, cytokeratin (epithelial), α-SMA, P4H (mesenchymal), and GAPDH (endogenous control) (**O**). Western blots were quantified and expressed as fold changed compared to expression on the lowest stiffness substrate using GAPDH as the endogenous control (**P**).

Epithelial cells display increasing cytoskeleton alignment, spreading, and cellular stiffness in proportion to substrate stiffness.

EMT is primarily characterized by decreases in epithelial markers and concomitant increases in mesenchymal markers, but is also accompanied by changes in cellular morphology, including increased cell spreading and cytoskeleton alignment. Therefore, stiffness-mediated EMT was further characterized through analysis of cell spreading and cytoskeletal organization/stress fiber formation. Alveolar epithelial cells were cultured on substrates of varying stiffness for 5 days, and then stained with Texas-red-X conjugated phalloidin to visualize the actin cytoskeleton (**Figure 5.3A-G**). Providing further evidence of the role of stiffness in driving EMT, cells cultured on lower stiffness substrates (E=2 kPa and 8 kPa) displayed the typical epithelial rounded morphology and diffuse cortical staining for actin, while cells cultured on higher stiffness substrates (E=16 kPA-32 kPA, and Fn-coated glass) became elongated and increasingly displayed aligned, thick actin filaments characteristic of stress fibers. Recapitulating the importance of the biochemical composition of the ECM in EMT, cells cultured on Ln-coated glass surfaces maintained a round epithelial morphology despite being cultured on non-physiologically relevant rigid substrates. Cell circularity was calculated to quantify differences observed in cell shape (**Figure 5.3H**); values closer to 1 indicate a more rounded cell. Cells exhibited statistically significant decreasing circularity values, and were therefore becoming more elongated, with increasing stiffness ($p<0.001$ each group compared to E=2 kPA) with cells exhibiting the following circularity values: E=2 kPA, 0.70; E=8 kPA, 0.62; E=16 kPA, 0.46; E=24 kPA, 0.44; E=32 kPA, 0.41; glass-Fn, 0.42; glass-Ln, 0.65.

It has previously been demonstrated that fibroblasts respond to a range of substrate stiffness by increasing their internal stiffness, up to a saturating level of approximately 8 kPa.(28) It is thought that cellular stiffness matching is the product of cytoskeleton rearrangements and activation of Rho-mediated contractility, therefore, based on the observations of cytoskeleton rearrangements in response to substrate stiffness, it was investigated whether epithelial cell stiffness also increases similarly with substrate stiffness. Using similar AFM methodology as with the lung slices, the average Young's modulus of individual cells and that of their underlying substrate were measured from force-indentation profiles (**Figure 5.3I**). The average epithelial cell stiffness increased as substrate stiffness increased, reaching a maximum at approximately 6 kPa on the stiffest gel and Fn-coated glass. Interestingly, cells on Ln-coated glass exhibited values similar to cells on the softest (2 kPa) substrate, with average Young's moduli around 0.5 kPa, suggesting that increases in cellular stiffness in response to substrate stiffness depend on the biochemical context. To determine the role of cell contractility in cellular stiffness-matching, the elasticity of cells on Fn-coated glass with the addition of 10 μM of the ROCK inhibitor Y-27632 was measured, and it was found that cell stiffness was decreased and exhibited values similar to cells on the softest (2 kPa) substrate and Ln-coated glass substrates.

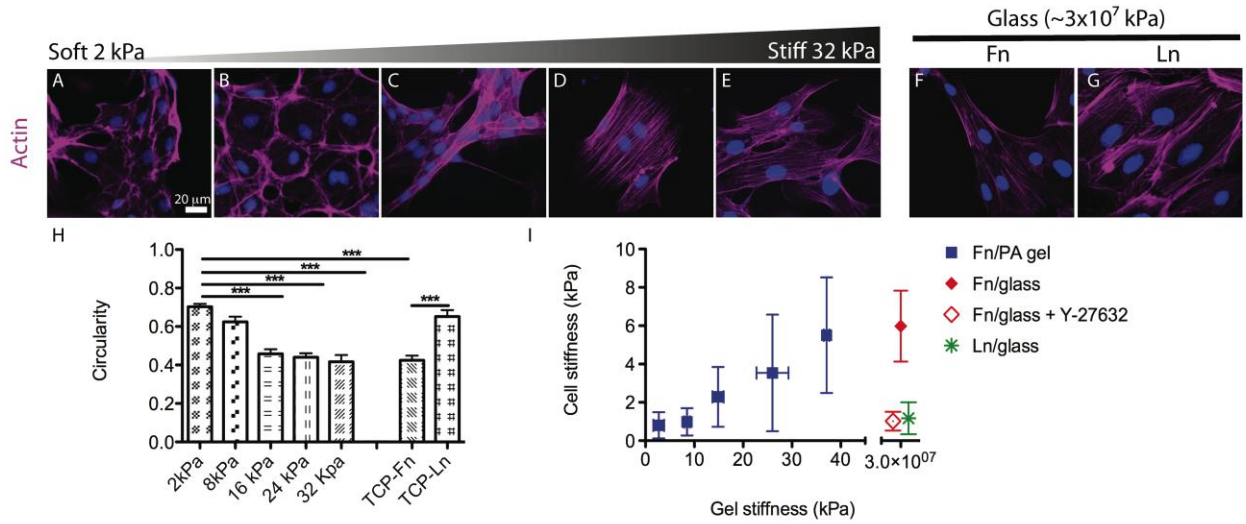

Figure 5.3: Substrate stiffness influences cell shape and actin cytoskeleton alignment, which corresponds to increases in single cell stiffness measurements. RLE-6TN cells were cultured for 5 days on substrates of increasing stiffness and then cell shape and stress fiber formation was analyzed. The actin cytoskeleton was visualized by staining with Texas-red phalloidin and the nuclei stained with Hoescht. (**A-G**) Cell circularity was calculated to quantify differences observed in cell shape (**H**); values closer to 1 indicate a more rounded cell. Fluorescent images were acquired with a Nikon Eclipse (TiE) inverted fluorescence microscope at 20X magnification. *** denotes $p<0.001$. Single cell elasticity was measured via AFM force mapping to characterize cell stiffening in response to substrate stiffness and/or ECM protein (**I**).

Stiffness-mediated EMT is dependent on cell contractility

Based on the observation that cellular stiffness increased with increasing stiffness and that cellular stiffness on Fn-coated glass could be decreased to levels observed for cells cultured on 2 kPa substrate by inhibiting cellular contractility, it was investigated if stiffness-mediated EMT was also dependent on contractility. Cells were cultured for 5 days on substrates of varying stiffness in the presence of Y-27632 and then EMT events characterized as previously described. In the presence of the ROCK inhibitor, cells maintained a round, epithelial morphology and displayed diffuse staining for actin regardless of the underlying substrate (**Figure 5.4A-G**). Furthermore, cells displayed positive staining for E-cadherin at cell-cell contacts (**Figure 5.4H-N**), minimal staining for α-SMA (**Figure 5.4O-U**), maintained equivalent protein expression levels of E-cadherin, cytokeratin, α-SMA, and P4H (**Figure 5.4V-W**), and remained circular in nature (**Figure 5.4X**), all of which were comparable to those observed on the lower stiffness substrates in the absence of ROCK inhibition. In other words, inhibition of cell contractility is sufficient to inhibit stiffness-mediated EMT. These results suggest that stiffness-mediated EMT is linked to changes in the cytoskeleton and increased cell contractility on increasingly rigid substrates.

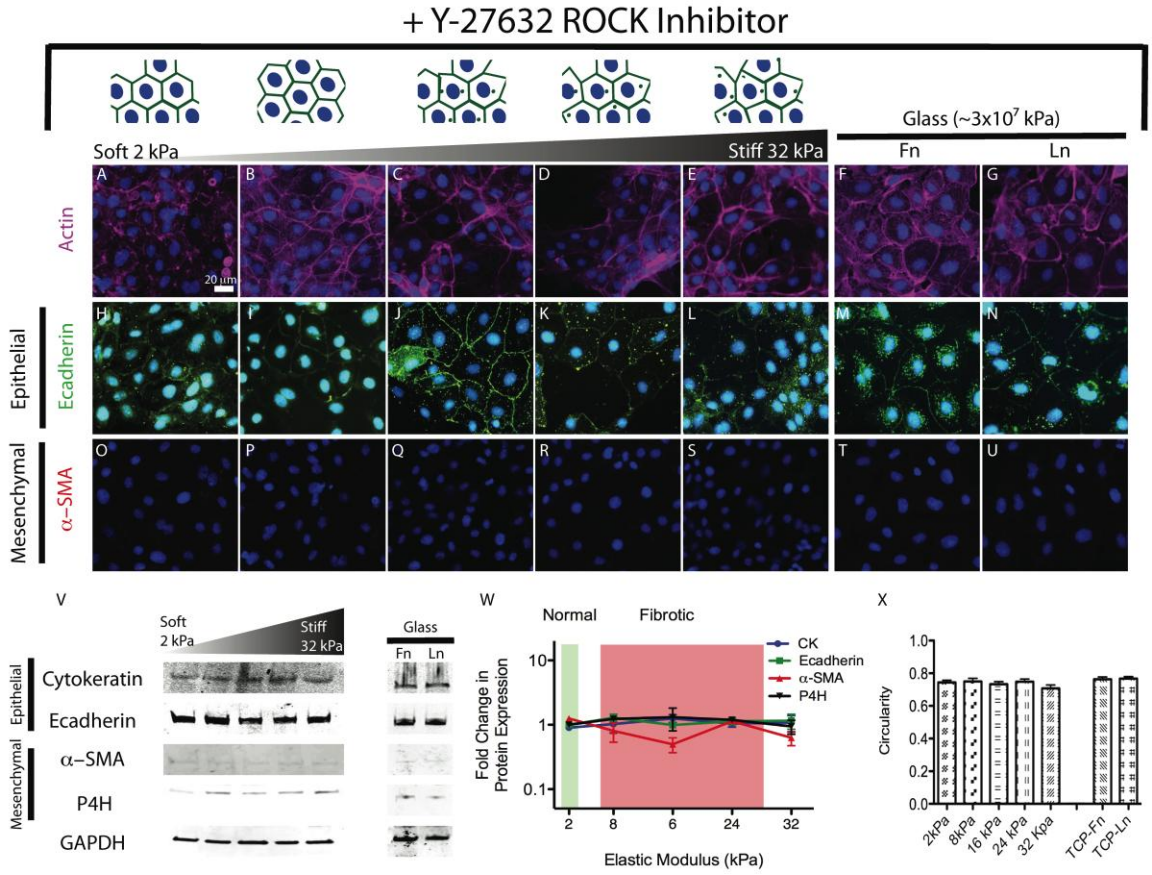

Figure 5.4: Substrate stiffness-mediated EMT is dependent on cell contractility. RLE-6TN cells were cultured on substrates of varying rigidities in the presence of 10 μM Y-27632 ROCK inhibitor for 5 days and then EMT responses were analyzed through changes in actin cytoskeleton alignment and cell circularity (**A-G, X**), and changes in epithelial and mesenchymal protein expression through immunofluorescence staining for E-cadherin (**H-N**) and α-SMA (**O-U**) and western blotting for E-cadherin, cytokeratin (epithelial), α-SMA, P4H (mesenchymal), and GAPDH (endogenous control) (**V**). Western blots were quantified and expressed as fold changed compared to expression on the lowest stiffness substrate using GAPDH as the endogenous control (**W**).

Epithelial cells display enhanced TGFβ activity when cultured on substrates of increasing stiffness.

It has been shown in the context of mesenchymal cells that fibroblasts increasingly activate latent TGFβ as substrate stiffness increases, through a process requiring high levels of cell contractile forces. Because TGFβ has been identified as one of the primary inducers of EMT and because inhibition of stiffness-mediated EMT was observed through inhibition of cell contractility, it was hypothesized that stiffness-mediated EMT could also be driven by a similar mechanism in epithelial cells. To determine if differences in substrate stiffness induced changes in TGFβ activation in epithelial cells, expression of Pai-1, a TGFβ-specific responsive gene, was analyzed by q-PCR (**Figure 5.5**). Cells displayed increased Pai-1 expression as substrate stiffness increased, with cells expressing significantly higher levels of Pai-1 when cultured on the highest stiffness substrate E= 32 kPa than cells cultured on substrates of stiffness E=2 kPa, 8 kPA, or 16 kPa ($p<0.01$) (**Figure 5.5A**), indicating that epithelial cells increasingly synthesize and/or activate TGFβ with increasing substrate stiffness. A slight twofold increase in TGFβ mRNA expression was observed on the highest stiffness substrates (32 kPa and Fn coated glass) compared to cells cultured on the lowest stiffness substrate (**Figure 5.6**). Alternatively, cells may display increased TGFβ signaling (i.e. sensitivity) in response to increasingly rigid substrates. The addition of Y-27632 abrogated this effect and no statistical significance was seen between groups cultured in the presence of the inhibitor (**Figure 5.5B**), indicating that TGFβ production, activation, and/or signaling and subsequent EMT, is dependent on cell contractility. As expected, control groups cultured on Fn-coated glass expressed significantly higher levels of Pai-1 than those cultured on

Ln-coated glass ($p<0.01$) and the addition of Y-27632 abrogated these differences (**Figure 5.5C**). Furthermore, no significant differences in Pai-1 mRNA were observed between cells cultured on Fn-coated glass in media only compared to media plus active TGFβ and Y-27632, indicating that the inhibition of ROCK does not inhibit normal TGFβ signaling, thus implicating TGFβ activation as the critical step. In addition, it was found that increased TGFβ activation on higher stiffness substrates (E=32 kPa) is not specific to ROCK signaling but rather more broadly on cell contractility. Pai-1 expression was found to significantly decrease in the presence of a variety of cell contractility inhibitors (**Figure 5.7**).

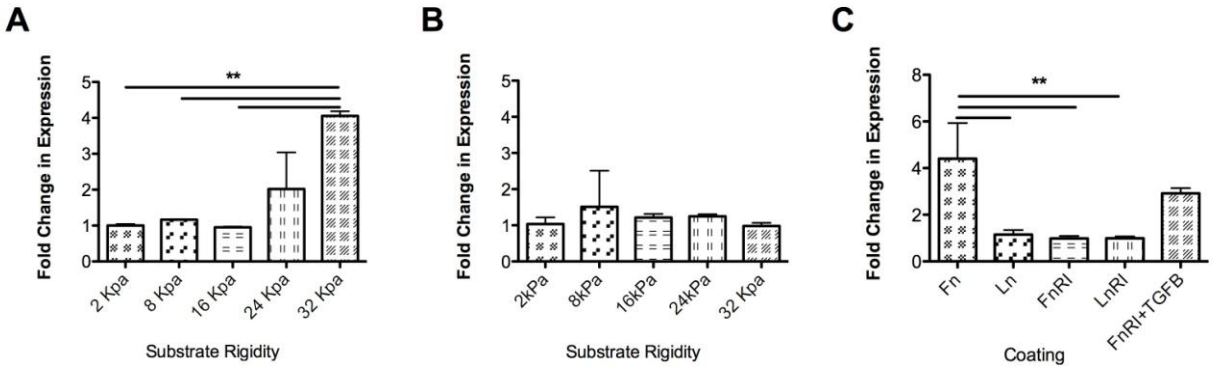

Figure 5.5: TGFβ activation increases with increases in substrate stiffness as determined through Pai-1 mRNA expression: RLE-6TN cells were cultured for 5 days on substrates of varying rigidities in the absence (**A**) or presence of 10 μM Y-27632 (**B**). Levels of expression of the TGFβ responsive gene Pai-1 were determined by q-PCR. Fold changes in gene expression were determined by ΔΔCT analysis using β-actin as the endogenous control and comparing expression to cells cultured on E=2 kPa in the absence or presence of ROCK inhibitor respectively. Controls included cells cultured on glass-Fn or glass-Ln in the absence or presence of Y-27632 (**C**). Reactions were performed in triplicate. ** denotes $p<0.01$

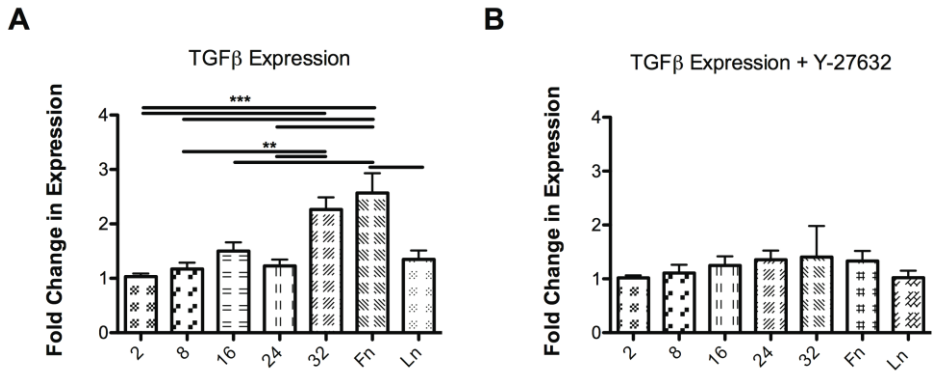

Figure 5.6: TGFβ mRNA expression on substrates of varying stiffness. RLE-6TN cells were cultured for 5 days on substrates of varying rigidities in the absence (**A**) or presence of 10 μM Y-27632 (**B**). Levels of expression of TGFβ mRNA were determined by q-PCR. Fold changes in gene expression were determined by ΔΔCT analysis using β-actin as the endogenous control and comparing expression to cells cultured on E=2 kPa in the absence or presence of ROCK inhibitor respectively. Reactions were performed in triplicate. ** denotes p <0.01, *** denotes p <0.001

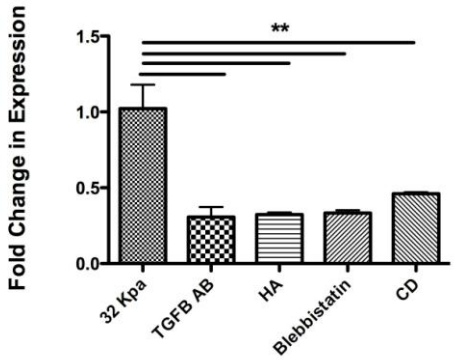

Figure 5.7: Pai-1 mRNA expression on high stiffness substrates is inhibited by a variety of cell contractility inhibitors. RLE-6TN cells were cultured for 48 hours on the highest stiffness substrate (E=32 kPA) in the presence of 10 ug/ml TGFβ neutralizing antibodies, 10 μM HA 1077, 50 μM Blebbistatin, 100 nM cytochaslin D, or media only and Pai-1 expression was analyzed. Pai-1 expression was significantly lower in the presence of all contractility inhibitors analyzed compared to cells cultured on 32 kPa surfaces in media alone (p<0.01).

Stiffness-mediated EMT is driven by TGFβ activation and subsequent signaling

To further confirm that stiffness-mediated EMT is due to TGFβ activation and not alterations in TGFβ signaling, EMT events were analyzed in the presence of active TGFβ on the lowest stiffness substrate (E=2 kPa) and in the presence of TGFβ neutralizing antibodies on the highest stiffness substrate (E=32 kPa, **Figure 5.8**). In the presence of active TGFβ, cells cultured on 2 kPa underwent EMT as evidenced by an elongated morphology, stress fiber formation, loss of E-cadherin at cell-cell contacts and positive staining for α-SMA (**Figure 5.8A-B, E-F**). Furthermore, western blot analysis demonstrated minimal expression of E-cadherin and cytokeratin, while expression of α-SMA and P4H increased compared to cells cultured on 2 kPa in the absence of exogenously added active TGFβ (**Figure 5.8I, K**). These EMT events were accompanied by a significant increase in Pai-1 expression ($p<0.05$), indicative of active TGFβ signaling (**Figure 5.8M**). The converse was observed on 32 kPa substrates in the presence of TGFβ neutralizing antibodies. Cells maintained a round, epithelial morphology accompanied by E-cadherin at cell-cell contacts and negative staining for α-SMA (**Figure 5.8C-D, G-H**). Western blot analysis demonstrated minimal expression of α-SMA and P4H, while expression of E-cadherin and cytokeratin as well as Pai-1 mRNA level were comparable to cells cultured on 2 kPa surfaces in media only (**Figure 5.8J, L, N**). These results demonstrate that EMT can occur on soft substrates in the presence of active TGFβ, indicating that cells on soft substrates are not less sensitive to TGFβ than those cultured on rigid substrates. Furthermore, these data, taken together with the results that inhibition of TGFβ signaling on rigid substrates inhibits EMT, further supports the

hypothesis that stiffness mediated EMT is a consequence of increased cell contractility leading to increased TGFβ activation.

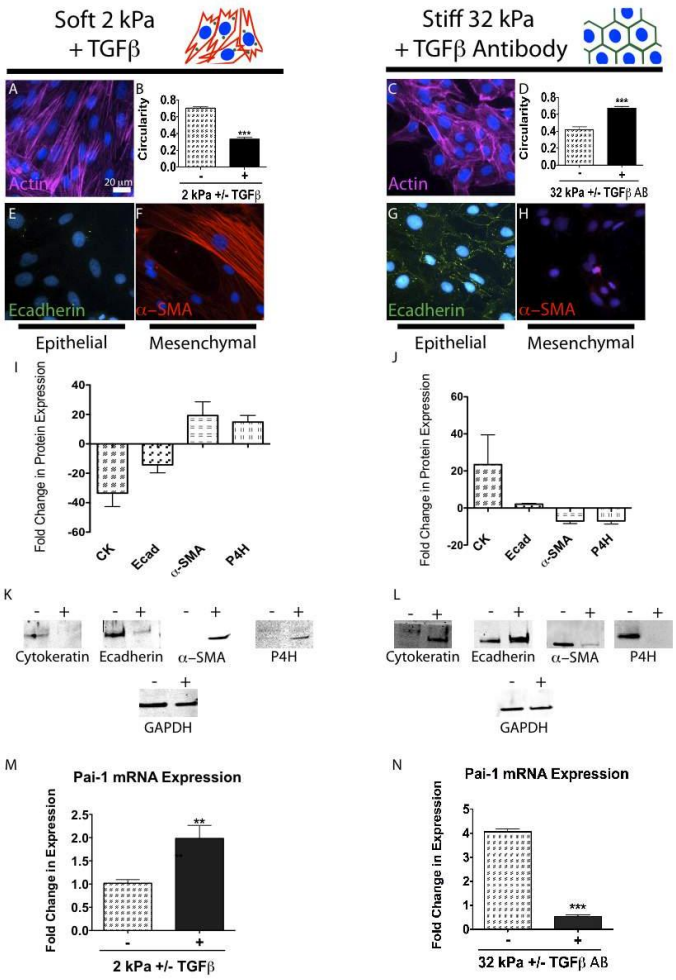

Figure 5.8: EMT events can be induced on low stiffness substrates in the presence of active TGFβ and inhibited on high stiffness substrates in the presence of TGFβ neutralizing antibodies. RLE-6TN cells were cultured for 5 days on the lowest stiffness substrate (E=2 kPA) in the presence of 5 ng/ml active TGFβ (**A-B, E-F, I, K, M**) or on the highest stiffness substrate (E=32 kPA) in the presence of 10 µg/ml TGFβ neutralizing antibodies (**C-D, G-H, J, L, N**). EMT events were analyzed though changes in actin cytoskeleton alignment and cell circularity (**A-D**), and changes in epithelial and mesenchymal protein expression through immunofluorescence staining for E-cadherin (**E; G**) and α-SMA (**F; H**) and western blotting for E-cadherin, cytokeratin (epithelial), α-SMA, P4H (mesenchymal), and GAPDH (endogenous control) (**K-L**). Western blots were quantified comparing expression to cells cultured on substrates in media only (E=2 kPa, **I;** E=32 kPa, **J**). Levels of mRNA expression of the TGFβ responsive gene Pai-1 were also determined by q-PCR, comparing expression to cells cultured on E=2 kPa (**M**) or E=32 kPa (**N**), respectively.

Discussion

EMT is a critical process in the progression of invasive pathologies like cancer and fibrosis and as such it is essential that the process is fully understood in order to gain therapeutic insights. This work provides evidence that the micromechanical environment with which epithelial cells interact is a strong driving force for EMT. The stiffer the matrix/substrate is, the stronger the pressure to undergo EMT and vice versa. This unique finding raises questions about what is currently known about EMT. Specifically, the vast majority of *in vitro* EMT research to date has been performed on substrates with non-physiological stiffness (i.e. GPa stiffness). (1, 4, 8, 29, 30)

While stiffness of the cellular microenvironment clearly plays a significant role in defining the resident cell phenotype, (13, 14, 20, 23) the origins of the increased tissue stiffness are still poorly understood. It is likely that stiffness emanates from the residential cell population and the over-production or activation of cross-linking enzymes. Fibroblasts that have differentiated down a contractile, myofibroblastic pathway are known to exhibit significant contractile force. (20) Such cell-derived forces are capable of stressing the surrounding ECM leading to increased microenvironmental stiffness. Additionally, recent evidence suggests that even normal fibroblast subpopulations, as in the case of Thy-1 surface expression, may display significant differences in their capacity to exert force on their matrix. (31, 32) Several investigations have shown that lysyl oxidase in the tumor microenvironment is sufficient to crosslink and stiffen the tumor stroma (33) and transglutaminases have long been known to catalyze ECM crosslinking and recently have been shown to result in tissue stiffening. (34) As mentioned previously, the prevailing thought is that EMT precedes tissue

stiffening, yet several reports indicate that tissue stiffening occurs prior to the onset of fibrosis.

The data here indicate that tissue/substrate stiffness is necessary but not sufficient to induce spontaneous EMT. The effect of stiffness in the context of EMT depends on the ECM ligand. Increased stiffness acts synergistically with Fn to promote EMT through contraction-mediated TGFβ activation whereas Ln substrates inhibit the effect of stiffness (**Figure 5.9**). These data corroborate previous findings on tissue culture plastic/glass regarding the role of ECM proteins on EMT (4) and also support recent evidence that integrin-specificity drives mechanotransduction/compliance matching.

Biochemical signaling through the ECM is clearly dependent on specific integrins binding to their extracellular counterpart. (35) How integrins interact with specific extracellular ligands to determine transduction of matrix mechanical properties is less understood. Integrin binding to an ECM ligand can result in physical linkage between integrin and the cytoskeleton, allowing force transmission through the attachment site and reinforcement of the protein complex. (36, 37) Recent studies suggest differential reinforcement of adhesions based on the dominant integrin being bound. (38, 39) Rosa-Cusachs *et al*. reported dynamic stiffening of the attachment site when physiological forces were applied via mainly αvβ3, whereas binding and clustering of α5β1 resulted in enhanced adhesion strength. The results presented in this aim reinforce the suggestion that different matrix ligands, and presumably their interaction with specific integrins, allow for differential transduction of matrix stiffness and importantly affect substrate-mediated alterations in cell phenotype.

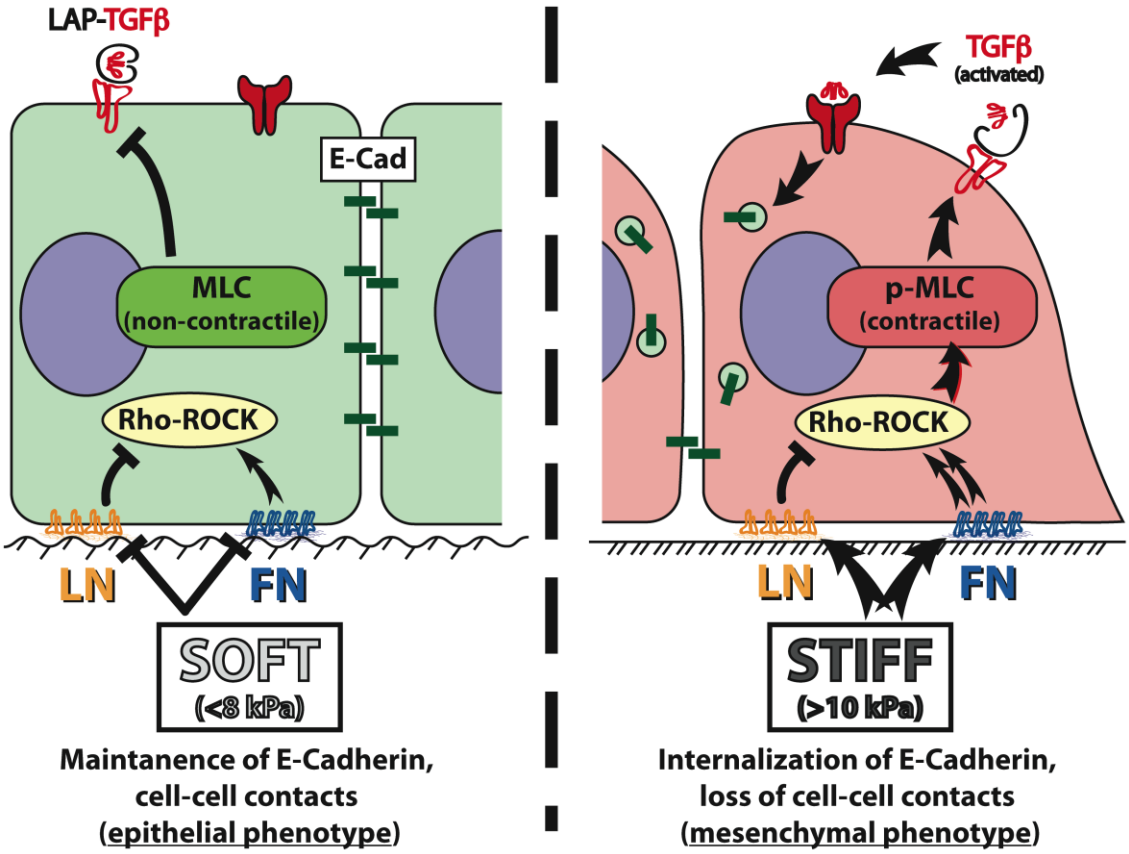

Figure 5.9: Schematic of hypothesized stiffness-mediated EMT mechanism. The results of this study indicate that tissue compliance is a synergistic signal that facilitates the activation of pro-contractile signals in the cell (i.e. Rho and ROCK) and subsequent contraction-mediated TGFβ activation. These effects are context dependent. The biochemical composition of the underlying ECM, and hence the integrin specificity of cell-ECM interaction, appears to be a master regulator of stiffness-mediated effects on epithelial cell phenotype. This proposed model suggests that therapeutic approaches to cancer and fibrosis need to focus equally on modification of the ECM microenvironmental properties in addition to the affected cells themselves.

Force application to the focal adhesion complex leads to recruitment and activation of signaling proteins like FAK, Src, and Shc whose major downstream targets are Rho GTPases. Importantly, activation of the Rho signaling cascade leads to cytoskeletal rearrangement and increased cell contractility. These cytoskeletal/contractile perturbations are now directly linked to activation of TGFβ via integrin-mediated release of the active growth factor from the Latency Associated Protein. (4, 20, 40) The consequence of this "secondary effect" of tissue stiffness is the transformation of cell types – fibroblasts to myofibroblasts, (20) epithelial to mesenchymal transition, etc.

In conclusion, these studies demonstrate, for the first time, that tissue compliance is a critical factor in the determination of EMT and that matrix stiffness acts synergistically with integrin-mediated compliance matching in the activation of cell contractility and subsequent TGFβ activation. These findings, along with others', suggest that therapeutic approaches to cancer metastasis and fibrosis that focus on the cell only are critically flawed. The pathological extracellular microenvironment (the ECM and its mechanical properties) presents pro-malignant signals that ensure the progression of the disease despite any acute eradication of the resident cells. How one modifies the biochemical and biophysical microenvironment may be a greater determinant in the success of future therapeutics.

References

1. Thiery JP, Sleeman JP. Complex networks orchestrate epithelial-mesenchymal transitions. Nat Rev Mol Cell Biol.7:131-42. 2006.

2. Jain R, Shaul PW, Borok Z, Willis BC. Endothelin-1 induces alveolar epithelial-mesenchymal transition through endothelin type A receptor-mediated production of TGF-beta1. Am J Respir Cell Mol Biol.37:38-47. 2007.

3. Kasai H, Allen JT, Mason RM, Kamimura T, Zhang Z. TGF-beta1 induces human alveolar epithelial to mesenchymal cell transition (EMT). Respir Res.6:56. 2005.

4. Kim KK, Kugler MC, Wolters PJ, Robillard L, Galvez MG, Brumwell AN, et al. Alveolar epithelial cell mesenchymal transition develops in vivo during pulmonary fibrosis and is regulated by the extracellular matrix. Proc Natl Acad Sci U S A.103:13180-5. 2006.

5. Lamouille S, Derynck R. Cell size and invasion in TGF-beta-induced epithelial to mesenchymal transition is regulated by activation of the mTOR pathway. J Cell Biol.178:437-51. 2007.

6. Lenferink AE, Magoon J, Cantin C, O'Connor-McCourt MD. Investigation of three new mouse mammary tumor cell lines as models for transforming growth factor (TGF)-beta and Neu pathway signaling studies: identification of a novel model for TGF-beta-induced epithelial-to-mesenchymal transition. Breast Cancer Res.6:R514-30. 2004.

7. Park SH, Choi MJ, Song IK, Choi SY, Nam JO, Kim CD, et al. Erythropoietin decreases renal fibrosis in mice with ureteral obstruction: role of inhibiting TGF-beta-induced epithelial-to-mesenchymal transition. J Am Soc Nephrol.18:1497-507. 2007.

8. Willis BC, Liebler JM, Luby-Phelps K, Nicholson AG, Crandall ED, du Bois RM, et al. Induction of epithelial-mesenchymal transition in alveolar epithelial cells by transforming growth factor-beta1: potential role in idiopathic pulmonary fibrosis. Am J Pathol.166:1321-32. 2005.

9. Wynn TA. Cellular and molecular mechanisms of fibrosis. J Pathol.214:199-210. 2008.

10. Xu J, Lamouille S, Derynck R. TGF-beta-induced epithelial to mesenchymal transition. Cell Res.19:156-72. 2009.

11. Brown AC, Rowe JA, Barker TH. Guiding epithelial cell phenotypes with engineered integrin-specific recombinant fibronectin fragments. Tissue Eng Part A.17:139-50.

12. Engler AJ, Griffin MA, Sen S, Bonnemann CG, Sweeney HL, Discher DE. Myotubes differentiate optimally on substrates with tissue-like stiffness: pathological implications for soft or stiff microenvironments. J Cell Biol.166:877-87. 2004.

13. Engler AJ, Sen S, Sweeney HL, Discher DE. Matrix elasticity directs stem cell lineage specification. Cell.126:677-89. 2006.

14. Paszek MJ, Zahir N, Johnson KR, Lakins JN, Rozenberg GI, Gefen A, et al. Tensional homeostasis and the malignant phenotype. Cancer Cell.8:241-54. 2005.

15. Wozniak MA, Desai R, Solski PA, Der CJ, Keely PJ. ROCK-generated contractility regulates breast epithelial cell differentiation in response to the physical properties of a three-dimensional collagen matrix. J Cell Biol.163:583-95. 2003.

16. Pelham RJ, Jr., Wang Y. Cell locomotion and focal adhesions are regulated by substrate flexibility. Proc Natl Acad Sci U S A.94:13661-5. 1997.

17. Pelham RJ, Jr., Wang YL. Cell locomotion and focal adhesions are regulated by the mechanical properties of the substrate. Biol Bull.194:348-9; discussion 9-50. 1998.

18. Vogel V, Sheetz M. Local force and geometry sensing regulate cell functions. Nat Rev Mol Cell Biol.7:265-75. 2006.

19. Georges PC, Janmey PA. Cell type-specific response to growth on soft materials. J Appl Physiol.98:1547-53. 2005.

20. Wipff PJ, Rifkin DB, Meister JJ, Hinz B. Myofibroblast contraction activates latent TGF-beta1 from the extracellular matrix. J Cell Biol.179:1311-23. 2007.

21. Spruit MA, Janssen DJ, Franssen FM, Wouters EF. Rehabilitation and palliative care in lung fibrosis. Respirology.14:781-7. 2009.

22. Selman M, Pardo A. Role of epithelial cells in idiopathic pulmonary fibrosis: from innocent targets to serial killers. Proc Am Thorac Soc.3:364-72. 2006.

23. Liu F, Mih JD, Shea BS, Kho AT, Sharif AS, Tager AM, et al. Feedback amplification of fibrosis through matrix stiffening and COX-2 suppression. J Cell Biol.190:693-706.

24. Tse JR, Engler AJ. Preparation of hydrogel substrates with tunable mechanical properties. Curr Protoc Cell Biol.Chapter 10:Unit 10 6.

25. Schefe JH, Lehmann KE, Buschmann IR, Unger T, Funke-Kaiser H. Quantitative real-time RT-PCR data analysis: current concepts and the novel "gene expression's CT difference" formula. J Mol Med.84:901-10. 2006.

26. Kim Y, Kugler MC, Wei Y, Kim KK, Li X, Brumwell AN, et al. Integrin alpha3beta1-dependent beta-catenin phosphorylation links epithelial Smad signaling to cell contacts. J Cell Biol.184:309-22. 2009.

27. Wang Z, Symons JM, Goldstein SL, McDonald A, Miner JH, Kreidberg JA. (Alpha)3(beta)1 integrin regulates epithelial cytoskeletal organization. J Cell Sci.112 (Pt 17):2925-35. 1999.

28. Solon J, Levental I, Sengupta K, Georges PC, Janmey PA. Fibroblast adaptation and stiffness matching to soft elastic substrates. Biophys J.93:4453-61. 2007.

29. Chang CJ, Chao CH, Xia W, Yang JY, Xiong Y, Li CW, et al. p53 regulates epithelial-mesenchymal transition and stem cell properties through modulating miRNAs. Nat Cell Biol.13:317-23.

30. Yang MH, Hsu DS, Wang HW, Wang HJ, Lan HY, Yang WH, et al. Bmi1 is essential in Twist1-induced epithelial-mesenchymal transition. Nat Cell Biol.12:982-92.

31. Barker TH, Grenett HE, MacEwen MW, Tilden SG, Fuller GM, Settleman J, et al. Thy-1 regulates fibroblast focal adhesions, cytoskeletal organization and migration through modulation of p190 RhoGAP and Rho GTPase activity. Exp Cell Res.295:488-96. 2004.

32. Zhou Y, Hagood JS, Lu B, Merryman WD, Murphy-Ullrich JE. Thy-1-integrin alphav beta5 interactions inhibit lung fibroblast contraction-induced latent transforming growth factor-beta1 activation and myofibroblast differentiation. J Biol Chem.285:22382-93.

33. Levental KR, Yu H, Kass L, Lakins JN, Egeblad M, Erler JT, et al. Matrix crosslinking forces tumor progression by enhancing integrin signaling. Cell.139:891-906. 2009.

34. Santhanam L, Tuday EC, Webb AK, Dowzicky P, Kim JH, Oh YJ, et al. Decreased S-nitrosylation of tissue transglutaminase contributes to age-related increases in vascular stiffness. Circ Res.107:117-25.

35. Hynes RO. The extracellular matrix: not just pretty fibrils. Science.326:1216-9. 2009.

36. Choquet D, Felsenfeld DP, Sheetz MP. Extracellular matrix rigidity causes strengthening of integrin-cytoskeleton linkages. Cell.88:39-48. 1997.

37. Grashoff C, Hoffman BD, Brenner MD, Zhou R, Parsons M, Yang MT, et al. Measuring mechanical tension across vinculin reveals regulation of focal adhesion dynamics. Nature.466:263-6.

38. Jiang G, Huang AH, Cai Y, Tanase M, Sheetz MP. Rigidity sensing at the leading edge through alphavbeta3 integrins and RPTPalpha. Biophys J.90:1804-9. 2006.

39. Roca-Cusachs P, Gauthier NC, Del Rio A, Sheetz MP. Clustering of alpha(5)beta(1) integrins determines adhesion strength whereas alpha(v)beta(3) and talin enable mechanotransduction. Proc Natl Acad Sci U S A.106:16245-50. 2009.

40. Hinz B. Tissue stiffness, latent TGF-beta1 activation, and mechanical signal transduction: implications for the pathogenesis and treatment of fibrosis. Curr Rheumatol Rep.11:120-6. 2009.

CHAPTER 6

FUTURE CONSIDERATIONS

EMT is a critical process in the progression of invasive pathologies like cancer and fibrosis, therefore, it is essential that this process is fully understood in order to gain therapeutic insights. This dissertation provides evidence that the micromechanical environment with which epithelial cells interact is a strong contributor to EMT; however, integrin specificity is the ultimate driving force behind EMT. The results presented here suggest that EMT following αv integrin binding on rigid substrates results in increased levels of TGFβ activation as a result of increased cell contractility. These results provide many insights into the onset and progression of pathological EMT and have implications in development of new treatment for fibrotic diseases. In addition, these results provide new design parameters for tissue engineering applications that seek to design cell instructive matrices.

One of the main contributions of this work is that it challenges current notions about the role of Fn in the progression of EMT. Many recent studies have implicated Fn as a key contributor to the onset of fibrotic pathologies by increasing cell contractility and TGFβ activation; (1-4) however, this work illustrates a different paradigm. Recent studies by Kim *et al.* showed *in vitro* that ATII epithelial cells undergo spontaneous EMT in response to provisional matrices (fibrin-fibronectin) but not in response to laminin-collagen matrices through a mechanism involving αvβ6 integrin mediated activation of endogenous TGFβ, suggesting that the mere presence of fibronectin would trigger a

cascade of EMT events in an epithelial tissue. Epithelial cells in the lung and other tissues routinely engage fibronectin matrices during wound repair and yet disease onset does not occur in the vast majority of these cases. This dissertation demonstrates Fn-mediated EMT is much more complicated than simple engagement of Fn, rather this work suggests two important concepts regarding epithelial engagement of Fn and the onset and progression of EMT. 1) The molecular conformation of Fn, for example folded vs. unfolded, determines integrin specific binding and subsequent inhibition or promotion of EMT. A more stabilized version of the molecule displaying RGD and PHSRN in close proximity engages α3β1 and α5β1 integrins promoting normal epithelial phenotypes, while a version of the molecule displaying only the RGD site however, cannot support binding of α3β1, but rather will engage αv integrins, become contractile, activate TGFβ and undergo EMT. 2) The mechano-environment in which cells interact with Fn is another critical determinant for the onset of EMT. Cells engaging Fn on soft substrates are not able to generate intracellular tension that is necessary to activate latent TGFβ and will maintain an epithelial phenotype. These points taken together suggest it is not merely interactions with Fn that lead to EMT, but rather uncontrolled interactions with Fn in perpetually unfolded conformations and/or stiff environments that lead to pathological EMT.

Fn-stiffness Mediated EMT

While this work provides new insights into how the ECM mechanical environment and integrin specificity induce or inhibit EMT, it opens the door for numerous additional questions. The work investigating Fn-stiffness mediated EMT defines a cyclic process of increased substrate stiffness leading to increased contractility, which in turn leads to

increased TGFβ activation, which drives EMT, resulting in more contractile phenotypes and further perpetuation of the process; however, the initiating factor of this cyclic process remains unclear. Interestingly, recent studies into the progression of renal fibrosis show that the ECM actually becomes stiff prior to the development of fibrosis, (5) implicating increased contractility on increasingly stiff surfaces as the initiating factor in this cyclic process. *In vitro*, this could be demonstrated experimentally by inducing contractility with pharmacological agents on soft substrates and observing TGFβ activation and EMT. Furthermore, inducing contractility on soft surfaces and inhibiting TGFβ should result in the maintenance of an epithelial phenotype. Experiments such as these would further implicate increased tissue stiffness in the onset and progression of EMT, however, it remains unknown what produces the initial stiffening of matrix. It seems most likely that some initial event, be it injury, viral infection, etc., would initiate the clotting cascade and inflammatory response, recruiting macrophages and matrix producing fibroblasts. If the inflammatory response was uncontrolled and lead to over activation of resident fibroblast populations and excessive ECM production, the result would be a decrease in the matrix compliance. The surrounding epithelial cells would sense these changes and potentially undergo EMT, leading to more ECM producing fibroblasts and further perpetuate the disease. Being that fibrosis is a progressive disease, this seems a likely mechanism through which the disease compounds. Studies investigating the progression of tissue stiffening in fibrotic diseases *in vivo* and correlating stiffening to the first signs of EMT would help to fully understand the dynamics of ECM stiffening and the onset of EMT. Using an SPC specific promoter, Kim et al. elegantly showed that ATII specific EMT does incur in vivo in bleomycin

induced pulmonary fibrosis. This system could be combined with AFM analysis of living lung slices utilized in this dissertation and by others (6) to fully elucidate the dynamics of EMT and tissue stiffening.

Integrin Specific Binding in EMT

While increased stiffness is clearly a driving factor in Fn-mediated EMT, the results presented here suggest that integrin specificity is the primary determinant of EMT vs. normal wound healing. (7) In addition to characterizing changes in tissue stiffness overtime in *in vivo* fibrotic models, studies characterizing dynamic changes in integrin expression and/or binding over time and correlating those to EMT responses *in vivo* could provide insight into these complex ECM/cell dynamics. In addition, little is known about integrin binding on rigid vs. soft substrates, however there is some evidence that α5β1 and αvβ3 binding is differential on soft vs. hard substrates. α5β1 binding has been shown to exhibit a "catch" bond type response on stiffer substrates, (8) and αvβ3 in complex with receptor-like protein tyrosine phosphatase α (RPTPα) contributes to stiffness sensing at the leading edge of fibroblasts. (9) However, neither of these studies considered the contribution of additional integrins. Because integrin binding seems to be the primary driver in the onset of EMT, it is critical to know and understand the differences in integrin binding on soft vs. hard substrates.

Another important concept presented by this work is the role of the Fn synergy site in EMT. While many studies have shown the implications of Fn unfolding and increases in the spacing between the RGD and PHSRN sites in directing cell fate (and in this study, EMT), it remains unclear to what degree, if at all, Fn unfolding occurs *in vivo.* Tools allowing for detection of Fn unfolding *in vivo* would provide much needed insight

into the role of alterations in the spacing between the RGD and PHSRN sites in physiologically relevant systems. If tools such as these were developed, they could be used in conjunction with the ATII cell tracking system described previously to potentially correlate increased spacing between the RGD and PHSRN sites and EMT *in vivo.* Interestingly, it has been shown *in vitro* using FRET techniques, that highly contractile fibroblasts associated with pulmonary fibrosis increasingly unfold Fn matrices. (10) EMT would result in an increasing number of contractile cells, which theoretically could increasingly unfold Fn in the surrounding ECM, further compounding EMT. Probes for detecting folded vs. unfolded Fn *in vivo* could provide critical insight into the existence of such hypothesized events and could potentially be engineered to target therapeutics to fibrotic regions containing chronic levels of unfolded Fn.

The degree of Fn unfolding *in vitro* on soft vs. stiff substrates also remains unclear. It has been suggested that Fn becomes unfolded when adsorbed to stiff substrates such as seen on tissue culture plastic. (11-13) It is unknown if the converse is true; does Fn exist as a more compact, i.e. less unfolded, molecule on soft substrates? It has been hypothesized that Fn is one of the key molecules in "mechano-sensing" (14) and, if true, could be one mechanism through which cells "sense" their mechanical environment. The studies presented here suggest that Fn-stiffness mediated EMT is the result of increased contractility with increasing stiffness, and subsequent increased TGFβ activation; If Fn becomes increasingly unfolded with increasing substrate stiffness, increased contractility could result from increased αv integrin engagement.

Once more highlighting the importance of the Fn synergy site in directing cell phenotype, this work shows for the first time that Fn binds the epithelial integrin α3β1 in a PHSRN-

dependent manner and, in the context of SPR studies, stabilized FnIII9'10 domains bind integrin α3β1 with affinities similar those of Ln. These results provide insight into how an epithelial cell might interact with a dynamic ECM in a wound healing environment to promote normal wound healing. As depicted in **Figure 6.1**, during normal homeostasis, an epithelial cell interacts predominantly with Ln through engagement of integrin α3β1. (15) In response to injury, epithelial cells will be exposed to Fn, and assuming Fn exists in a more compact form in which PHSRN and RGD are in close proximity, the epithelial cell will continue to engage integrin α3β1. This could potentially facilitate α5β1 binding, resulting in normal wound repair and a smooth transition back to a normal Ln matrix (**Figure 6.1A**). However, if after initial injury cells interact with a more unfolded conformation of Fn, as a result of any of the afore mentioned modes of unfolding, in which the RGD and PHSRN sites are no longer in close proximity, the epithelial cell will no longer be able to engage integrin α3β1 and will rather result in αv integrin binding, leading to altered wound healing. Unregulated αv integrin engagement has been linked to a host of pathological conditions associated with fibrotic conditions, including increased contractility, increased TGFβ activation, and increased EMT. (1) This proposed interaction highlights the importance of the ECM microenvironment in directing proper wound healing.

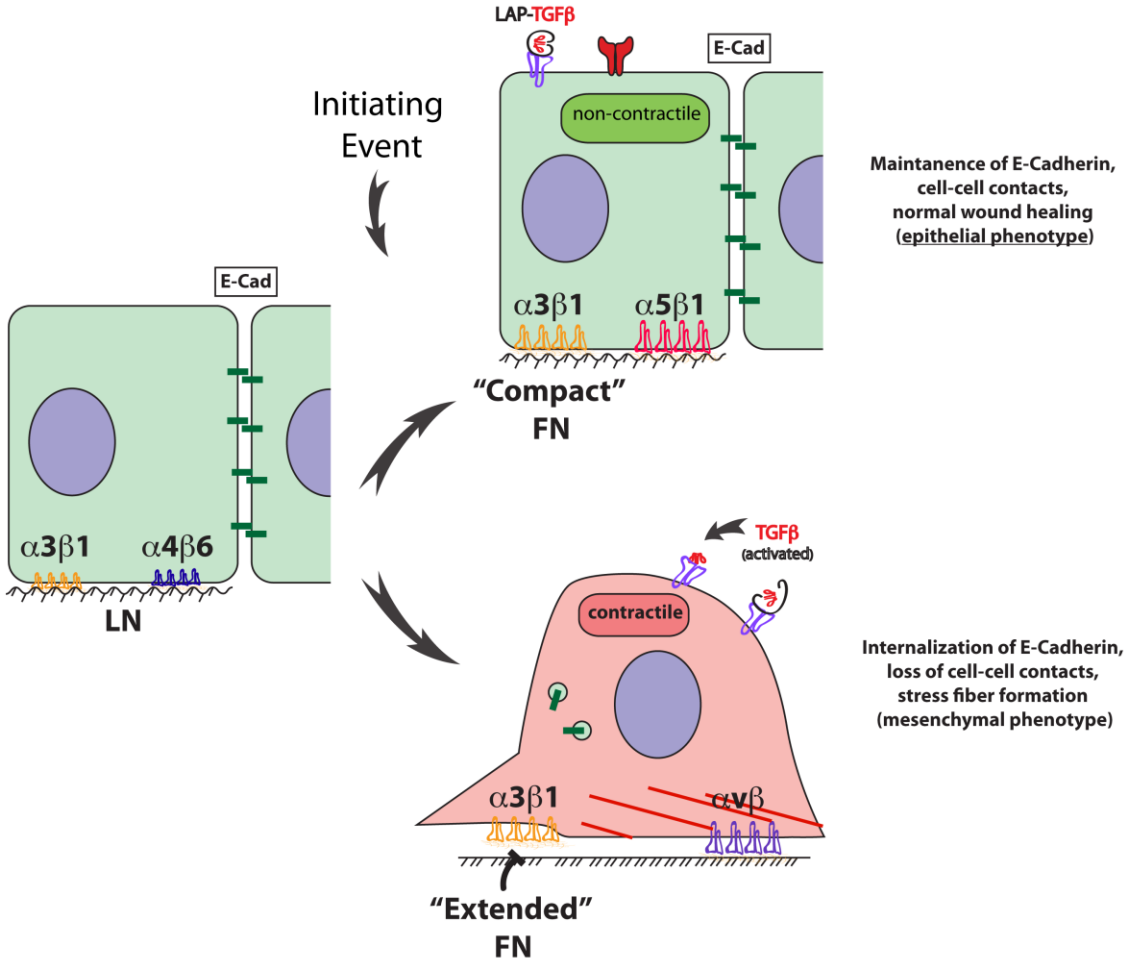

Figure 6.1: Proposed role of Fn unfolding on epithelial wound healing events: The studies presented here indicate that the Fn synergy site contributes to integrin α3β1 binding. The compact form of the molecule, with the RGD and PHSRN sites in close proximity, promotes integrin α3β1 binding and inhibits contractile signaling and TGFβ activation. The extended form of the molecule, with the RGD and PHSRN sites at a distance to great to be bound by the same integrin, promotes integrin αv binding and leads to the activation of pro-contractile signals in the cell (i.e. Rho and ROCK) and subsequent contraction-mediated TGFβ activation and EMT. This proposed model suggests that understanding the dynamics of Fn conformational changes *in vitro* are essential for understanding the pathological progression of fibrotic pathologies.

Fibrosis Therapeutics

From a therapeutic point of view, this work provides many insights into designing effective therapeutics for fibrotic pathologies. Because TGFβ is a primary inducer of EMT many recent therapeutic strategies have targeted TGFβ or TGFβ activating integrins such as αvβ6, for example through monoclonal antibodies or knock-out models. (16-18) The studies presented here suggest that cell contractility is a primary contributor to EMT through TGFβ activation and that it can occur in response to increased stiffness and the underlying ECM. Therapeutic schemes targeting "relaxing" the underlying ECM could prove to be more effective. This could be achieved through reducing a cell's ability to respond to a stiff matrix by inhibiting cell contractility, directly decreasing matrix stiffness by matrix metalloproteases, or combinatorial methods encompassing both of these approaches. However, inhibiting cell contractility in the lung could prove to be highly detrimental to breathing, so approaches such as these would need to be highly controlled and specifically targeted to fibrotic regions. These methods could potentially prove to be effective methods for inhibiting EMT in that they will get to the root of the problem of uncontrolled TGFβ activation.

Implications in Biomaterial Design and Regenerative Medicine Applications

The findings of this dissertation also have implications in traditional biomaterial design. Biomaterials often elicit fibrotic responses, which are characterized by excessive deposition of extracellular matrix (ECM) and hardening of the surrounding tissue. Biomaterial-induced fibrosis, best known as the foreign body capsule, consists of a thick collagen capsule surrounding the biomaterial. (19) Similarities exist between

biomaterials-induced fibrosis and many other fibrotic pathologies, including pulmonary fibrosis. As with many fibrotic pathologies, biomaterials-induced fibrosis is thought to result from unresolved inflammation. Biomaterials-induced-fibrosis can lead to a host of problems including loss of material function and loss of function in the surrounding tissue due to excessive scar tissue formation. This work suggests that that EMT could result in response to increasingly rigid materials. In order to design effective biomaterials, the effects of material properties, such as elasticity, on cellular responses to materials should be considered. In particular, as evidence of mechanical effects on biology continue to mount, it is clear that biomaterial scientists must strive harder to mimic the physiological environment of cells, from growth factor concentrations and ECM molecules displayed to micromechanical properties.

These results also open many possibilities in the field of tissue engineering and regenerative medicine. Directing specific cell behaviors, particularly differentiation, in response to biomaterials for regenerative medicine applications is thus far a mostly unrealized goal. (20, 21) Many current technologies have been inspired by the reductionist point of view and have focused on developing simple and merely adequate environments that facilitate simple cell processes, such as cellular adhesion. For example, many groups have used the RGD motif to serve as an 'ECM mimetic' in the context of synthetic biomaterials. (22) However, even if ECM-derived peptides have largely demonstrated their utility through supporting cell adhesion, the lack of biological specificity of many of these peptide motifs is simply not optimal for controlling more integrated processes, such as differentiation. (23) Inducing complex cellular processes, which is the goal of many tissue engineering endeavors, requires more specific integrin-

signaling scaffolds. However, the use of full length ECM molecules is also not ideal due to the inherent capacity of ECM to bind multiple and diverse integrins and growth factors. For that reason, many groups have begun to incorporate engineered ECM variants that display only a fraction of the native ECM protein complexity yet still attempt to provide sufficient instruction for directing cell phenotype. (23-25) The FnIII9'10 fragments created here can provide new tools for designing these integrin-specific microenvironments for directing epithelial cell fate. Similar fragments have been used recently to induce stem cell differentiation in 3D gels and promote osseointegration *in vivo*. (23, 25) Though this work has mainly focused on the role of EMT in pathological conditions, induction of EMT may be favorable for some tissue engineering applications aiming to create complex cellular tissues which require epithelial and mesenchymal cells in close proximity. To design such a complex tissue, one could imagine patterning epithelial promoting fragments, such as FnIII9'10, and mesenchymal promoting fragments, such as FnIII10, in defined spatial orientations and patterns. Furthermore, fragments could be incorporated into more complex systems, featuring varying levels of elasticity, to induce epithelial or mesenchymal phenotypes. Utilizing integrin-specific fragments in conjunction with well defined elastic moduli creates many new design opportunities for tissue engineering applications.

In conclusion, this dissertation shows for the first time that alveolar epithelial cell EMT is influenced by both integrin-specific engagements to the central cell binding domain of Fn as well as substrate stiffness. These EMT events are likely due to an increase in cell contractility, ultimately resulting in increasing TGFβ activation. Furthermore, these studies show that Fn can engage α3β1 with high affinity through

interactions with the 9th and 10th type III domains when the RGD and PHSRN sites are in close proximity. This work highlights that EMT is a complicated process, likely resulting from a shift in both the protein composition and the mechanical microenvironment of the surrounding ECM. Furthermore, this work highlights that epithelial cell interactions with Fn are complex and if not tightly controlled can lead to pathological progression of fibrotic conditions. These findings open new paths for potential treatments of fibrotic diseases, offer new tools for designing cell instructive matrices, and provide insight into designing effective biomaterials. Further investigation into the role of Fn-mediated EMT could provide many new avenues for discovery in the field of mechanotransduction.

References

1. Kim KK, Kugler MC, Wolters PJ, Robillard L, Galvez MG, Brumwell AN, et al. Alveolar epithelial cell mesenchymal transition develops in vivo during pulmonary fibrosis and is regulated by the extracellular matrix. Proc Natl Acad Sci U S A.103:13180-5. 2006.

2. Kim Y, Kugler MC, Wei Y, Kim KK, Li X, Brumwell AN, et al. Integrin alpha3beta1-dependent beta-catenin phosphorylation links epithelial Smad signaling to cell contacts. The Journal of cell biology.184:309-22. 2009.

3. Camara J, Jarai G. Epithelial-mesenchymal transition in primary human bronchial epithelial cells is Smad-dependent and enhanced by fibronectin and TNF-alpha. Fibrogenesis Tissue Repair.3:2.

4. Kim KK, Wei Y, Szekeres C, Kugler MC, Wolters PJ, Hill ML, et al. Epithelial cell alpha3beta1 integrin links beta-catenin and Smad signaling to promote myofibroblast formation and pulmonary fibrosis. J Clin Invest.119:213-24. 2009.

5. Georges PC, Hui JJ, Gombos Z, McCormick ME, Wang AY, Uemura M, et al. Increased stiffness of the rat liver precedes matrix deposition: implications for fibrosis. Am J Physiol Gastrointest Liver Physiol.293:G1147-54. 2007.

6. Liu F, Mih JD, Shea BS, Kho AT, Sharif AS, Tager AM, et al. Feedback amplification of fibrosis through matrix stiffening and COX-2 suppression. The Journal of cell biology.190:693-706.

7. Brown AC, Rowe JA, Barker TH. Guiding epithelial cell phenotypes with engineered integrin-specific recombinant fibronectin fragments. Tissue Eng Part A.17:139-50.

8. Friedland JC, Lee MH, Boettiger D. Mechanically activated integrin switch controls alpha5beta1 function. Science.323:642-4. 2009.

9. Jiang G, Huang AH, Cai Y, Tanase M, Sheetz MP. Rigidity sensing at the leading edge through alphavbeta3 integrins and RPTPalpha. Biophys J.90:1804-9. 2006.

10. Barker TH, Baneyx G, Cardo-Vila M, Workman GA, Weaver M, Menon PM, et al. SPARC regulates extracellular matrix organization through its modulation of integrin-linked kinase activity. The Journal of biological chemistry.280:36483-93. 2005.

11. Narasimhan C, Lai CS. Conformational changes of plasma fibronectin detected upon adsorption to solid substrates: a spin-label study. Biochemistry.28:5041-6. 1989.

12. Pitt WG, Weaver DR, Cooper SL. Fibronectin adsorpton kinetics on phase segregated polyurethaneureas. J Biomater Sci Polym Ed.4:337-46. 1993.

13. Underwood PA, Steele JG, Dalton BA. Effects of polystyrene surface chemistry on the biological activity of solid phase fibronectin and vitronectin, analysed with monoclonal antibodies. J Cell Sci.104 (Pt 3):793-803. 1993.

14. Vogel V. Mechanotransduction involving multimodular proteins: converting force into biochemical signals. Annu Rev Biophys Biomol Struct.35:459-88. 2006.

15. Fehrenbach H. Alveolar epithelial type II cell: defender of the alveolus revisited. Respir Res.2:33-46. 2001.

16. Mullamitha SA, Ton NC, Parker GJ, Jackson A, Julyan PJ, Roberts C, et al. Phase I evaluation of a fully human anti-alphav integrin monoclonal antibody (CNTO 95) in patients with advanced solid tumors. Clin Cancer Res.13:2128-35. 2007.

17. Yang Z, Mu Z, Dabovic B, Jurukovski V, Yu D, Sung J, et al. Absence of integrin-mediated TGFbeta1 activation in vivo recapitulates the phenotype of TGFbeta1-null mice. The Journal of cell biology.176:787-93. 2007.

18. Horan GS, Wood S, Ona V, Li DJ, Lukashev ME, Weinreb PH, et al. Partial inhibition of integrin alpha(v)beta6 prevents pulmonary fibrosis without exacerbating inflammation. American journal of respiratory and critical care medicine.177:56-65. 2008.

19. Anderson JM, Rodriguez A, Chang DT. Foreign body reaction to biomaterials. Semin Immunol.20:86-100. 2008.

20. Hubbell JA. Bioactive biomaterials. Curr Opin Biotechnol.10:123-9. 1999.

21. Hubbell JA. Materials as morphogenetic guides in tissue engineering. Curr Opin Biotechnol.14:551-8. 2003.

22. Ruoslahti E. RGD and other recognition sequences for integrins. Annu Rev Cell Dev Biol.12:697-715. 1996.

23. Petrie TA, Capadona JR, Reyes CD, Garcia AJ. Integrin specificity and enhanced cellular activities associated with surfaces presenting a recombinant fibronectin fragment compared to RGD supports. Biomaterials.27:5459-70. 2006.

24. Carson AE, Barker TH. Emerging concepts in engineering extracellular matrix variants for directing cell phenotype. Regen Med.4:593-600. 2009.

25. Martino MM, Mochizuki M, Rothenfluh DA, Rempel SA, Hubbell JA, Barker TH. Controlling integrin specificity and stem cell differentiation in 2D and 3D environments through regulation of fibronectin domain stability. Biomaterials.30:1089-97. 2009.

APPENDIX A

FIBRONECTIN-INDUCED STIFFNESS-MEDIATED EMT: ANALYSIS IN L2 CELLS

Initial studies investigating the role of substrate stiffness in Fn-induced EMT were performed using L2 cells, an ATII-like cell line. Initial characterization of PA-gels utilized for analysis are presented here, along with analysis of proliferation, mRNA expression of epithelial and mesenchymal markers, and cell spreading in response to increases in substrate stiffness. The results presented here indicate that Fn-induced stiffness-mediated EMT is not specific to RLE-6TN cells, but rather, can occur in multiple epithelial cell lines.

Materials and Methods

Poly-acrylamide gel production

To determine the role of substrate stiffness on EMT events, poly-acrylamide (PA) gels of varying bis concentrations were created. PA gel solutions were produced by combining acrylamide and bis to final concentrations of 10% acrylamide (Biorad, Hercules, CA, USA) and 0.3%, 0.07%, 0.13%, or 0.26% bis (Biorad) and then polymerized under nitrogen by the addition of ammonium persulfate (VWR, West Chester, PA, USA) and N,N,N',N'-tetramethylethylenediamine (Biorad, Hercules, CA, USA) (0.05% final concentration each). The gels were allowed to polymerize under nitrogen for

approximately 15 minutes. Because PA is anti-adhesive, human plasma fibronectin (Fn) (BD Bioscience, San Jose, California, USA) was attached to the surface using the heterobifunctional crosslinker sulfosuccinimidyl-6-(4'-azido-2' nitrophenyl-amino)hexanoate (sulfo-SANPAH; Pierce Chemical Co., Rockford, IL., USA).

PA gel elasticity determination

The relationship between Young's modulus of the gel and bis concentration was determined macroscopically as previously described by Pelham *et al*. Briefly, 3 x 2 x1 mm gels of varying bis concentrations were produced and a weight was attached to the end. The change in length upon attachment of the weight was measured and E determined by the following equation:

$$E= \sigma/\varepsilon$$

E as a function of bis concentration was determined through linear regression. 3 independent experiments were performed.

Cell culture

L2 cells, an alveolar epithelial cell line (a generous gift from Prof. Douglas Eaton, Emory University, Atlanta, GA), were maintained in Coons modified media supplemented with 10% FBS, 1% P/S. To determine the affect of substrate stiffness on L2 cell fate, cells were plated on PA gels with Fn cross-linked on the surface with the following rigidities: E=8.5 kPA, 13.3 kPA, 20.5 kPA, 36.1 kPA, or on tissue culture plastic (TCP) coated with Fn or Ln as a control. Cells were plated at a density of 25,000 cells/cm^2 in Coon's modified media supplemented with 10% FBS, and 1% Penicillin/ Streptomycin in the absence or presence of 10 μM Y-27632 (EMD Biosciences, Gibbstown, NJ, USA). Media was changed every 48 hours.

BrdU proliferation assay

Proliferation in response to substrate stiffness was determined with a standard Bromodeoxyuridine (BrdU) proliferation assay (Exalpha Biologicals, Shirley, MA, USA). L2 cells were plated on substrates of varying stiffness and cultured for 24, then BrdU was added to the media and incubated for 24 hours. Cells were then fixed with glutaraldehyde and an ELISA performed for BrdU according to manufacturer's specifications. Three independent triplicate experiments were performed. Data shown is pooled for all experiments performed. Proliferation was normalized to the lowest and highest levels of proliferation, such that cells cultured on the lowest stiffness substrate, E=8.5 kPA, was equivalent to 0%, and cells cultured on E=26.5 was equivalent to 100% proliferation.

Analysis of gene expression

L2 cells were cultured on substrates of varying stiffness for 1 week in the absence or presence of 10 μM Y-27632. Cells were trypsinized, mRNA isolated (RNAeasy, Qiagen, Valencia, CA, USA) and c-DNA generated (High Capacity cDNA Reverse Transcription Kit, Applied Biosystems, Foster City, CA, USA). Primers (Invitrogen, Carlsbad, CA, USA) used for q-PCR reactions were as follows: N-cadherin forward AGGGCCTTAAAGCTGCTGACA; N-cadherin reverse TCATAGTCGAAGACTAAAAGGGAGTCATAT; Vimentin forward CCCAGATTCAGGAACAGCAT; Vimentin reverse CACCTGTCTCCGGTATTCGT (designed using Primer3Plus software); E-cadherin forward TGAGCATGCCCCAGTATCG ; E-cadherin reverse CTGCCTTCAGGTTTTCATCGA; β-actin forward ACCCGCCACCAGTTCGCCAT; β-actin reverse

CTTGCTCTGGGCCTCGTCGC; surfactant protein C (SPC) forward GTGGTTGTGGTGGTAGTC; SPC reverse AATAGAGAAGGTAGCGATGG: Plasminogen activator inhibitor-1 (Pai-1) forward CACAGTGCTGGGTGTAATGG; Pai-1 reverse GTTTGTGGGGCAGCTATTGT (designed using Primer3Plus software). Q-PCR was performed on a Step One Plus ABI thermocycler (Applied Biosystems) using Power SYBR Green Master Mix (Applied Biosystems). Data was analyzed using the ΔΔCT method using β-actin as the endogenous control and comparing expression levels to cells cultured on the lowest stiffness substrate (E=8.6 kPA). Q-PCR reactions were run in triplicate and performed for 3 independent experiments. Data shown was pooled from 3 independent experiments.

Analysis of cell shape and cytoskeleton organization

L2 cell contractility in response to substrate stiffness was determined through analysis of stress fiber formation by culturing cells on Fn-substrates of varying stiffness and Fn or Ln-coated glass slides in the absence or presence of 10 μM Y-27632 for 1 week. Media was changed every 48 hours. Cells were then fixed with 4% formaldehyde, actin was stained with Texas-red phalloidin (Invitrogen) and nuclei were stained with Hoescht stain (Invitrogen). Coverslips were mounted and images acquired with a Nikon Eclipse (TiE) inverted fluorescence microscope at 20X magnification (PlanApo 100X, 1.4 NA oil-immersion objective) with a CoolSNAP HQ2 Monochromatic CCD camera. Representative images are presented.

Analysis of circularity

Cells were cultured on substrates of varying stiffness for 1 week in the absence or presence of 10 μM Y-27632 and the cytoskeleton visualized as described above. Area

and perimeter of individual cells was determined for each condition using Image J (NIH Freeware) image processing software, then circularity was determined using the equation circularity = $4\pi(\text{area}/\text{perimeter}^2)$. Three independent images were analyzed for each condition, and at least 10 cells were analyzed per image. Data is pooled from all 3 images analyzed per condition.

Statistical Analysis

All statistical analysis was performed by multi-variate ANOVA using Prism (Graphpad Software Inc., La Jolla, CA, USA). Statistical significance is achieved for $p<0.05$.

Results

Young's Modulus directly correlates with percent bis concentration

To determine the relationship between percent bis concentration of the PA gels and Young's modulus (E), 3 x 2 x1 mm gels of varying bis concentrations were produced and a weight was attached to the end. The change in length upon attachment of the weight was measured and E determined by Hooke's law using the following equation:

$$E = \sigma/\varepsilon$$

where σ=force/area and $\varepsilon=\Delta l/l$. E as a function of bis concentration was determined through linear regression. It was found that E increases linearly with percent bis concentration (%bc), and this relationship can characterized by the following equation:

$$E = 120.12(\%bc) + 4.9$$

Using regression analysis, this relationship was found to have an R^2 value of 0.986 (**Figure A.1A**). To determine if the amount of Fn cross-linked to the surface of the gels was equivalent for PA gels of varying rigidities, gels were produced with 0.03%, 0.07%, 0.13%, and 0.26% bis concentrations and then Fn was cross-linked to the surface of the gels using sulfo-SANPAH. Relative concentrations of Fn on the surface of the PA gels was determined using a modified ELISA approach. A One-way ANOVA showed there was no statistically significant difference in the amount of Fn cross-linked to the surface between the 4 rigidities (**Figure A.1B**).

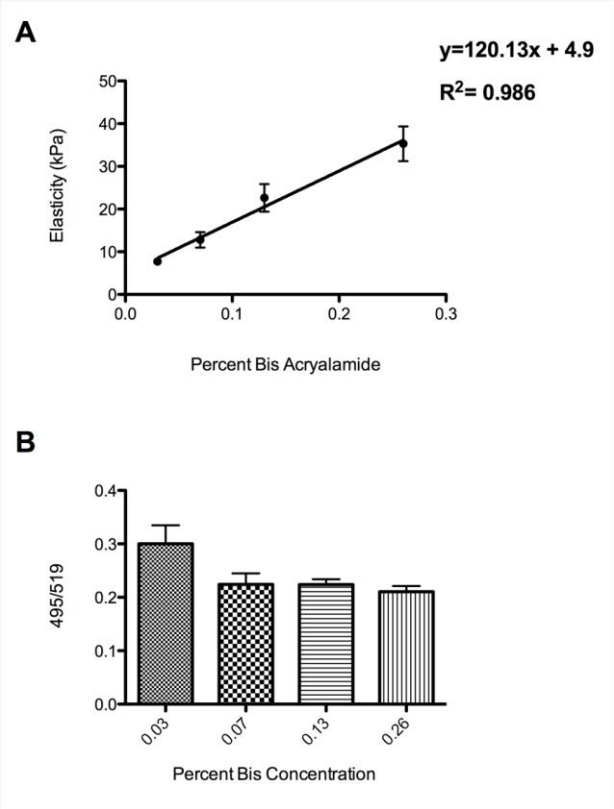

Figure A.1: Young's modulus directly correlates with percent bis concentration. Young's modulus was determined as a function of bis concentration by creating PA gels of varying percent bis concentration and measuring σ and ε (**A**). Alexa Flour 488 conjugated Fn was cross-linked to gels of varying percent bis concentration and then relative amounts of Fn on the surface of the gels was determined by measuring fluorescence with excitation and emission at 495 and 519 nm respectively (**B**).

Cells display increasing levels of proliferation with increasing stiffness

To investigate if substrate stiffness modulates L2 cellular behavior, L2 proliferation was analyzed. L2 cells were cultured on Fn-substrates of varying stiffness or Ln coated TCP for 24 hours in the absence or presence of 10 μM Y-27632, at which point proliferation was analyzed by BrdU incorporation (**Figure A.2**). A standard ELISA was performed for BrdU and absorbance measured at 450 nm, and proliferation was normalized to the lowest and highest levels of proliferation, such that cells cultured on the lowest stiffness

substrate, E=8.5 kPA, was equivalent to 0%, and cells cultured on E=26.5 was equivalent to 100% proliferation. L2 cells cultured on the lowest stiffness substrate, E=8.5 kPa, displayed minimal proliferation (0% +/- 20.42). To confirm that the lack of proliferation observed was not due to cell death, a live:dead assay was performed, and it was found that cells displayed a high percentage of viable cells on all substrates analyzed (data not shown). Proliferation was found to display a biphasic response, with proliferation increasing with increasing stiffness on gels of E=13.3 kPA and E=20.5 kPA (71.53% +/- 27.89 and 100 +/- 21.25 respectively) then decreasing slightly on the highest stiffness gel, E= 36.1 kPA, (60.05% +/- 10.97) and on TCP (29.58% +/- 1.778). One-way ANOVA analysis showed significant difference in proliferation on the lowest stiffness gels, E=8.5 kPa, and gels with E=20.5 kPa, $p<0.01$. In addition, proliferation on gels with E=20.5 kPA was significantly higher than proliferation on TCP, $p<0.05$. Differences in proliferation were abrogated through the addition of 10 μM Y-27632, and no statistical differences in proliferation were observed in the presence of the ROCK inhibitor ($p=0.86$).

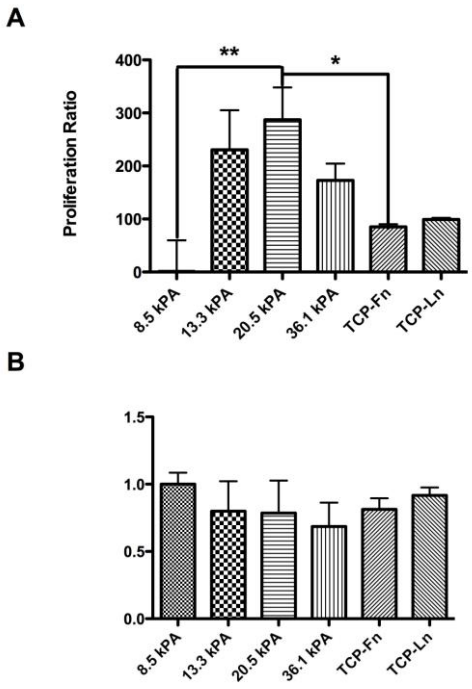

Figure A.2: Proliferation of L2 cells cultured on substrates of varying stiffness after 24 hours. Cells were cultured for 24 hours on PA gels of varying stiffnesss, Fn, or Ln-coated TCP in the absence (**A**) or presence (**B**) of 10 μM Y-27632 ROCK inhibitor, then proliferation was measured with a BRDU assay. Data is pooled from three independent triplicate experiments and is expressed as percent proliferation; E=8.5 kPA, 0% and E=25.6=100%. A One-way ANOVA analysis was performed. ****** denotes $p<0.01$, and ***** denotes $p<0.05$.

Cells increase expression of mesenchymal markers when cultured on gels of increasing stiffness and this is inhibited by the addition of ROCK inhibitor

To determine if observed differences in morphology of L2 cells cultured on substrates of varying stiffness resulted in differences in gene expression, expression of epithelial (SPC, alveolar specific and E-cadherin) and mesenchymal (vimentin, N-cadherin) genes by q-PCR were analyzed. mRNA was isolated from cells cultured for 1 week on gels with E= 8.5 kPA, 13.3 kPA, 20.5 kPA, 36.1 kPA, or Fn or Ln-coated TCP in the absence (green bars) or presence (red bars) of 10 μM Y-27632 (**Figure A.3**). qPCR data was analyzed

using the ΔΔCt method, using β-actin as the control gene and comparing all samples to cells cultured on the lowest stiffness substrate (E=8.5 kPA). In general, cells increased expression of vimentin and N-cadherin as substrate stiffness increased, which coincided with a concomitant decrease in expression of SPC and E-cadherin. Upon addition of Y-27632 to the culture media, these differences were abrogated. A one-way ANOVA showed no significant differences in expression of any genes analyzed between cells cultured on substrates of varying rigidities in the presence of Y-27632.

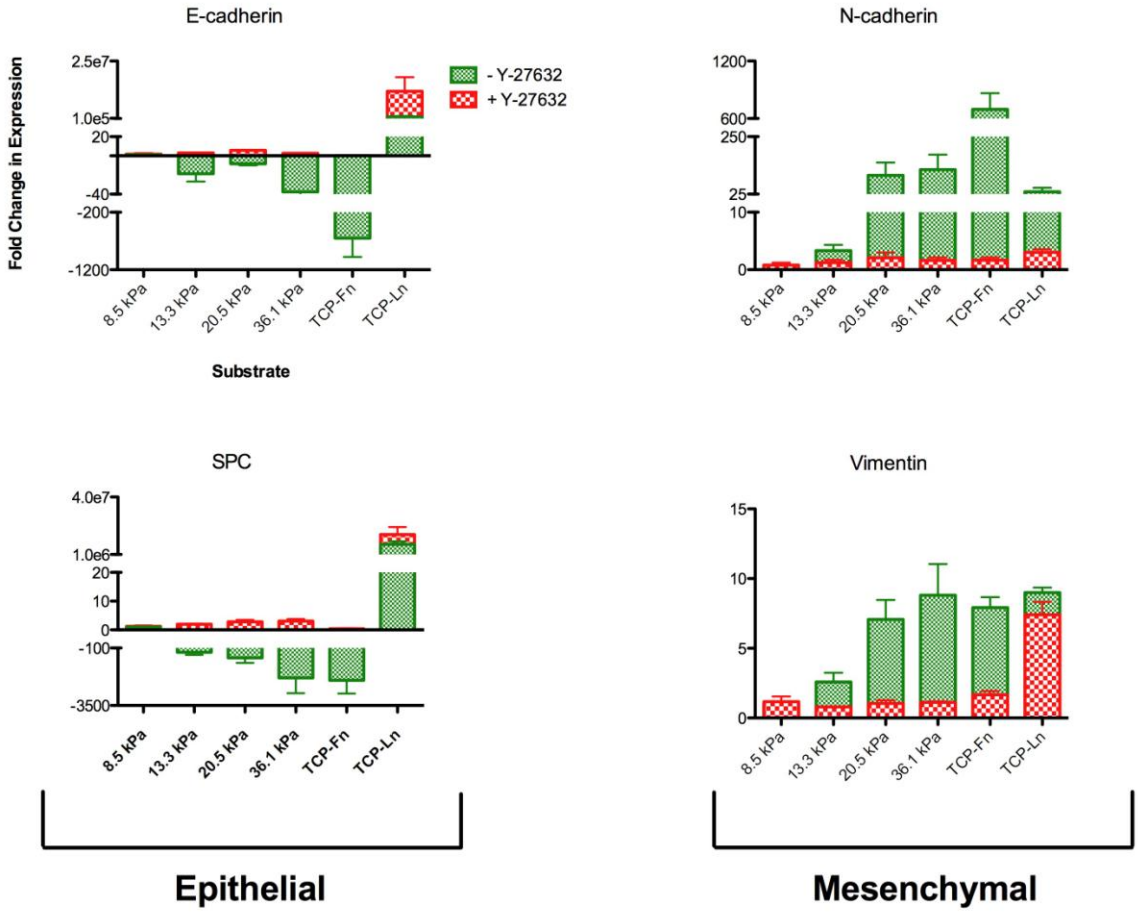

Figure A.3: q-PCR analysis of gene expression of L2 cells cultured on substrates of varying stiffness in the absence or presence of Y-27632. L2 cells were cultured on substrates of varying stiffness or Fn or Ln-coated TCP for 1 week. RNA was isolated and q-PCR performed for various epithelial and mesenchymal markers. Cells cultured in the absence of Y-27632 are presented as green bars, and cells cultured in the presence of 10 μM Y-2632 are presented as red bars. Data was analysed using the ΔΔCT method taking reaction efficiency into consideration, using β-actin as the control gene and comparing all samples to cells cultured on the lowest stiffness substrate (E=8.6 kPA).

Cells display different degrees of cytoskeleton alignment on gels of varying stiffness, and these differences are negated by the addition of ROCK inhibitor

Next, cytoskeletal organization and stress fiber formation were analyzed by culturing L2 cells on substrates of varying stiffness in the absence (**Figure A.4A, C, E, G, I**) or presence (**Figure A.4B, D, F, H, J**) of 10 μM Y-27632. Cells were also cultured on Ln in the absence or presence of Y-27632 (**Figure A.4K, L**) due to Ln known role in preventing EMT. After 1 week in culture, cells were stained with Texas-red phallodin to visualize the actin cytoskeleton. In the absence of Y-27632, cells cultured on the lowest stiffness substrate (E=8.5 kPA, **Figure A.4A**) displayed a round morphology and diffuse staining for actin. Cells cultured on the next highest stiffness substrate (E=13.3 kPA, **Figure A.4C**) displayed a slightly more elongated morphology, but continued to display on diffuse staining for actin. On the higher stiffness substrates (E=20.5 kPA, 36.1 kPA, and TCP **Figure A.4E, G, I** respectively) cells became more elongated and increasingly displayed aligned, thick actin filaments characteristic of stress fibers, and as expected, cells cultured on Ln surfaces maintained an epithelial phenotype. Cells cultured in the presence of Y-27632 displayed a round morphology and diffuse staining for actin regardless of the stiffness of the underlying substrate. Cell circularity was calculated to quantify differences observed in cell shape (**Figure A.4M**); values closer to 1 indicated a more rounded cell. Cells exhibited statically significant decreasing circularity values with increasing stiffness ($p<0.001$ each group compared to E=8.5 kPA) with cells exhibiting the following circularity values: E=8.5 kPA, 0.48; E=13.3 kPA, 0.35; E=20.5 kPA, 0.29; E=36.1 kPA, 0.28; Fn-TCP, 0.33. The addition of 10 μM Y-27632 resulted in circularity values greater than 0.42. The addition of Y-27632 to cells cultured on

E=20.5 kPA, E=36.1 kPA, and Fn-TCP significantly decreased the increased their circularity values compared to the respective stiffness in the absence of Y-27632 inhibitor ($p<0.001$). Cells cultured on Ln-TCP exhibited similar circularity values in both the absence and presence of Y-27632 with circularity values of 0.53 and 0.55, respectively.

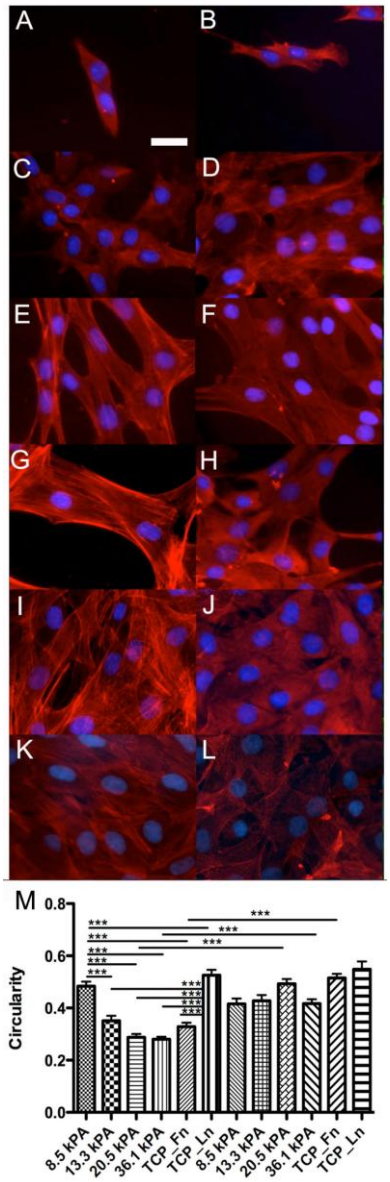

Figure A.4: Actin cytoskeleton alignment, stress fiber formation, and changes in cell circularity in response to substrate stiffness. L2 cells were cultured for 1 week on Fn substrates of increasing stiffness in the absence (**A, C, E, G, I**) of presence (**B, D, F, H, J)** of 10 μM Y-27632. Cells were also cultured on Ln in the absence or presence of Y-27632 (**Figure K, L**). To analyze stress fiber formation, the actin cytoskeleton was visualized by staining with Texas-red phalloidin and the nuclei stained with Hoescht. Images are of representative of at least 3 independent experiments. Cell circularity was calculated to quantify differences observed in cell shape (**M**); values closer to 1 indicate a more rounded cell. Fluorescent images were acquired with a Nikon Eclipse (TiE) inverted fluorescence microscope at 20X magnification. Three independent images were analyzed for each condition and 10 cells were analyzed per image. Data is pooled from all 3 images analyzed per condition. *** denotes $p<0.001$.

Epithelial cells exhibit differences in pai-1 expression when cultured on substrates of increasing stiffness.

To determine if differences in substrate stiffness induced changes in Pai-1, a TGFβ-specific responsive gene, L2 cells were cultured on substrates of varying stiffness or Fn or Ln-coated TCP for 1 week in the absence or presence of 10 μM Y-27632 ROCK inhibitor and then expression of the Pai-1 gene was determined by q-PCR (**Figure A.5**). In general, cells increased Pai-1 expression as substrate stiffness increased, with cells cultured on TCP expressing significantly more Pai-1 than cells cultured on substrates of stiffness E=8.5 kPa, 20.5 kPA, and 36.1 kPA ($p<0.05$). The addition of 10 μM Y-27632 abrogated this trend, and no statistical significance was seen between groups cultured in the presence of the inhibitor.

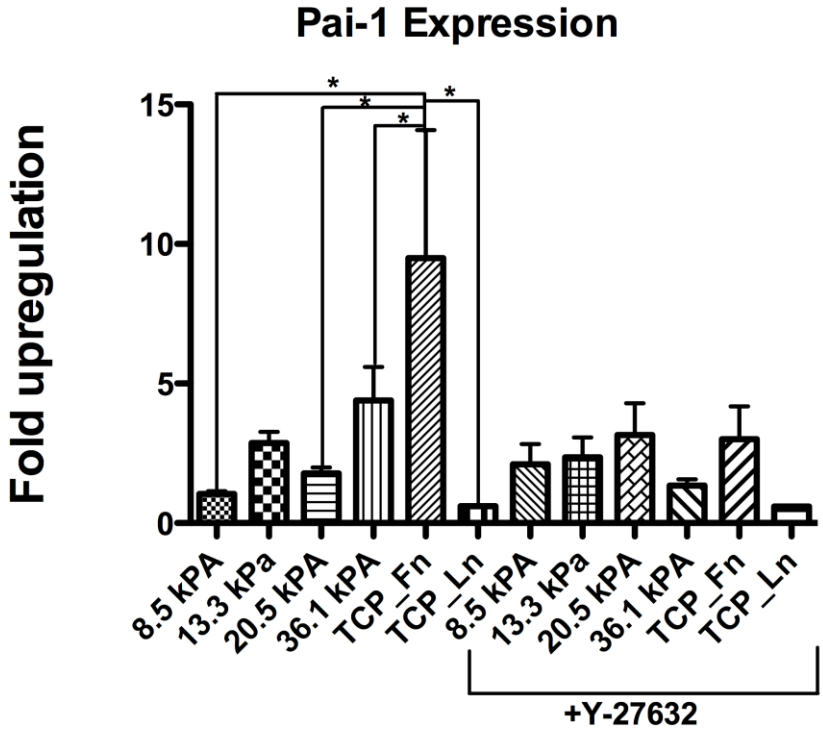

Figure A.5: Pai-1 gene expression analysis. L2 cells were cultured for 1 week on substrates of varying stiffnesss or on Fn or Ln-coated TCP in the absence or presence of 10 μM Y-27632. Levels of expression of the TGFβ responsive gene Pai-1 were determined by q-PCR. Fold changes in gene expression were determined by ΔΔCT analysis using GAPDH as the endogenous control and comparing expression to cells cultured on E=8.5 kPa. Reactions were performed in triplicate. * denotes $p < 0.05$

VITA

ASHLEY C. BROWN

Ashley C. Brown was born in Greenville, South Carolina. She attended public schools in Greer, South Carolina, received a B.S. in Biosystems Engineering from Clemson University, Clemson, South Carolina in 2006 before coming to Georgia Tech to pursue a doctorate in Biomedical Engineering. When she is not working on her research, Mrs. Brown enjoys practicing Ashtanga yoga, running marathons with her husband Chris, and spending time with their two dogs, Dobby and Gryffin.